Structural Insights into Omp85-Mediated Protein Translocation and Insertion in the Bacterial Outer Membrane

Inauguraldissertation

zur

Erlangung der Würde eines Doktors der Philosophie

vorgelegt der

Philosophisch-Naturwissenschaftlichen Fakultät

der Universität Basel

von

Fabian Gruss

aus Deutschland

Basel, 2015

Genehmigt von der Philosophisch-Naturwissenschaftlichen Fakultät
auf Antrag von

Prof. Dr. Timm Maier
Prof. Dr. Martin Spiess

Basel, den 13.10.2015

Prof. Dr. Jörg Schibler
Dekan

Summary

Proteins of the Omp85 superfamily reside in the outer membranes of Gram-negative bacteria, mitochondria and chloroplasts and are responsible for the insertion of outer membrane β-barrel proteins into or the translocation of soluble proteins across the membrane. They contain a C-terminal membrane-embedded 16-stranded β-barrel and soluble substrate-interacting POTRA domains, which in Gram-negative bacteria locate to the periplasm. The underlying translocation and insertion mechanisms are poorly understood and atomic structures of Omp85 insertases have been missing.

This thesis provides the structural basis for the insertion mechanism of substrates by the *Escherichia coli* Omp85 insertase TamA. The crystal structure of TamA reveals minimal interactions between the first and the last β-strand of the barrel with a lipid-occupied lateral gate, suggesting substrate β-barrel assembly via hybrid barrel formation and lateral release. Exemplified by the crystallization of TamA, a general crystal seeding protocol for optimization of membrane protein crystals grown from bicelle solution is described. Furthermore, interactions of TamA with its associated periplasmic complex partner TamB are investigated by experimental approaches and bioinformatics, revealing potential interaction sites between these two proteins. The organization of Omp85 insertases is then compared to Omp85 translocases, represented by FhaC from *Bordetella pertussis*, and a mechanism for substrate selection by FhaC is deduced from a newly determined crystal structure of an FhaC double mutant defective in substrate recognition.

Whereas protein import into chloroplasts is mediated by a member of the Omp85 superfamily, in mitochondria this task is fulfilled by Tom40, a 19-stranded β-barrel outer membrane protein that lacks POTRA domains. As a basis for experimental *in vitro* approaches to gaining insights into the Tom40 translocation mechanism, a protocol for recombinant Tom40 over-expression, refolding and sample preparation is provided. NMR spectroscopy of isotope-labeled protein evidences the presence of folded Tom40 in our samples.

Table of Contents

List of Figures

List of Tables

List of Abbreviations

A_{280}	Absorbance at 280 nm
AIEX	Anion exchange chromatography
AT	Autotransporter
ATP	Adenosine triphosphate
BAM	β-Barrel assembly machinery
CdiA	Contact-dependent growth inhibition protein A
CHAPSO	3-[(3-Cholamidopropyl)dimethylammonio]-2-hydroxy-1-propanesulfonate
CIEX	Cation exchange chromatography
C/o	Cut off
δ	Chemical shift
DDM	n-Dodecyl-β-D-maltopyranoside
DMPC	1,2-Dimyristoyl-sn-glycero-3-phosphocholine
DNA	Deoxyribonucleic acid
DTT	Dithiothreitol

E. coli	*Escherichia coli*
EDTA	Ethylenediaminetetraacetic acid
FHA	Filamentous hemagglutinin
FhaC	Filamentous hemagglutinin transporter protein C
$FhaC_{DIS}$	FhaC disruption
Gu-HCl	Guanidine hydrochloride
HEPES	4-(2-hydroxyethyl)-1-piperazineethanesulfonic acid
HMW	High molecular weight protein
HSQC	Heteronuclear single quantum coherence
IEM	Inner envelope membrane
IM	Inner membrane
IMAC	Immobilized metal affinity chromatography
IMM	Inner mitochondrial membrane
IMP	Inner membrane protein
IMS	Intermembrane space
IPTG	Isopropyl β-D-thiogalactopyranoside
ITC	Isothermal titration calorimetry
κ	Conductivity
K_D	Dissociation constant
kDa	Kilodalton
LamB	Phage lambda receptor protein B
LB	Luria broth
LDAO	n-Dodecyl-N,N-dimethylamine-N-oxide
LoI	Lipoprotein localization
LPP	Major outer membrane lipoprotein
LPS	Lipopolysaccharides
LptD	Lipopolysaccharide transport protein D
mAU	Milli absorbance units
MBP	Maltose binding protein
β-ME	β-Mercaptoethanol
MSA	Multiple sequence alignment
MW	Molecular weight
NCBI	National Center for Biotechnology Information
NMR	Nuclear magnetic resonance
OD_{600}	Optical density at 600 nm
OEM	Outer envelope membrane

OEP	Outer envelope membrane protein
β-OG	n-Octyl-β-D-glucopyranoside
OM	Outer membrane
OMM	Outer mitochondrial membrane
OMP	Outer membrane protein
O/n	Over night
PAGE	Polyacrylamide gelelectrophoresis
PBS	Phosphate-buffered saline
PDB	Protein Data Bank
PEG	Polyethylene glycol
PG	Peptidoglycan
PhoE	Phosphoporin protein E
PM	Plasma membrane
POTRA	Polypeptide transport associated
SAM	Sorting and assembly machinery
SDS	Sodium dodecylsulfate
Sec	Secretory translocase
SEC	Size exclusion chromatography
ShlA	Serratio hemolysin A
Skp	Seventeen kilodalton protein
SRP	Signal recognition particle
SurA	Survival protein A
TAM	Translocation and assembly module
Tat	Twin-arginine translocation
TE	Tris-EDTA
TEV	Tobacco etch virus
TF	Trigger factor
TOC	Translocase of the outer envelope membrane of chloroplasts
TOM	Translocase of the outer membrane of mitochondria
TonB	Transport energizer protein B
TPS	Two-partner secretion
Tris	2-Amino-2-hydroxymethyl-propane-1,3-diol
TROSY	Transverse relaxation-optimized spectroscopy
TxSS	Type x secretion system
VDAC	Voltage-dependent anion channel
WTFhaC	Wild-type FhaC

CHAPTER 1:

Introduction

1.1. Gram-positive and Gram-negative bacteria

In the 1880s, when looking for a method to selectively stain cytosol and nuclei of cells in human tissue, Hans Christian Gram invented a method that leaves eukaryotic cells unstained, but instead stains bacteria (Gram 1884). Furthermore, this method, now commonly known as Gram-staining, classifies bacteria into two major groups according to their staining behavior: Certain types of bacteria keep the primary crystal violet – iodine complex stain during the decolorization and counterstaining process and therefore are referred to as “Gram-positive” bacteria; others lose it and instead adopt the secondary safranin stain, and are thus called “Gram-negative” bacteria.

It took decades until electron microscopy of thin-sectioned bacteria revealed that morphological differences in the cell envelope are the cause of the different staining properties (Glauert and Thornley 1969). In Gram-positive bacteria, a thick peptidoglycan (PG; also called murein) network of 30-100 nm thickness stabilizes the cell by surrounding the plasma membrane (PM) and a narrow periplasmic space (Silhavy *et al.* 2010) (Fig. 1.1a). PG is the actual component being stained by crystal violet in Gram-staining. Gram-negative bacteria contain a much thinner PG layer. In *E. coli*, for instance, most of the PG is single layered and has a maximum thickness of 7.5 nm (Labischinski *et al.* 1991). Additionally, Gram-negative bacteria possess an outer membrane (OM) (Glauert and Thornley 1969) (Fig. 1.1b). The thin PG layer, located in the periplasmic space between OM and PM, here also called inner membrane (IM), incorporates the stain during Gram’s method, but does not retain it.

A few bacterial genera do not show canonical behavior in Gram-staining with respect to the number of cell membranes. Mycoplasma, for instance, show a negative response towards Gram-staining despite having only a single membrane, because they completely lack a PG cell wall (Rottem 2003, Vollmer *et al.* 2008a). Nevertheless, throughout the literature and in the following, “Gram-positive” generally refers to bacteria with a single membrane and “Gram-negative” to bacteria with an additional OM.

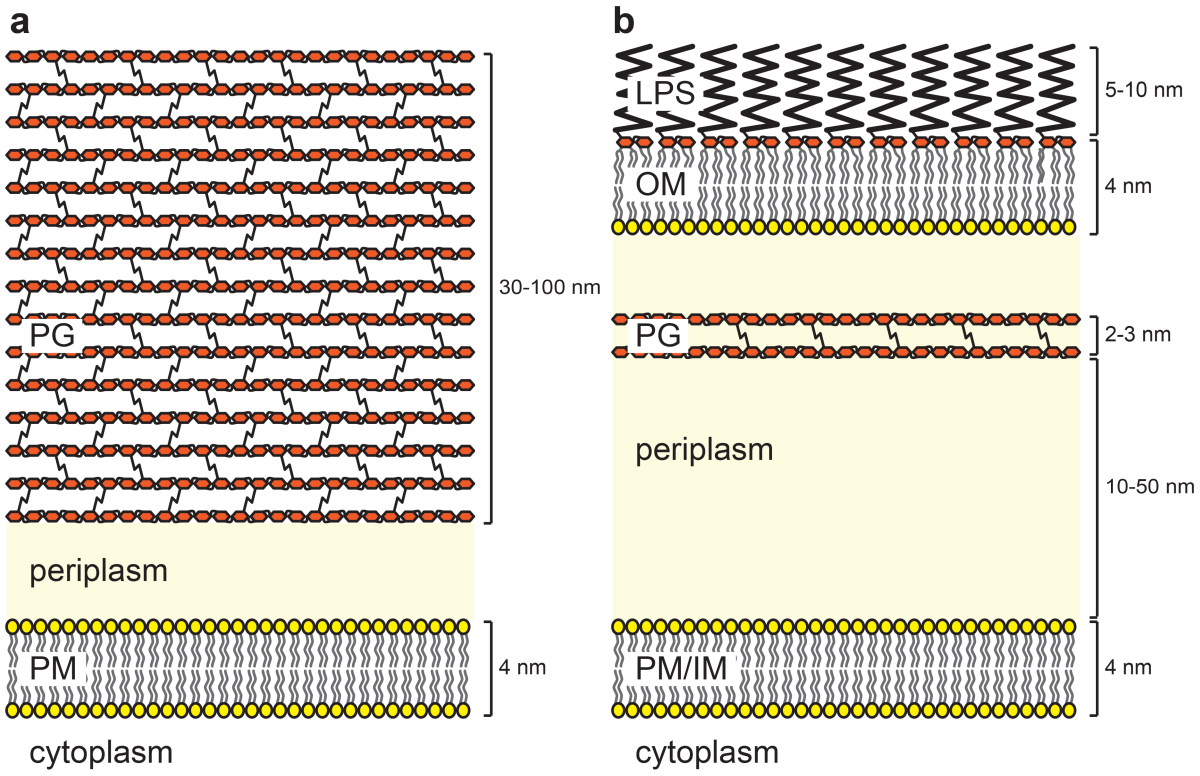

Figure 1.1 Cell envelopes in Gram-positive and Gram-negative bacteria.
(**a**) The cell envelope of Gram-positive bacteria is constituted by the plasma membrane (PM), a narrow periplasmic space (highlighted in light yellow) and a thick peptidoglycan (PG) layer. (**b**) Gram-negative bacteria contain a PM, here also called inner membrane (IM), a wider periplasmic space (highlighted in light yellow) with a thin PG layer, and additionally an outer membrane (OM) with an outer leaflet that is formed by lipopolysaccharides (LPS). Typical lengths are indicated.

1.2. The bacterial cell envelope

PG layer and membranes have different functions. In both Gram-positive and Gram-negative bacteria the rigid yet elastic PG layer conveys stability to the cell and protects it from lysis due to mechanical and osmotic forces. Moreover, it gives rise to characteristic shapes of different bacteria (Silhavy *et al.* 2010). PG is composed of polymers of N-acetylglucosamine and N-acetylmuramic acid disaccharides. The average chain length of the polymers can vary depending on species and growth conditions between 20 and several hundreds of disaccharide units, but it does not correlate with the thickness of the PG layer. The chains are crosslinked via short stem peptides, which contain non-proteinogenic amino acids as *e.g.* D-enantiomers (Krause and McCarty 1961, Strange and Dark 1956, Typas *et al.* 2012, Vollmer *et al.* 2008a).

In Gram-negative bacteria, the PG layer is connected to the OM via the small lipoprotein Lpp, the most abundant protein in *E. coli* (Braun 1975). Lpp contains an N-terminal cysteine,

covalently modified with a lipid group that is buried in the inner leaflet of the OM. The PG mesh has a porous structure, through which small compounds can easily diffuse and even proteins of up to a size of 50 – 100 kDa are able to cross it. For larger protein complexes, peptidoglycan hydrolases may locally disrupt the layer (Scheurwater and Burrows 2011, Silhavy *et al.* 2010, Vollmer and Bertsche 2008, Vollmer *et al.* 2008b).

In contrast, cell membranes act as permeability barriers not only for macromolecules, but also for many small molecules and ions. Hence, they are responsible for keeping the integrity of the cell-interior intact and for protecting it from potentially harmful compounds. The OM of Gram-negative bacteria thus constitutes a protecting barrier in addition to the IM (Nikaido 2003, Silhavy *et al.* 2010), which makes Gram-negative bacteria generally more tolerant towards antibiotics than Gram-positive bacteria (Page 2012, Silhavy *et al.* 2010).

Bacterial plasma membranes form a lipid bilayer, composed of phospholipids as the major components in both leaflets. The most abundant phospholipids found in bacterial membranes are phosphatidylethanolamines (approx. 75%), followed by phosphatidylglycerols (approx. 20%) and cardiolipins (approx. 5%) (Cronan 2003), which have acyl chains with between 14 and 20 carbon atoms (Zhang and Rock 2008). The OM of Gram-negative bacteria, however, is distinct from the IM, as its outer leaflet contains lipopolysaccharides (LPS) and therefore the OM is asymmetric. LPS consist of lipid-A, containing six to seven hydrophobic acyl chains, and a branched polysaccharide chain attached to it facing the extracellular space (Chatterjee and Chaudhuri 2012, Silhavy *et al.* 2010, Whitfield and Trent 2014). Furthermore, a substantial amount of both membranes is composed of proteins that are embedded in or attached to the membranes.

The OM and its integrity are essential for survival of Gram-negative bacteria. Contributing to this fact is plausibly the thin PG layer and the circumstance that essential periplasmic proteins rely on the OM to be kept in proximity, whereas corresponding proteins in Gram-positive bacteria are either attached to the plasma membrane or the thick PG layer (Silhavy *et al.* 2010).

1.3. Membrane proteins in bacteria

Inner membrane proteins (IMPs) in all bacteria typically adopt α-helical secondary structure within the lipid bilayer of the membrane. These proteins can span the membrane with only one (single-pass) or with several α-helices (multi-pass), which are enriched in hydrophobic amino acids (Fig. 1.2a). Transmembrane α-helices of multi-pass IMPs interact with neighboring helices to form defined arrangements within the membrane. Homo- and hetero-oligomerization of IMPs to form membrane complexes is quite frequent. Homo-

oligomers usually form rotation-symmetrical complexes in the layer of the membrane (Vinothkumar and Henderson 2010, von Heijne 2006).

In addition to the transmembrane part, many IMPs contain cytoplasmic and/or periplasmic domains that can be N- or C-terminal or embedded in loops connecting transmembrane helices. These soluble domains can contain both α-helical and β-sheet structures (Du *et al.* 2014, Kumazaki *et al.* 2014). Bacteria possess a lot of different IMPs. For instance, in *E. coli* approx. 20 – 30% of all genes encode for them (Facey and Kuhn 2010). Their functions are diverse and include synthesis of cell envelope components, ATP synthesis, signal transduction and transport of molecules across the IM (Vinothkumar and Henderson 2010). In contrast, outer membrane proteins (OMPs) in Gram-negative bacteria constitute only approx. 2% of all proteins and their functions are less diverse. Usually, they are involved in transport and cell adhesion, even though a few enzymatically active OMPs exist (Facey and Kuhn 2010, Tamm *et al.* 2004, Vinothkumar and Henderson 2010, Wimley 2003).

Structurally, OMPs are completely different from IMPs, as they form β-barrels in the lipid bilayer. These consist of a β-sheet with antiparallel strands wrapping up to form a cylindrical shape in which the first and the last β-strand interact via hydrogen bonds (Fig. 1.2b). The number of strands is usually even and varies between 8 as in OmpA (Pautsch and Schulz 1998) and 26 as in LptD (Qiao *et al.* 2014). The membrane-spanning part of β-strands in OMPs is amphipathic. It shows a typical alternating pattern of hydrophobic and hydrophilic residues, as sidechains alternatingly point to the hydrophobic lipid bilayer and the hydrophilic β-barrel lumen. Some OMPs form homo-oligomers, such as trimers (Cowan *et al.* 1992). A few special OMPs, like trimeric autotransporters and TolC, have a single homo-oligomeric β-barrel, in which each of the three proteins contributes four strands to form one trimeric 12-stranded β-barrel (Koronakis *et al.* 2000, Shahid *et al.* 2012).

Like IMPs, also OMPs can have additional periplasmic and/or extracellular domains that can contain both α-helical and β-sheet structures. These domains are often found N-terminal or embedded in extracellular loops between strands (Phan *et al.* 2011). C-terminal soluble domains are rare due to OMP biogenesis, but can be found as well, *e.g.* in OmpA (Pautsch and Schulz 1998) and in inverse autotransporters (Oberhettinger *et al.* 2015).

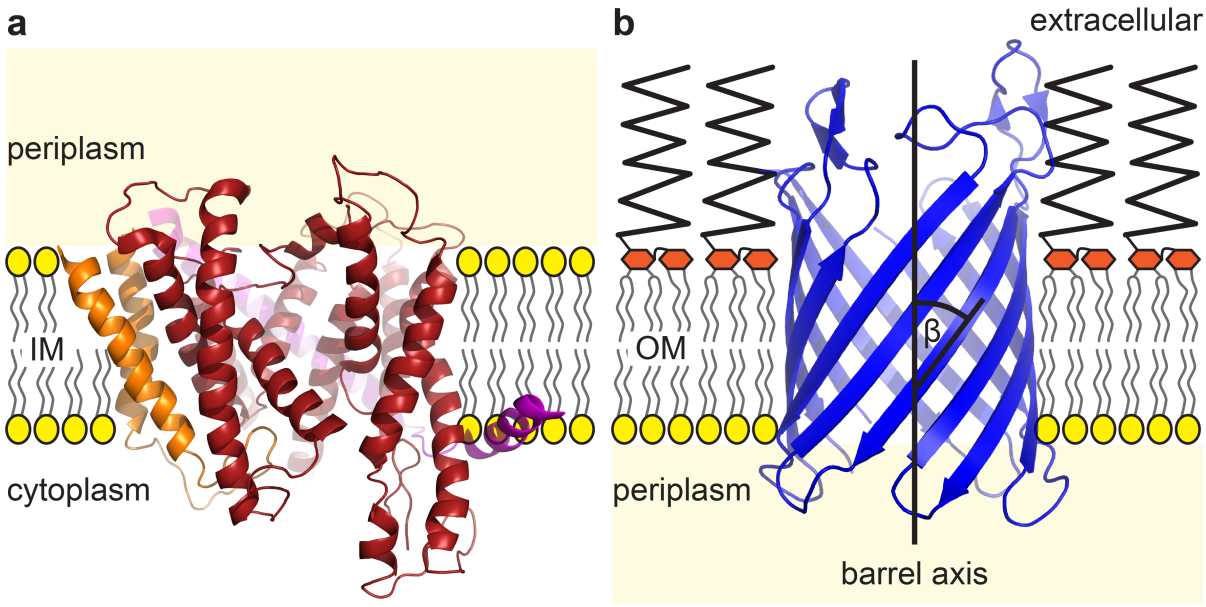

Figure 1.2 α-Helical and β-barrel transmembrane proteins.
(**a**) The inner membrane of Gram-negative bacteria contains transmembrane proteins of α-helical structure. As an example the hetero-trimeric SecYEG is shown (SecY in red, SecE in purple and SecG in orange; PDB entry 3DIN (Zimmer *et al.* 2008)). (**b**) The outer membrane contains transmembrane proteins of β-barrel structure. As an example NanC (blue) is shown (PDB entry 2WJR (Wirth *et al.* 2009)). The tilt angle β for this β-barrel is indicated.

Geometrically, β-barrels can be described by their number of strands, tilt angle (Fig. 1.2b), and shear number (Pali and Marsh 2001). Importantly, all β-barrels with solved structure to date tilt to the same direction with similar angles between 35° and 45° (Pali and Marsh 2001). Viewed from the top, β-barrels can adopt different shapes; they can be almost perfectly round but they can also be *e.g.* elliptic or kidney-shaped. However, they may be intrinsically flexible if no further structures lead to stabilization of a certain shape. Another common feature of β-barrels is that the loops on the extracellular site connecting two neighboring strands are usually significantly longer than the periplasmic turns (Mirus *et al.* 2010).

Whereas α-helical membrane proteins can also be found in most membranes of eukaryotic cells, β-barrels are restricted to outer membranes of eukaryotic organelles that derive from endosymbiosis like mitochondria and chloroplasts. The mitochondrial outer membrane protein VDAC is the only OMP to date with solved structure that has an uneven number of strands (19) and therefore, in this special case, the first and the last strand are parallel to each other (Hiller *et al.* 2008).

Even though the OM is essential in Gram-negative bacteria, only two OMPs are essential: One is the protein LptD, which, together with periplasmic, IM and cytoplasmic proteins, is responsible for the transport of LPS molecules from the IM across the periplasmic space into the outer leaflet of the OM (Braun and Silhavy 2002, Qiao *et al.* 2014, Tokuda 2009, Whitfield

and Trent 2014). The other essential OMP is BamA. This protein forms a complex with non-transmembrane but OM-anchored lipoproteins and is indispensable for the integration of new OMPs into the OM, including LptD and other BamA molecules (Doerrler and Raetz 2005, Voulhoux *et al.* 2003, Werner and Misra 2005, Wu *et al.* 2005).

1.4. Transport of nutrients across membranes

Whereas small hydrophobic molecules can cross lipid bilayers by passive diffusion at reasonable rates, ions and most nutrients cannot pass them. Therefore, it is essential for bacteria to be able to import them. This is achieved through transmembrane proteins embedded in the lipid bilayers of IM and OM that can be divided into two groups: The first group facilitates diffusion of certain molecules or ions by providing an aqueous path from one side of the membrane to the other. This group can be subdivided into channels and pores. The second group constitutes transporters that do not contain a continuous path through the membrane but can utilize energy sources to undergo conformational changes and thereby transport substrates against concentration gradients across membranes (Noinaj and Buchanan 2014, Vinothkumar and Henderson 2010).

Pores provide a hydrophilic environment across the membrane between helices of IMPs or within the β-barrel of OMPs. These pores are often substrate-unspecific and facilitate diffusion of different molecules and ions across a membrane as long as their sizes do not exceed the pore diameter. Uncharged molecules diffuse solely along their concentration gradients, whereas for charged molecules additionally the membrane potential plays a role and therefore they diffuse along their electrochemical gradient. Channels contain specificity filters, which for instance let only certain ions pass. Many channels are not constitutively open; instead they can be gated and only open upon specific stimuli. These can include mechanical or chemical signals and changes in membrane potential (Alberts *et al.* 2008, Vinothkumar and Henderson 2010) (Fig. 1.3a).

Transporters, or carriers, also completely span the membrane, but in contrast to channels and pores, they do not constitute a continuous aqueous path across the membrane. Instead, they bind molecules or ions to be transported very specifically on one side of the membrane and then undergo conformational changes that take the cargo to the other side of the membrane, where it is released. Therefore, the transport rates are usually significantly slower than for pores or channels. There are transporters that facilitate diffusion without input of external energy, but others are energized and can transport molecules against concentration resp. electrochemical gradients. These latter ones can be subdivided into primary active transporters, which couple transport to ATP hydrolysis, and secondary active transporters, which couple the transport of a molecule against its electrochemical gradient to

the transport of one or several others along their electrochemical gradient. The latter gradient is however in the first place established by ATP-driven transport, hence the term “secondary active” (Alberts *et al.* 2008, Chen 2013, Jaehme and Slotboom 2015, Noinaj and Buchanan 2014, Robertson *et al.* 2012, Shi 2013, Vinothkumar and Henderson 2010, Wilkens 2015) (Fig. 1.3a).

Whereas in the IM channels and pores for facilitated diffusion as well as energized transporters exist, the OM is usually constricted to channels and pores, due to the lack of energy sources like ATP in the periplasm or an electrochemical potential across the OM. OMP pores, called porins, contain a β-barrel with typically 16 or 18 strands, and form trimers of β-barrels in the membrane (Galdiero *et al.* 2012). Porins in *E. coli*, which allow nonspecific facilitated diffusion of ions, water and small molecules (<600 Da) like glucose, include OmpC, OmpF and PhoE (Cowan *et al.* 1992). More substrate-specific porins include *e.g.* the maltooligosaccharide-specific maltoporin LamB (Koebnik *et al.* 2000, Schirmer *et al.* 1995). Once maltose has entered the periplasm after diffusion through the LamB pore, it is bound by the maltose binding protein (MBP) and therefore pulled out from the pool of freely diffusing maltose molecules across the OM. MBP then binds to a specific maltose transporter at the inner membrane, which takes over the maltose and transports it across the IM under ATP consumption (Chen 2013, Oldham *et al.* 2007) (Fig. 1.3b).

There are also exceptions of OMPs that constitute energy-driven transporters. Those usually release siderophores to the extracellular space to bind ferric chelates, nickel complexes, vitamin B12 or carbohydrates. The re-uptake of these siderophores is a process that requires energy. Due to the lack of energy sources at the OM, energy from the proton motif force at the IM is delivered from the TonB-ExbB-ExbD complex in the IM to these transporters in the OM. Those are therefore called TonB-dependent transporters but little is known about the details of energy transfer (Noinaj *et al.* 2010, Vinothkumar and Henderson 2010).

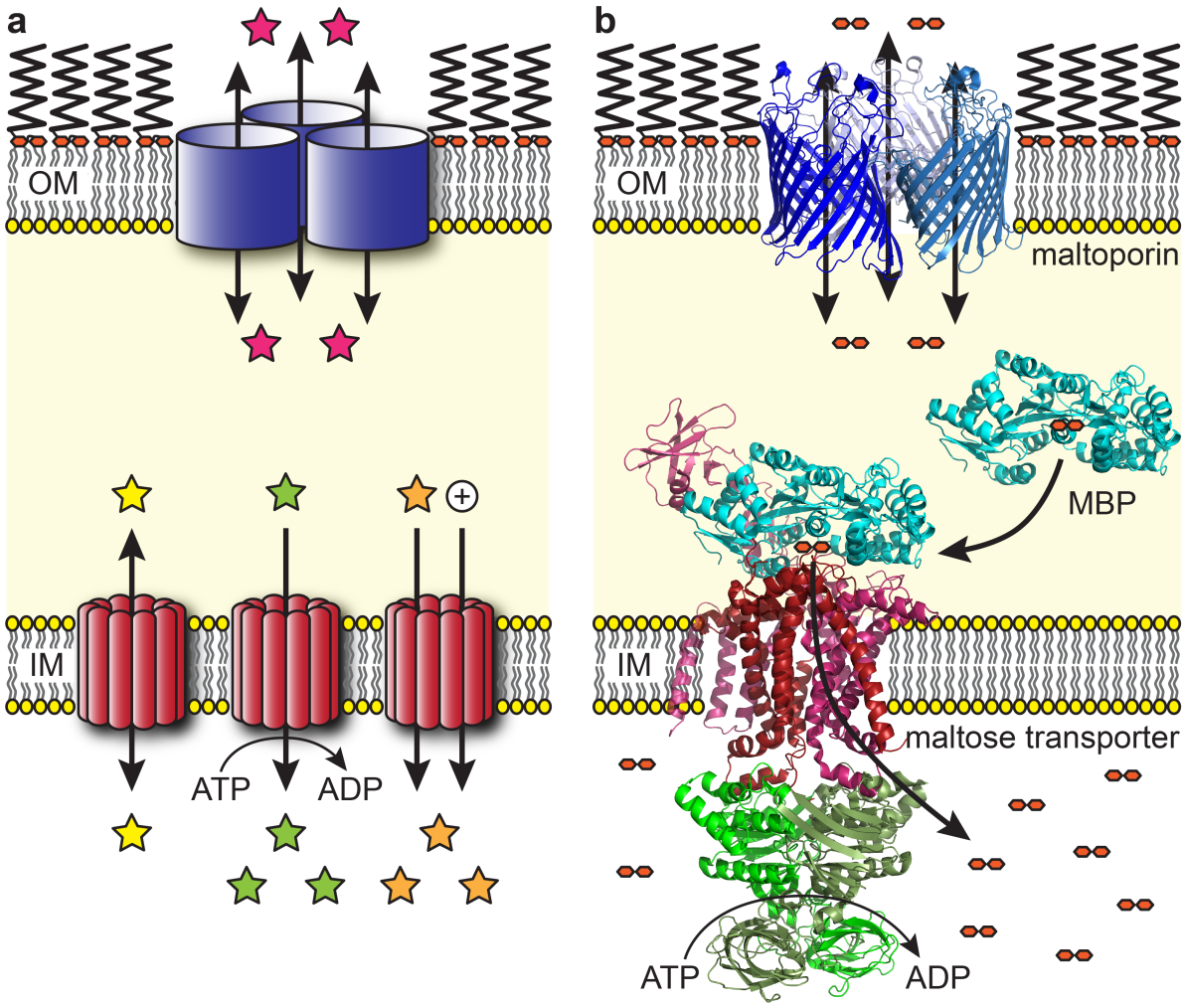

Figure 1.3 Transport of small molecules across membranes.
(**a**) Schematic representation of a trimeric OM porin (blue, top), IM channel or pore (red, bottom left), IM primary active transporter (red, bottom center) and IM secondary active transporter, depicted as a cation symporter (red, bottom right). Small molecule or ion substrates are represented by colored stars. (**b**) Depiction of maltose import from the extracellular space to the cytoplasm across OM, periplasm and IM. Maltoporin LamB (blue, top; PDB entry 1MAL (Schirmer *et al.* 1995)) facilitates diffusion of maltose across the OM. Periplasmic maltose binding protein MBP/MalE (cyan) binds maltose and takes it to the IM maltose transporter MalFG (MalF in magenta and MalG in red), which is energized by the dimeric ATPase MalK (green) to transport maltose across the IM against its concentration gradient (MalEFGK: PDB entry 2R6G (Oldham *et al.* 2007)).

1.5. Assembly of inner membrane proteins by SecYEG

Both IMPs and OMPs, as well as all other bacterial proteins, are synthesized by ribosomes in the cytoplasm. Since integral membrane proteins naturally contain a lot of hydrophobic residues in the parts that will later face the lipid bilayer environment of the membranes, these proteins are prone to aggregation as long as they do not adopt their final

membrane-embedded structure. To reach their destination, IMPs are directly integrated into the IM, whereas OMPs first need to be transported to the periplasm and then cross it, before being integrated into the OM.

IMPs contain a hydrophobic signal anchor sequence, which will also be the most N-terminal transmembrane helix in the folded protein. When it emerges from the ribosome early in the translation process, it interacts with the ribosome-associated chaperone trigger factor (TF), as most nascent chains do (Facey and Kuhn 2010, Hoffmann *et al.* 2010, Maier *et al.* 2005). Subsequently, signal recognition particle (SRP) competes with TF for interaction with the nascent chain as it has especially high affinity to hydrophobic sequences like the signal anchor sequence. Translation is stalled and SRP targets the ribosome – nascent chain – SRP complex to the inner membrane where it interacts with the membrane-bound SRP-receptor FtsY (Akopian *et al.* 2013, Facey and Kuhn 2010, Valent *et al.* 1998). SRP dissociates from the signal anchor sequence, which is transferred to the inner membrane protein complex SecYEG. Translation continues and the emerging nascent polypeptide chain threads through the membrane pore formed by SecYEG (Cannon *et al.* 2005, Gogala *et al.* 2014, Park *et al.* 2014, Spiess 2014, Van den Berg *et al.* 2004), pushed by the polypeptide synthesis at the ribosome (Facey and Kuhn 2010, Park and Rapoport 2012). When a hydrophobic stretch of amino acids, which will be a transmembrane helix in the mature protein, is recognized, it is transferred laterally into the IM through a lateral gate between two transmembrane helices (2 and 7) of SecY that opens up (Egea and Stroud 2010, Gogala *et al.* 2014, Park *et al.* 2014, Van den Berg *et al.* 2004). The nascent chain continues threading through SecYEG and with every new transmembrane helix a lateral insertion procedure takes place until the translation at the ribosome is finished and the IMP is completely inserted in the IM (Facey and Kuhn 2010, Xie and Dalbey 2008) (Fig. 1.4).

This process of co-translational insertion overcomes the problem that a hydrophobic polypeptide chain may aggregate in the cytoplasm. Besides this canonical pathway for IMP insertion, other pathways also play a role for distinct proteins, involving another IMP insertase called YidC (Dalbey *et al.* 2014, Hennon *et al.* 2015, Xie and Dalbey 2008).

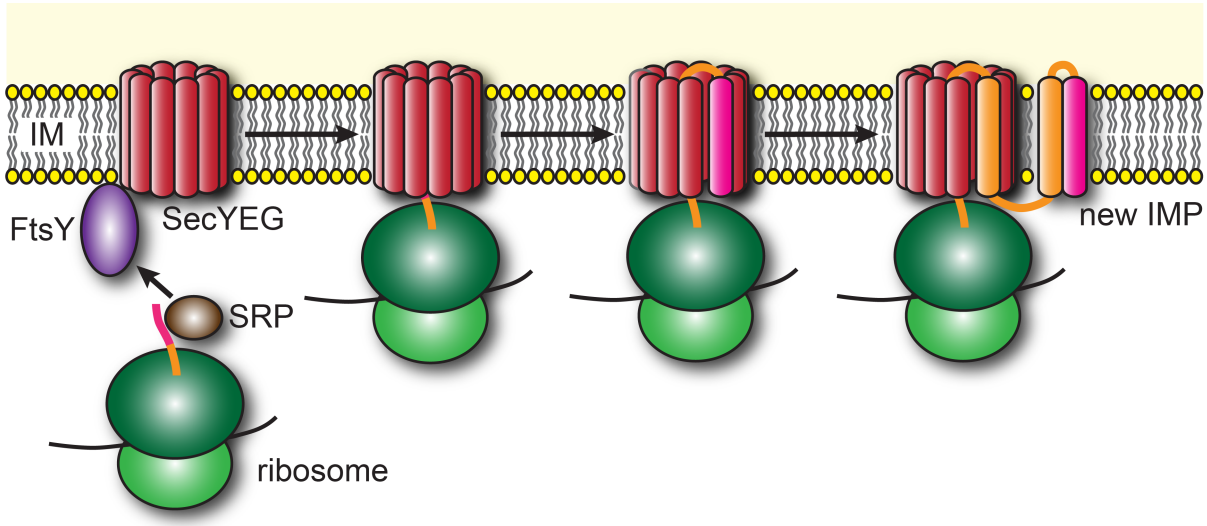

Figure 1.4 IMP biogenesis.
SRP (brown) directs the stalled nascent chain (orange, signal anchor sequence in magenta) – ribosome (green) – mRNA (black) complex to the SRP receptor FtsY (purple) at the IM. Subsequently, the nascent chain is handed over to SecYEG (red). Translation continues and the nascent chain is threaded through SecYEG. Hydrophobic transmembrane α-helices of the newly synthesized IMP are recognized and released laterally into the membrane by SecYEG.

1.6. Transport of proteins across the inner membrane by SecYEG

OMPs and most periplasmic proteins use the Sec translocase for IM traversal. A co-translational process is in some cases used, but usually OMPs and soluble periplasmic proteins are post-translationally transported to the periplasm. In this pathway, an N-terminal tripartite signal sequence (Hutchings *et al.* 2009) is recognized by trigger factor (TF) when emerging from the ribosome during translation of OMPs and periplasmic proteins. Subsequently, SecB chaperone molecules are recruited, displace TF and stabilize the nascent polypeptide chain (Bechtluft *et al.* 2010, Facey and Kuhn 2010). When the translation process is finished, the unfolded, chaperone-stabilized OMP or periplasmic protein is delivered to the IM, where the signal sequence is bound by SecYEG and the polypeptide it is threaded through the SecYEG translocon in a hairpin fashion in N- to C-terminal direction (Cannon *et al.* 2005, Gogala *et al.* 2014, Park *et al.* 2014). This process is energetically mainly driven by the ATPase SecA (Papanikou *et al.* 2007, Park and Rapoport 2012). As β-barrel OMPs do not contain stretches of purely hydrophobic amino acids as in transmembrane α-helices of IMPs, a lateral membrane insertion process into the IM is not triggered and instead the whole polypeptide chain is threaded through. Once this translocation process is completed, the N-terminal signal sequence, still bound to SecYEG,

is cleaved from the rest of the polypeptide chain by signal peptidase (SP) (Facey and Kuhn 2010, Papanikou *et al.* 2007) (Fig. 1.5).

In addition to OMPs and soluble periplasmic proteins, most lipoproteins from the IM and OM use this pathway as well to reach the periplasm. After translocation, these lipoproteins are still bound to Sec via their N-terminal signal sequence. A conserved cysteine residue directly behind the signal sequence is then modified with a lipid and the signal sequence is cleaved, which leaves the lipoprotein anchored with the lipid moiety in the outer leaflet of the IM. Most lipoproteins are then transported by the lipoprotein localization (Lol) pathway to the OM, where they are anchored to the inner leaflet. Lipoproteins that are destined to remain IM-anchored avoid this translocation pathway by containing special Lol avoidance signals (Hutchings *et al.* 2009, Zückert 2014).

Besides the Sec pathway, which transports still unfolded proteins to the periplasm, another pathway for folded substrates exists, called the twin-arginine translocation (Tat) pathway. Certain proteins, including some lipoproteins, use this pathway instead of Sec to be transported in a folded state, but insights into its structural and mechanistic aspects are still limited (Kudva *et al.* 2013, Palmer and Berks 2012, Patel *et al.* 2014).

1.7. Transport of outer membrane proteins across the periplasm

Similarly to the recruitment of the chaperones TF and SecB during translation in the cytoplasm, periplasmic chaperones are recruited when an unfolded OMP is threaded through Sec in the IM and arrives at the periplasmic side of the membrane. The chaperone that is mainly involved in this process in *E. coli* is called SurA (Sklar *et al.* 2007b, Volokhina *et al.* 2011) and multiple SurA molecules bind as monomers or dimers to multiple aromatic residue-rich sites of unfolded OMPs (Xu *et al.* 2007). Besides the SurA pathway, another pathway for OMPs exists, involving the chaperones Skp and DegP (Sklar *et al.* 2007b, Volokhina *et al.* 2011). This pathway is thought to work as a backup system for SurA in *E. coli*. Here, SurA is the generally preferred chaperone, but both pathways can substitute each other, whereas in other Gram-negative bacteria the Skp/DegP pathway may be the preferred one (Sklar *et al.* 2007b, Tommassen 2010, Ulrich and Rapaport 2015, Volokhina *et al.* 2011). Skp binds OMPs in a very different fashion than SurA by providing a cavity between three “arms” of this trimeric protein, where the substrate is kept in a fluid globule state (Burmann *et al.* 2013, Callon *et al.* 2014, Qu *et al.* 2007). The chaperones transport the unfolded OMP through the periplasm to the OM, where they hand it over to the BAM complex, which finally integrates this polypeptide as a β-barrel into the OM (Kim *et al.* 2012) (Fig. 1.5).

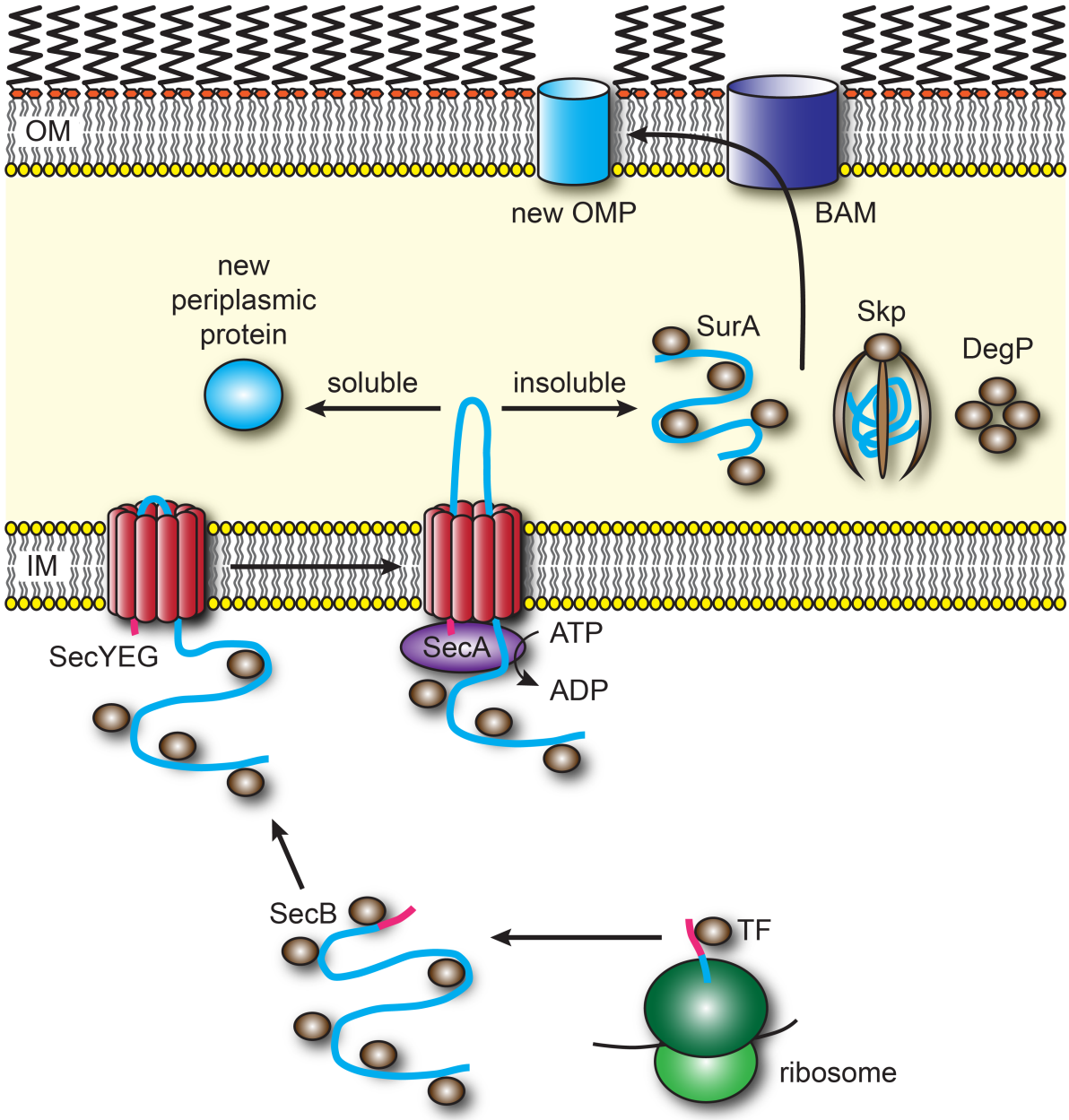

Figure 1.5 OMP biogenesis.

During translation of an OMP at a ribosome (green) in the cytosol, TF (brown) is displaced by SecB chaperone molecules (brown), which guide the unfolded OMP (cyan, signal sequence in magenta) to SecYEG (red) in the IM. SecA ATPase (purple) drives the translocation of the substrate through SecYEG, after which the signal sequence is removed. Unfolded OMPs use either the SurA or the Skp/DegP chaperone (brown) pathway to be stabilized in the periplasm. The chaperones guide the unfolded OMP to the OM, where it is assembled by the BAM complex (blue).

1.8. Assembly of outer membrane proteins by BAM

The BAM complex is responsible for the integration of newly synthesized OMPs into the OM of Gram-negative bacteria (Doerrler and Raetz 2005, Voulhoux *et al.* 2003, Werner and Misra 2005, Wu *et al.* 2005), ranging from the smallest OMPs, containing 8 β-strands to the largest ones with 26 β-strands (Doerrler and Raetz 2005, Palomino *et al.* 2011, Qiao *et al.* 2014, Voulhoux *et al.* 2003, Werner and Misra 2005). It consists of BamA, which is an OMP itself (Flack *et al.* 1995, Manning *et al.* 1998, Ruffolo and Adler 1996, Thomas *et al.* 1990), and several lipoproteins, which are BamBCDE in *E. coli* (Anwari *et al.* 2012, Volokhina *et al.* 2009, Wu *et al.* 2005). Despite consisting of five subunits, only BamA and BamD are essential for a functional BAM complex and cell viability (Malinverni *et al.* 2006, Rossiter *et al.* 2011, Voulhoux *et al.* 2003). However, deletions of any of the non-essential lipoproteins lead to compromised cell growth and OMP insertion. Furthermore, for BamA, which comprises a 16-stranded membrane-integrated β-barrel and five periplasmic POTRA (for "polypeptide transport associated", (Sanchez-Pulido *et al.* 2003)) domains, only POTRA domain 5, which is most proximal to the barrel, and the barrel itself are essential in *Neisseria meningitides* (Bos *et al.* 2007). In *E. coli*, POTRA domains 3-5 and the barrel are essential (Kim *et al.* 2007), and deletions of non-essential POTRA domains compromise BAM function.

POTRA domains share a typical β-α-α-β-β fold with a 3-stranded β-sheet and two proximal α-helices (Gatzeva-Topalova *et al.* 2008, Gatzeva-Topalova *et al.* 2010, Kim *et al.* 2007, Zhang *et al.* 2011). BamA POTRA domain 5 interacts with BamD (Kim *et al.* 2007, Ricci *et al.* 2012), which in turn binds BamC and BamE (Kim *et al.* 2011a, Malinverni *et al.* 2006, Rigel *et al.* 2012, Sklar *et al.* 2007a). BamB interacts directly with BamA POTRA domain 3 (Dong *et al.* 2012b, Jansen *et al.* 2015, Vuong *et al.* 2008) (Fig. 1.6).

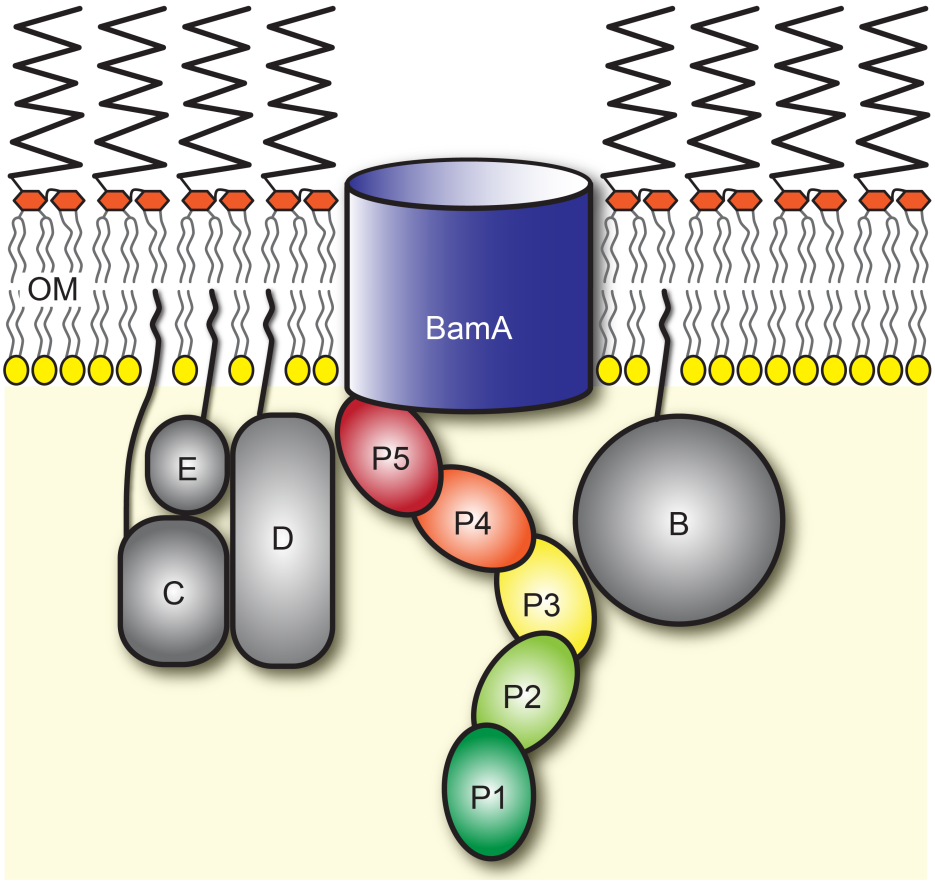

Figure 1.6 Schematic representation of the BAM complex.
Blue: the BamA β-barrel. Green – light green – yellow – orange – red: The BamA POTRA domains 1 to 5. Grey: BamB, BamC, BamD and BamE, labeled with the respective letters.

The process of OMP substrate processing by the BAM complex after delivery via the SurA or Skp/DegP chaperone pathways is not understood in detail. SurA interacts with BamA POTRA domain 1 (Bennion *et al.* 2010, Sauri *et al.* 2009, Sklar *et al.* 2007b). Upon arrival at the BAM complex, substrates are released from the chaperone, when presumably the conserved C-terminal "β-signal" motif, which is located in the last β-strand of a mature OMP and has a phenylalanine as the most frequent C-terminal residue (Struyvé *et al.* 1991), is recognized by the BAM complex. BamA POTRA domains interact with peptides corresponding to β-signals of OMPs (Knowles *et al.* 2008). The suggested mechanism is based on β-augmentation (Harrison 1996), which means that unfolded OMP substrates extend the 3-stranded β-sheets of the POTRA domains by providing one or more additional strands to transiently form larger β-sheets (Kim *et al.* 2012). Substrates may slide along the POTRA domains under reformation of β-augmentation interactions. This process has not been demonstrated directly, but in several crystal structures of BamA POTRA domains, crystal contacts between POTRA domains mimic β-augmentation (Gatzeva-Topalova *et al.* 2008, Kim *et al.* 2007, Koenig *et al.* 2010).

The essential BamD interacts with β-signal motifs as well (Albrecht and Zeth 2011) and BamC may have a regulatory function, as in the BamCD crystal structure it binds to the presumable β-signal binding groove of BamD (Kim *et al.* 2011a). β-Augmentation is also proposed to take place with BamB, which forms a β-propeller with eight WD40 repeats, and therefore would offer several sites for β-sheet extension (Heuck *et al.* 2011). The non-essential BamB may thus be especially important for OMPs containing many β-strands by providing additional interaction sites (Heuck *et al.* 2011, Palomino *et al.* 2011). BamE stabilizes the BAM complex (Sklar *et al.* 2007a) and binds phosphatidylglycerols (Knowles *et al.* 2011). Thereby, it may locate the BAM complex to regions rich in this lipid, which was shown to facilitate spontaneous membrane insertion of the BAM substrate OmpA *in vitro* (Patel *et al.* 2009).

Despite available high-resolution structures for all BAM lipoproteins (Albrecht and Zeth 2011, Dong *et al.* 2012a, Dong *et al.* 2012b, Heuck *et al.* 2011, Jansen *et al.* 2012, Kim *et al.* 2011a, Kim *et al.* 2011b, Kim *et al.* 2011c, Kim and Paetzel 2011, Knowles *et al.* 2011, Noinaj *et al.* 2011, Sandoval *et al.* 2011) and for all BamA POTRA domains (Gatzeva-Topalova *et al.* 2008, Gatzeva-Topalova *et al.* 2010, Kim *et al.* 2007, Zhang *et al.* 2011), the main mechanistic characterization of OMP assembly in the bacterial OM, especially of the final steps, is still missing.

The conformation of the flexible BamA barrel (Stegmeier and Andersen 2006) is influenced by interactions with unfolded substrates and their C-terminal β-signals (Robert *et al.* 2006). The interaction of substrates and the BamA barrel happens at a late stage of OMP assembly since the barrel is the part of the BAM complex closest to and even inside the OM, the final destination of the substrates (Kim *et al.* 2012).

The β-barrel formation process generally works without external energy provision, as the periplasm is devoid of ATP and the OM is not energized by an electrochemical potential. Moreover, proteoliposome-reconstituted BAM complex (Hagan and Kahne 2011, Hagan *et al.* 2010, Norell *et al.* 2014) and BamA alone (Patel and Kleinschmidt 2013) show OMP insertion activity without additional energy. Thus, the folding of such polypeptide chains into a membrane-embedded β-barrel is an energetic downhill process, driven by the energetically favorable formation of hydrogen bonds between β-strands, catalytically facilitated by the insertase BamA. This finding is well in line with the observation that several β-barrels can also fold spontaneously into lipid bilayers *in vitro* on their own, but with a rate much lower than observed *in vivo* (Burgess *et al.* 2008, Huysmans *et al.* 2010, Patel *et al.* 2009, Patel and Kleinschmidt 2013, Pocanschi *et al.* 2006, Surrey and Jahnig 1992, Surrey *et al.* 1996).

Another reason why BamA is the central subunit in the BAM complex for the assembly of new OMPs is that it belongs to the Omp85 superfamily (Gentle *et al.* 2004). Omp85 proteins share a C-terminal 16-stranded β-barrel and a varying number of N-terminal POTRA

domains (Gentle *et al.* 2005). This protein family also exists in the OM of eukaryotic mitochondria and plastids. There, Omp85 proteins belong to complexes that utilize membrane assembly of OMPs as well. Furthermore, they are the only homologous proteins between the different complexes and therefore evolutionary most conserved and functionally most relevant (Gentle *et al.* 2004, Gentle *et al.* 2005, Walther *et al.* 2009).

1.9. Transport of proteins across the outer membrane in two-partner secretion

BamA is one of several Omp85 proteins found in Gram-negative bacteria. There is also TamA with three POTRA domains (formerly YtfM) (Stegmeier *et al.* 2007) and TpsB proteins with two POTRA domains (Jacob-Dubuisson *et al.* 2013), including the best-characterized member FhaC from the whooping cough agent *Bordetella pertussis*.

TpsB proteins function in two-partner secretion (TPS) (Jacob-Dubuisson *et al.* 2000), which is also classified as type 5b secretion system (T5bSS) (Henderson *et al.* 2000). The name TPS derives from the fact that most TpsB Omp85 proteins have one distinct substrate protein, called TpsA, which is usually encoded in the same operon as the TpsB protein and which is in contrast to OMPs not integrated into, but instead translocated across the OM to the extracellular space (Barenkamp and St Geme 1994, Schiebel *et al.* 1989, Willems *et al.* 1994). This transport through the OM is performed solely by the TpsB partner, which does not have complex partners, in contrast to Omp85 proteins from OMP insertion machineries (Fan *et al.* 2012). In some bacteria one TpsB protein can have several TpsA substrates (Julio and Cotter 2005, Plamondon *et al.* 2007).

To date, in addition to type5 secretion systems (T5SS), five other secretion systems (T1SS to T4SS and T6SS) have been characterized in Gram-negative bacteria, which are all much more complex than T5SS. Those secretion systems are composed of large hetero-oligomeric complexes that span both IM and OM and often can form a complete tunnel from the cytoplasm to the extracellular space, through which proteins, DNA or small molecules can be ejected (Costa *et al.* 2015). However, T5SS is the most abundant secretion pathway for proteins in Gram-negative bacteria.

The general pathway of TpsA protein biogenesis is very similar to the one of OMPs. They are synthesized in the cytoplasm, containing an N-terminal, often extended signal sequence, which directs them through the IM and is cleaved off after arrival in the periplasm. There, even though still unfolded, they are less prone to aggregation than OMPs since they do not contain transmembrane regions and therefore not as many hydrophobic residues. There is however evidence that the chaperone DegP may play a role when they cross the periplasm to reach the OM (Baud *et al.* 2009). The greatest difference to the biogenesis of OMPs lies in the final step, when in contrast to unfolded OMPs, unfolded TpsA proteins are not processed

by the BAM complex, but instead by the TpsB partner protein, which mediates secretion to the extracellular space (Fig. 1.7a).

Secreted TpsA proteins usually adopt similar overall folds as they form extended β-helical structures (Kajava and Steven 2006), but they vary in size from a few hundred to several thousand amino acids. Moreover, despite being structurally similar, TpsA functions are diverse. For instance, in the pathogenic bacterium *Bordetella pertussis*, filamentous hemagglutinin (FHA) is crucially involved in cell adhesion and biofilm formation during colonization of the respiratory tract (Serra *et al.* 2011), in *Serratia marcenscens*, Serratia hemolysin (ShlA) lyses erythrocytes by forming pores in their membrane (Poole *et al.* 1988, Schiebel *et al.* 1989) and in *Haemophilus influenzae*, two high-molecular-weight proteins (HMW-1 and HMW-2) mediate attachment to epithelial cells (St Geme *et al.* 1993). No TpsA proteins exist in laboratory *E. coli* K-12 strains, but in uropathogenic *E. coli*, where CdiA mediates contact-dependent growth inhibition to other bacteria (Aoki *et al.* 2005). Despite fulfilling important virulence functions, TPS systems also exist in non-pathogenic bacteria, where they are generally involved in attachment between bacteria and interactions of bacteria with their environment (Jacob-Dubuisson *et al.* 2013), but those TPS systems are less well studied.

TpsA proteins share an N-terminal TPS domain as the most conserved region. It has a length of around 250 amino acids and is located directly behind the signal sequence. The TPS domain is necessary and sufficient for recognition and transport by the respective TpsB partner (Grass and St Geme 2000, Jacob-Dubuisson *et al.* 1997, Renauld-Mongenie *et al.* 1996, Schönherr *et al.* 1993). This domain contains a conserved NPNG(I/M) motif, crucial for secretion (Hodak *et al.* 2006, Jacob-Dubuisson *et al.* 1997, Schönherr *et al.* 1993, St Geme and Grass 1998). Recognition of TpsA substrates by TpsB proteins is initially mediated via interactions of the unfolded TPS domain with the two POTRA domains of TpsB (Delattre *et al.* 2011, Hodak *et al.* 2006, Surana *et al.* 2004), presumably by β-augmentation (Jacob-Dubuisson *et al.* 2013), and after secretion of the TpsA protein through the TpsB pore (Baud *et al.* 2014), the TPS domain adopts β-helical structure like usually most of the rest of the TpsA protein (Clantin *et al.* 2004, Weaver *et al.* 2009, Yeo *et al.* 2007) (Fig. 1.7b). For some TpsA proteins, as HMW-1, the TPS domain is cleaved off after translocation of the entire protein and released to the extracellular space (Grass and St Geme 2000, van Ulsen *et al.* 2014). Many TpsA proteins also contain a C-terminal domain, which is not secreted, but tethers the protein to the membrane via interactions with the TpsB partner (Buscher *et al.* 2006, Grass and St Geme 2000, Julio and Cotter 2005). For certain TpsA proteins, like FHA, this C-terminal domain can be cleaved off and is subsequently degraded in the periplasm (Julio and Cotter 2005, Noel *et al.* 2012, van Ulsen *et al.* 2008).

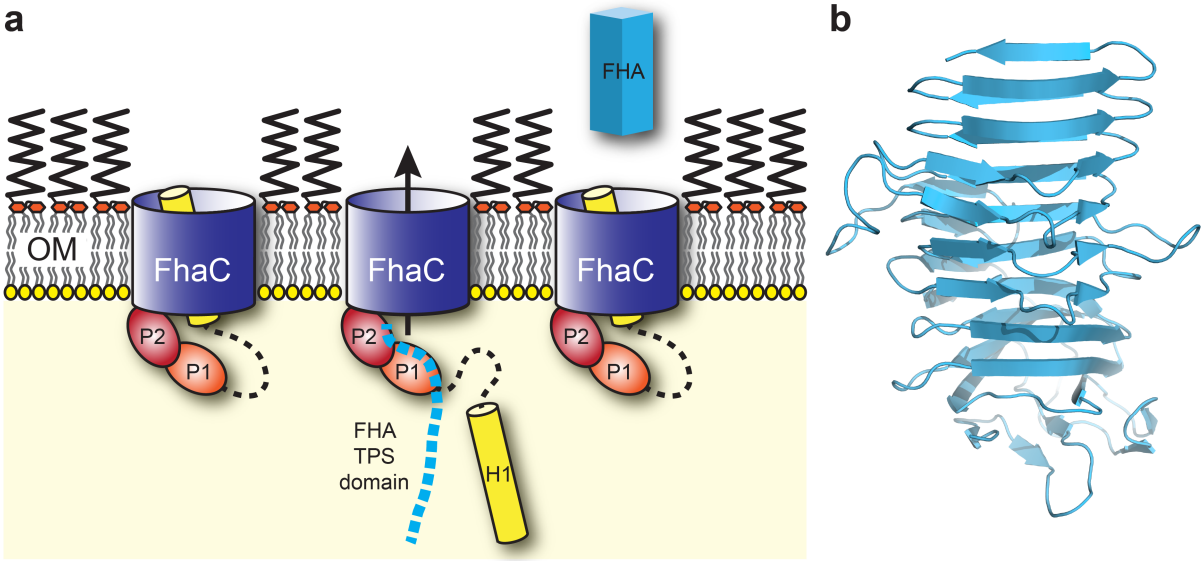

Figure 1.7 FHA translocation by FhaC and FHA TPS domain crystal structure.
(**a**) Unfolded FHA arrives at the OM, where it engages in initial interactions of its TPS domain sequence with the FhaC POTRA domains. Subsequently, the plug helix is removed from the FhaC barrel and FHA is transported to the extracellular space, where it folds. (**b**) β-helical fold of the FHA TPS domain (PDB entry 1RWR (Clantin *et al.* 2004)).

Like the BAM complex for the insertion of OMPs, TpsB proteins do not need external energy for the translocation of their TpsA substrates. *In vitro* assays demonstrated TpsA translocation into proteoliposomes containing only the corresponding TpsB transporter (Fan *et al.* 2012, Norell *et al.* 2014). The driving force for the directed translocation process is probably the initiation of folding that does not allow back diffusion. It is still under debate, how and in which direction translocation of TpsA proteins occurs. The two discussed possibilities include (i) N- to C-terminal translocation, so the TPS domain is transported first and initiates folding in the extracellular space, which gives the rest of the protein directionality in translocation, and (ii) a hairpin model, in which after recognition by the respective TpsB protein the TPS domain stays in the periplasm until the rest of the protein is threaded through the pore (Jacob-Dubuisson *et al.* 2013).

FhaC is the only TpsB protein for which the three-dimensional full-length structure has been solved (Clantin *et al.* 2007). It reveals a 16-stranded C-terminal β-barrel with two periplasmic POTRA domains and an N-terminal α-helix, which is inside the β-barrel pore. This helix is connected to the first POTRA domain via a linker (Fig. 1.8). The crystal structure conformation exemplifies a resting state of TpsB proteins (Gabel *et al.* 2014), most of which contain an N-terminal α-helix that is removed from the pore during secretion and locates to the periplasm (Guérin *et al.* 2014) (Fig. 1.7a).

A remarkable feature of Omp85 proteins in general is that they share the same overall fold with periplasmic POTRA domains and a 16-stranded membrane-embedded β-barrel, but do not share high sequence identities. However, all Omp85 proteins contain two highly conserved sequence motifs, which are (G/F)xDxG (Jacob-Dubuisson *et al.* 2013) and VRG(Y/F) (Delattre *et al.* 2010). The FhaC crystal structure reveals that the former one is located in barrel strand 13, pointing the sidechains to the inside of the barrel, approximately at half barrel height. The latter one is located at the tip of the long extracellular L6 loop, which in the structure reaches all the way through the barrel to its periplasmic rim. Despite showing the general locations of these two highly conserved motifs, the crystal structure does not suffice for the elucidation of their functional importance nor does it allow the deduction of details about the transport mechanism in general.

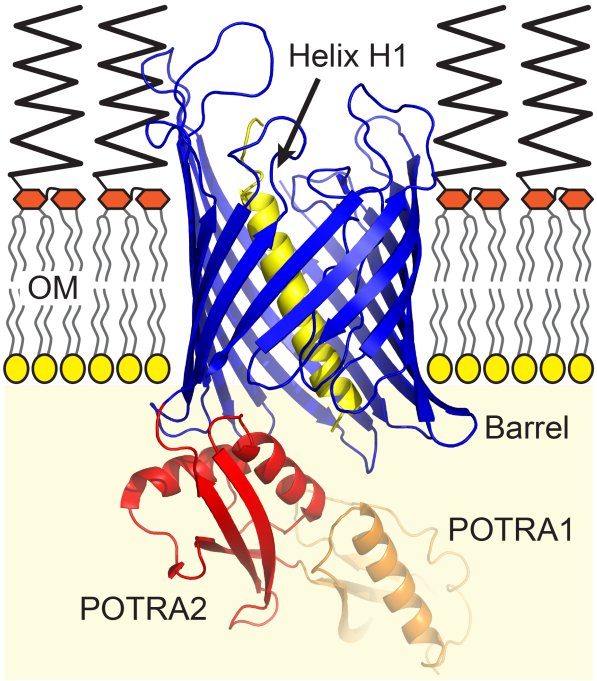

Figure 1.8 FhaC crystal structure.
The crystal structure of FhaC (PDB entry 2QDZ (Clantin *et al.* 2007)) shows the C-terminal transmembrane β-barrel (blue), POTRA domains 1 (orange) and 2 (red), and the N-terminal plug helix (yellow). The linker connecting the plug helix to POTRA1 is not resolved in the electron density.

1.10. Assembly of autotransporters by TAM

The function of the Omp85 protein TamA (Stegmeier *et al.* 2007) is less well understood. Whereas BamA is present and essential in all Gram-negative bacteria and TpsB proteins are especially but not only found in pathogenic ones and contribute to virulence (Jacob-Dubuisson *et al.* 2013), TamA is present in many but not all Gram-negative bacteria,

including pathogenic and non-pathogenic species (Heinz and Lithgow 2014, Selkrig *et al.* 2012). In contrast to BamA, TamA is non-essential in *E. coli*, but TamA deletion mutants exhibit growth defects (Stegmeier *et al.* 2007).

Its DNA usually appears in an operon together with a large protein (1259 amino acids in *E. coli*) called TamB (formerly YtfN) and thus resembles TPS systems with respect to its genomic organization. In Gammaproteobacteria, for instance in *E. coli* K-12 strains, another gene is found in this operon encoding a small cytoplasmic protein YtfP (113 amino acids in *E. coli*) with a gamma-glutamyl cyclotransferase-like fold (Aramini *et al.* 2007, Aramini *et al.* 2005), but its functional relevance remains unclear.

The structure of TamB is unknown. An N-terminal stretch of approx. 10 hydrophobic amino acids, included in the signal sequence, which is initially not cleaved, most likely forms a transmembrane helix, traversing the IM (Selkrig *et al.* 2012). There are also two domains annotated as members of the AsmA_2 superfamily in the NCBI database. One of the domains constitutes the C-terminal 336 residues of TamB and is additionally annotated as a DUF490 domain. The other AsmA_2 domain has a length of only 179 residues and ends 27 residues before the C-terminal AsmA_2 domain starts. AsmA proteins, however, are structurally not characterized and are inconsistently described to be located either in the IM and to be involved in LPS biogenesis in *E. coli* (Deng and Misra 1996) or in the OM and to contribute to virulence in *Salmonella* (Prieto *et al.* 2009). In general, a large part of the TamB structure is predicted to adopt β-helical structure like TpsA proteins. Noteworthy, the very C-terminus of TamB resembles a β-signal that is usually found in the last transmembrane β-strand of OMPs (Struyvé *et al.* 1991), but TamB is not predicted to include a transmembrane β-barrel.

In comparison to BamA and TpsB proteins, which have five and two POTRA domains, respectively, TamA contains three POTRAs (Stegmeier *et al.* 2007) and like BamA lacks an N-terminal plug-helix (Fig. 1.9a). On the one hand, TamA and TamB are genomically organized similar as TPS systems and TamB shares structural features with TpsA proteins, on the other hand, TamA shares higher sequence similarity to BamA than to TpsB proteins (Selkrig *et al.* 2012) and since crucial sequence motifs indicating a TPS domain are missing, TamB is clearly no TpsA protein.

Instead of being translocase and substrate, TamA and TamB were shown to interact with each other and to be involved in the biogenesis of a subgroup of special OMPs called autotransporters (ATs), including Ag43 in *E. coli* (Selkrig *et al.* 2012). These proteins are classified as type 5a secretion systems (T5aSS) (Leo *et al.* 2012) and contain a 12-stranded C-terminal membrane-embedded β-barrel (Oomen *et al.* 2004) and an often large N-terminal extracellular passenger domain. This domain is for most ATs of β-helical structure, just like TpsA proteins (Kajava and Steven 2006, van Ulsen *et al.* 2014). Structurally, ATs can

therefore be seen as a fusion of an OMP, whose membrane integration usually depends on the BAM complex, and a TpsA protein, whose translocation depends on a conjugate TpsB protein. AT passenger domains can mediate diverse functions, which are in general similar to TpsA proteins, since they often contribute to virulence, work as proteases and mediate cell adhesion (van Ulsen *et al.* 2014).

The name autotransporter derives from the initial idea that first the barrel of an AT is integrated into the OM and then the unfolded extracellular domain threads through the barrel without the need of other cofactors (Henderson *et al.* 1998, Pohlner *et al.* 1987). After completion, the extracellular domain is folded and connected to the first strand of the barrel at the periplasmic side via an α-helical linker through the barrel as can be seen in the full-length crystal structure of an autotransporter (van den Berg 2010). For many autotransporters, this linker is subsequently autocatalytically cleaved within the barrel pore to release the passenger domain to the extracellular space (van Ulsen *et al.* 2014).

The mechanism of autotransporter assembly has been controversially discussed (Bernstein 2007), as engineered folded secondary structure elements can be transported as well, for which the 12-stranded autotransporter barrel is actually too narrow (Jong *et al.* 2007, Skillman *et al.* 2005). Moreover, barrel integration and passenger domain translocation appear to be coupled processes (Pavlova *et al.* 2013) and some AT proteins could be crosslinked to BamA *in vivo* (Ieva and Bernstein 2009, Ieva *et al.* 2011, Sauri *et al.* 2009). Therefore, it seems that in T5aSS, ATs depend on the Omp85 proteins BamA or TamA for their OM barrel integration and passenger domain translocation (Figure 1.9b), whereas in T5bSS/TPS passenger domain-like TpsA proteins depend on a specific Omp85 TpsB partner protein for translocation.

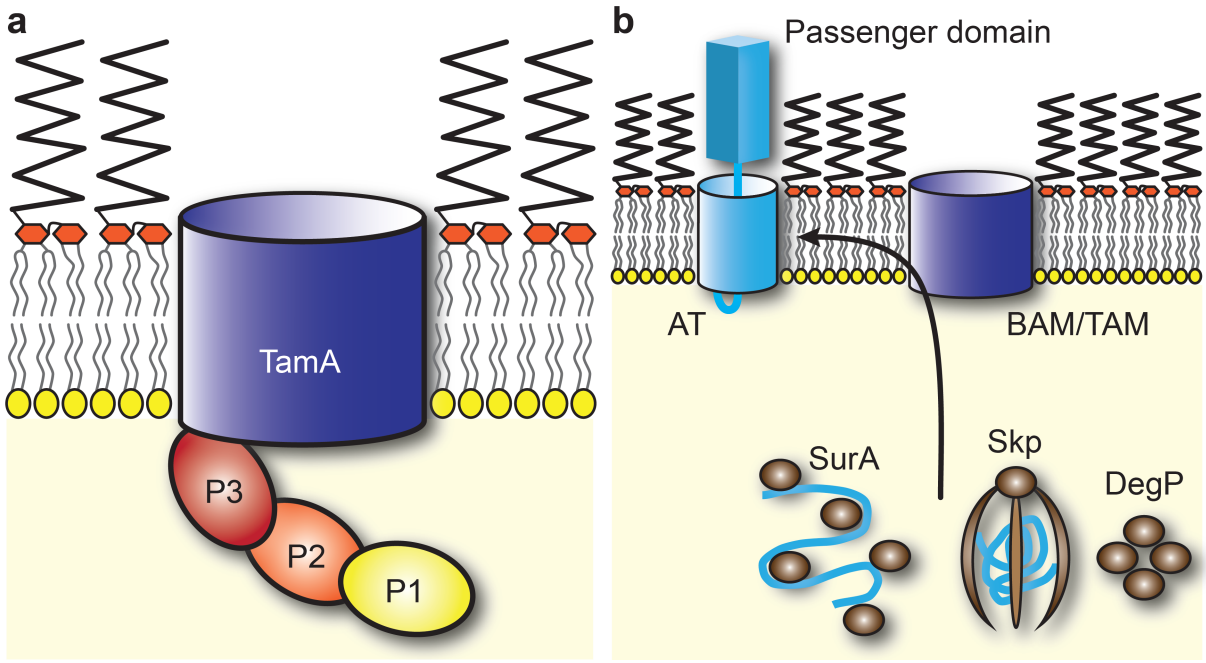

Figure 1.9 Schematic representation of TamA and autotransporter assembly.
(**a**) TamA consists of three N-terminal POTRA domains (yellow – orange – red) and a transmembrane β-barrel (blue). (**b**) Autotransporters are like other OMPs guided to the OM by SurA or Skp/DegP and then processed by the BAM or TAM complex for assembly into the OM.

1.11. Translocation and assembly of proteins in outer membranes of mitochondria and chloroplasts

In eukaryotic cells, proteins homologous to bacterial Omp85 proteins can be found as well. They are located in the outer membranes of mitochondria and chloroplasts (Jacob-Dubuisson *et al.* 2013), which are the organelles that derive from endosymbiosis (Keeling 2010, Kutschera and Niklas 2005, Timmis *et al.* 2004). This observation shows that Omp85 proteins have been functionally conserved over billions of years.

In the chloroplast outer envelope membrane (OEM), several Omp85 proteins can be found, some of which do not possess POTRA domains and have yet unknown functions (Hsueh *et al.* 2014, Nicolaisen *et al.* 2015). The essential Omp85 proteins Toc75-III and OEP80 (also called Toc75-V), however, contain three POTRA domains and are involved in translocation of nucleus-encoded proteins that are destined for one of the several chloroplast compartments, and probably in OMP insertion into the OEM. Whereas Toc75-III was shown to mediate the former task as part of the TOC complex together with the receptors Toc159 and Toc34 (Paila *et al.* 2015, Schnell *et al.* 1994, Tranel *et al.* 1995, Walther *et al.* 2009), OEP80 is believed to mediate the latter (Eckart *et al.* 2002, Hsu *et al.* 2008, Paila *et al.*

2015). As more than 95% of chloroplast proteins are encoded in the nucleus and translated in the cytosol, the protein import routes into this organelle are of essential importance.

Imported chloroplast proteins that are not OMPs usually contain an N-terminal targeting sequence, called transit peptide, which first directs them across the OEM and then to their final subcompartment within the chloroplast (Paila *et al.* 2015). Chloroplast OMPs usually do not contain this signal, but instead intrinsic targeting signals to be sorted to the OEM (Shi and Theg 2013). There is only one exception: the translocase Toc75-III itself. Its N-terminal transit peptide directs the protein not only across the OEM to the intermembrane space (IMS), the equivalent of the bacterial periplasm, but even further across the inner envelope membrane (IEM). There, it is cleaved off before the rest of the protein is released to the IMS, from where it is then probably integrated into the OEM (Tranel and Keegstra 1996, Ulrich and Rapaport 2015).

Interestingly, the orientation of the Omp85 proteins may have inversed as compared to bacterial homologues: the POTRA domains seem to face the cytosol instead of the IMS (Sommer *et al.* 2011), but controversial results about the topology exist (Sveshnikova *et al.* 2000). For Toc75-III an inversion would make sense from a mechanistic point of view, as the transportation direction of its substrates is inversed as compared to TpsA proteins. For β-barrel insertion however, in regard to the import route of Toc75-III, this would suggest that OMPs are inserted into the membrane from the side of the Omp85 proteins that does not contain the POTRA domains, in contrast to bacterial Omp85 insertases. However, since OMP biogenesis in chloroplasts is not yet well investigated, more research needs to be conducted before mechanistic conclusions can be drawn (Fig. 1.10a).

Similar as for chloroplasts, most mitochondrial proteins (approx. 99%) are encoded in the nucleus and post-translationally imported. They usually contain an N-terminal sorting signal, called presequence, but some proteins like OMPs contain intrinsic targeting signals instead (Höhr *et al.* 2015). For the insertion of OMPs into the outer mitochondrial membrane (OMM) a mitochondrial Omp85 protein exists, called Sam50 (or Tob55), which forms a complex with the proteins Sam35 and Sam37 (Gentle *et al.* 2004, Milenkovic *et al.* 2004, Neupert and Herrmann 2007, Paschen *et al.* 2003, Pfanner *et al.* 2004, Walther *et al.* 2009, Wiedemann *et al.* 2003). The latter two proteins are embedded in the OMM via a single α-helix and contain cytosolic domains. The SAM complex can be seen as the mitochondrial pendant of the BAM complex; it assembles OMPs that were imported from the cytosol in an unfolded state to the IMS between OMM and inner mitochondrial membrane (IMM). The single POTRA domain of Sam50 is located in the IMS, and therefore Sam50 has the same orientation in the membrane and towards substrates as Omp85 proteins in Gram-negative bacteria (Paschen *et al.* 2003). The other subunits Sam35 and Sam37 cannot be compared to any of the BAM complex subunits, as their soluble parts are located in the cytosol rather

than the IMS. Nevertheless, the essential Sam35 was shown to interact with C-terminal β-signals of OMP substrates (Chan and Lithgow 2008, Kutik *et al.* 2008), which also *e.g.* the BamD subunit in the BAM complex does. The function of the non-essential Sam37 involves release of an OMP substrate into the membrane (Chan and Lithgow 2008).

In mitochondria the OMP integration is done by a complex containing an Omp85 protein, but the protein import, in contrast to chloroplasts, is performed by a different protein complex, called the TOM (translocase of outer mitochondrial membrane) with its β-barrel pore formed by Tom40 (Chacinska *et al.* 2009, Hill *et al.* 1998, Suzuki *et al.* 2004, Vestweber *et al.* 1989). Like the homologous OMM protein VDAC (Hiller *et al.* 2008), Tom40 contains 19 β-strands (Gessmann *et al.* 2011, Lackey *et al.* 2014), but its structure has not been determined.

Tom40 does not contain POTRA domains, but an N-terminal α-helical region and forms a complex with six other proteins: the small proteins Tom5, Tom6, Tom7 belong to the TOM core and presumably have a stabilizing function and Tom20, Tom22 and Tom70 are associated receptors (Ahting *et al.* 1999, Kato and Mihara 2008, Künkele *et al.* 1998, Model *et al.* 2002, Schmitt *et al.* 2005). These proteins are embedded in the OMM via a single-pass α-helix and contain cytosolic domains, Tom22 and Tom7 in addition possess small IMS domains. Tom20 and Tom22 recognize the N-terminal presequences of substrates (Brix *et al.* 1997, Mayer *et al.* 1995, Yamamoto *et al.* 2011). Those sequences usually have a length of 15 to 50 residues, are positively charged and form an amphipathic α-helix (Neupert and Herrmann 2007, Schmidt *et al.* 2010). Tom70 with its tetratricopeptide repeats preferably recognizes substrates with intrinsic sorting signals like OMPs (Brix *et al.* 1997, Neupert and Herrmann 2007). The import mechanism is not understood in detail, but usually proteins are translocated in N- to C-terminal direction and it is thought that affinities for the substrates increase from the cytosolic parts of the receptors across the Tom40 pore to the IMS exposed domains, which thus directs the translocation through the OMM (Neupert and Herrmann 2007). Depending on the final destination of the imported protein, which may be the OMM, the IMS, the IMM or the inner matrix, further processing differs. For the insertion of β-barrel OMPs into the OMM, the substrates are handed over to the SAM complex (Neupert and Herrmann 2007, Schmidt *et al.* 2010, Wiedemann *et al.* 2003) (Fig. 1.10b).

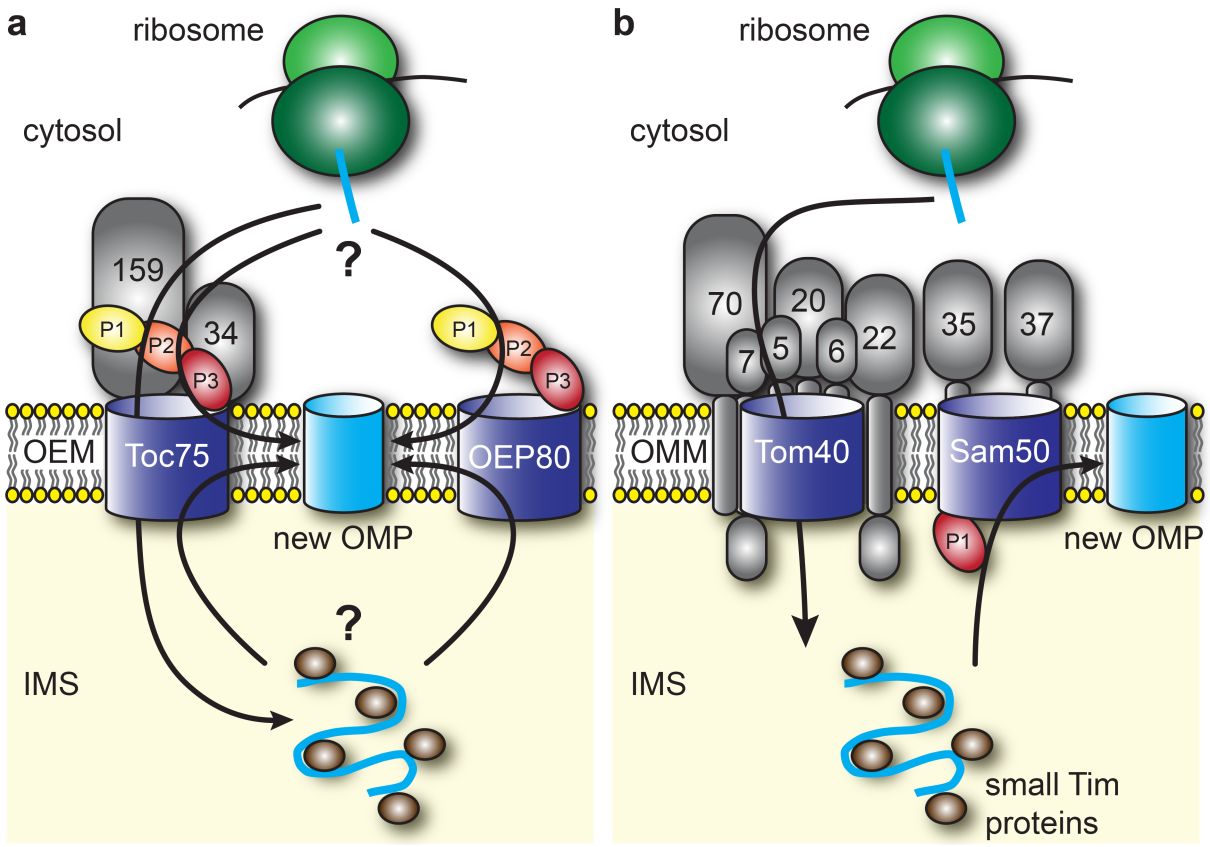

Figure 1.10 OMP biogenesis in mitochondria and chloroplasts.
(**a**) Chloroplast proteins are imported from the cytosol across the OEM via the TOC complex containing the Omp85 protein Toc75-III and the receptors Toc159 and Toc34. Assembly of β-barrels into the OEM has remained elusive but possibly involves the Omp85 protein OEP80. (**b**) Mitochondrial proteins are translocated from the cytosol across the OMM via the TOM complex containing the β-barrel protein Tom40, the receptors Tom70, Tom22 and Tom20 and the small subunits Tom5, Tom6 and Tom7. Mitochondrial OMPs are inserted from the IMS into the OMM by the SAM complex containing the Omp85 protein Sam50 and the subunits Sam35 and Sam37.

1.12. Aims of the thesis

For translocation of protein substrates across the outer membranes of Gram-negative bacteria, mitochondria and chloroplasts, and for the insertion of β-barrels into these membranes, the general protein complexes and their components have been identified. However, the underlying translocation and insertion mechanisms have remained enigmatic, even though for the BAM complex structures of all complex members except for the barrel of the insertase BamA itself have been solved. Moreover, even the full-length structure of the translocase FhaC has not been able to suffice for the deduction of a *bona fide* translocation mechanism. Since translocation and insertion are two distinct processes, it has not been clear whether they share a common mechanistic basis, even though TpsB translocases and

the central components of the other translocation and insertion complexes, except for Tom40, all belong to one superfamily of proteins. All these Omp85 proteins share the same principle architecture and therefore an evolutionary conserved common mechanistic basis for both insertion and translocation may exist.

The general aim of my thesis was therefore to gain insights into insertion and translocation mechanisms at outer membranes. The newly discovered TAM complex is specialized in autotransporter assembly, which in essence is a coupled insertion and translocation process. Furthermore, as compared to the BAM complex, its architecture is relatively simple as the TAM most probably consists of only two subunits: the Omp85 protein TamA and the IM-associated protein TamB. Thus, TamA is an ideal target to reveal insights into Omp85-mediated translocation and insertion mechanisms at outer membranes. The first goal was therefore the structure determination at the atomic level. Knowledge of the structure is a good basis for the design of further experiments to answer mechanistic questions. It also provides a comparison with the existing structure of the translocase FhaC, yielding insights into common structural and mechanistic principles.

The structure determination of TamA by X-ray crystallography is described in Chapter 2. It provides a structural basis for the deduction of a mechanism for the complex assembly of OMP autotransporter proteins. In a simplified version this mechanism can also hold true for OMP assembly in general. This chapter is reproduced from the publication “The structural basis of autotransporter translocation by TamA” (Gruss F, Zähringer F, Jakob RP, Burmann BM, Hiller S, Maier T, *Nat Struct Mol Biol*, 2013).

Chapter 3 provides a step-by-step protocol for TamA production and crystallization as well as a general protocol for seeding in lipid phase membrane protein crystallization, exemplified for TamA. This chapter is reproduced from the publication “Purification and bicelle crystallization for structure determination of the *E. coli* outer membrane protein TamA” (Gruss F, Hiller S, Maier T, *Methods Mol Biol*, 2015, in press).

Chapter 4 describes production and purification of the large TamA complex partner TamB in full-length. In addition, *in vitro* binding experiments using analytical size exclusion chromatography (SEC) and isothermal titration calorimetry (ITC) for TamB in combination with different TamA POTRA domain constructs are demonstrated and yield complementary information to published data about TamA – TamB interactions. Furthermore, a bioinformatics analysis of co-evolved residue pairs between TamA and TamB allows the mapping of the binding site of TamB at the TamA POTRA domains and reveals an additional binding site at the TamA barrel. The experimental work and bioinformatics were done by myself.

The structural results from these chapters and the deduced mechanisms are generally consistent with the simultaneously published crystal structure of the general OMP insertase

BamA (Noinaj *et al.* 2013). However, important structural features in these two proteins, involving the two most conserved regions in Omp85 proteins in general, are inconsistent with the previously published crystal structure of the translocase FhaC (Clantin *et al.* 2007).

Therefore, in Chapter 5 the determination of the crystal structure of an FhaC variant defective in substrate recognition is described. The determined crystal structure has better resolution and higher quality than the previously determined FhaC wild-type crystal structure. The results reveal that the previous model of wild-type FhaC is mistraced in the most highly conserved region within Omp85 proteins. The corrected structure is generally consistent with the structures of TamA and BamA and therefore a common structural basis for insertion and translocation mechanisms of Omp85 proteins is demonstrated. In addition, the FhaC variant structure reveals insights into substrate recognition mechanisms. This chapter is reproduced from the publication “Conserved Omp85 lid-lock structure and substrate recognition in FhaC” (Maier T, Clantin B, Gruss F, Dewitte F, Delattre AS, Jacob-Dubuisson F, Hiller S, Villeret V, *Nat Commun*, 2015)

Chapter 6 delineates inclusion body expression, purification and refolding of human Tom40 for the preparation of samples for NMR spectroscopy. Whereas functionally refolded Tom40 has been described on a single molecule level, it has so far resisted structure determination via NMR spectroscopy or X-ray crystallography. The majority of Tom40 molecules in the NMR samples within this work form micro-aggregates, as evaluated from SEC chromatograms. Consequently, the obtained NMR spectra show low signal intensity in comparison to equivalently prepared VDAC samples. However, the data demonstrate that folded Tom40 can be obtained in macroscopic amounts, and therefore can be used as a basis for further sample optimization towards crystallization or NMR structure determination. The protein expression, purification and NMR spectroscopy experiments were done by myself.

CHAPTER 2:

The Structural Basis of Autotransporter Translocation by TamA

Reproduced from:

Nature Structural and Molecular Biology, 20(11):1318-1320; November 2013
The structural basis of autotransporter translocation by TamA.
Fabian Gruss, Franziska Zähringer, Roman P. Jakob, Björn M. Burmann, Sebastian Hiller, and Timm Maier
Epub September, 22nd 2013
DOI 10.1038/nsmb.2689

2.1. Abstract

TamA is an *Escherichia coli* Omp85 protein involved in autotransporter biogenesis. It comprises a 16-stranded transmembrane β-barrel and three POTRA domains. The 2.3 Å crystal structure reveals that the TamA barrel is closed at the extracellular face by a conserved lid loop. The C-terminal β-strand of the barrel forms an unusual inward kink, which weakens the lateral barrel wall and creates a gate for substrate access to the lipid bilayer.

2.2. Introduction

Proteins of the Omp85 superfamily are responsible for the insertion of β-barrel outer membrane proteins (OMPs) and the translocation of protein substrates across the outer membrane in bacteria, mitochondria and plastids (Chacinska *et al.* 2009, Fan *et al.* 2012, Kim *et al.* 2007, Walther *et al.* 2009). The membrane protein–biogenesis subclass of Omp85 proteins catalyzes the insertion and folding of β-barrel OMPs and autotransporters, and this subclass includes bacterial BamA and mitochondrial Sam50 (Hagan *et al.* 2011, Wiedemann *et al.* 2003). A second subclass of Omp85 proteins includes bacterial two-partner secretion systems that translocate a specific partner protein across the outer membrane (Jacob-Dubuisson *et al.* 2013). A well-characterized member of this subclass is FhaC (Clantin *et al.* 2007). The 65-kDa *Escherichia coli* protein TamA is an Omp85 superfamily protein, which is evolutionarily more closely related to BamA than to FhaC (Supplementary Fig. 2.1) (Selkrig *et al.* 2012, Stegmeier *et al.* 2007). Although most autotransporters are processed by BamA, TamA has recently been implicated in passenger-domain translocation of a subset of autotransporters, but structural and mechanistic details of this function are unknown (Selkrig *et al.* 2012). Remarkably, TamA is the closest bacterial homolog of eukaryotic Tom40, which forms the functional pore of the mitochondrial translocase of the outer membrane (Pusnik *et al.* 2011, Vestweber *et al.* 1989).

2.3. Results and Discussion

To analyze how TamA contributes to the translocation of passenger domains, we determined the structure of full-length TamA, crystallized from bicelle solution, at 2.25 Å resolution (Supplementary Table 2.1). TamA comprises three N-terminal periplasmic polypeptide transport–associated (POTRA) domains (aa 22–264) followed by a 16-stranded membrane-integral β-barrel (aa 265–577) (Fig. 2.1a). We also separately determined the structure of a soluble fragment of TamA consisting of the three POTRA domains and the N-terminal strand of the TamA β-barrel at 1.9 Å resolution (Supplementary Table 2.1).

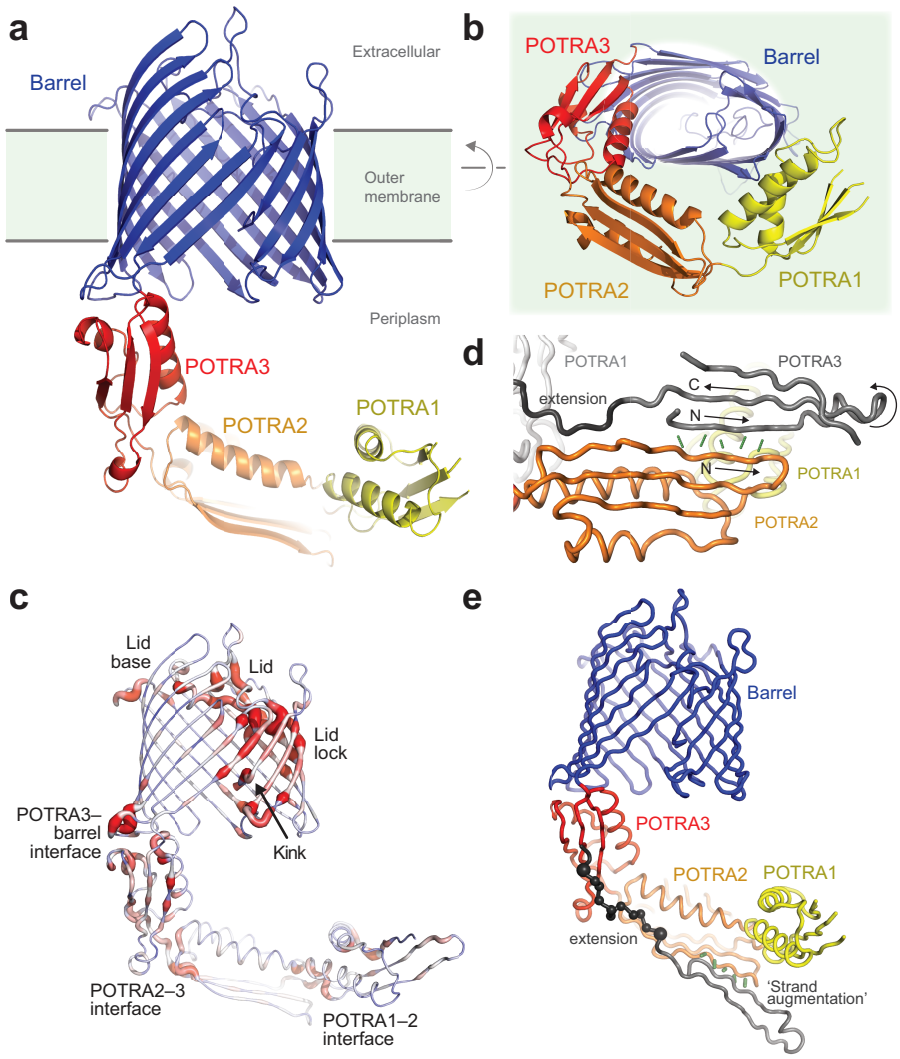

Figure 2.1 TamA structure and interactions of its POTRA domains.
(**a**) Structure of TamA in ribbon representation. TamA comprises a C-terminal 16-stranded β-barrel (blue) in the outer membrane and the periplasmic N-terminal POTRA domains 1–3 (yellow, orange and red). (**b**) View from the periplasm. (**c**) Conservation between TamA and BamA, indicated by cartoon representation (thin and blue, low conservation; thick and red, high conservation). (**d**) β-augmentation between POTRA2 (orange) and POTRA3 of a symmetry-related molecule (grey). (**e**) Part of the POTRA1–3 crystal structure positioned onto full-length TamA on the basis of the observed β-augmentation mode.

The POTRA domains in full-length TamA wind ~50 Å in the periplasmic direction, away from their barrel-attachment site, in a C-shaped arrangement (Fig. 2.1b). The three domains adopt the same spatial organization in the isolated TamA POTRA1–3 fragment and in full-length TamA, stabilized by substantial interdomain contacts (Supplementary Fig. 2.2). In comparison, the relative orientations of BamA POTRA3–4 and POTRA4–5 in the available fragment structures (Gatzeva-Topalova *et al.* 2010, Kim *et al.* 2007) reconstitute a similar C-shaped arrangement (Supplementary Fig. 2.2), and the corresponding interface regions

are conserved between BamA and TamA (Fig. 2.1c). The functional role of Omp85 POTRA domains is presumably the initial recognition of substrates mediated by β-strand augmentation, both in two-partner secretion and insertion of β-barrel membrane proteins, as evidenced biochemically for FhaC (Delattre *et al.* 2011) and in crystal structures of BamA POTRA domains (Kim *et al.* 2007), respectively. In the crystal structure of the soluble TamA fragment, an intermolecular β-strand augmentation is observed between POTRA domains 2 and 3 (Fig. 2.1d). This interaction mode would position an extended substrate intermediate toward POTRA3 and the periplasmic face of the TamA barrel (Fig. 2.1e). These results suggest that both BamA and TamA can use similar β-strand-augmentation mechanisms to presumably guide unfolded substrate proteins from the periplasmic space toward the barrel.

All Omp85 proteins feature a C-terminal 16-stranded β-barrel as a central structural element. The TamA β-barrel has a pronounced kidney shape with cross-section dimensions of 45 Å x 25 Å. At its periplasmic face, it is partly occluded by turns T4 and T5 (Supplementary Fig. 2.3) opposite the POTRA-domain attachment site; the remaining opening has a diameter of 15 Å x 18 Å. The extracellular face is completely closed by a large lid formed by the 40-residue loop L6 (aa 456–495), such that a central hydrophilic cavity of ~23 Å depth is formed (Fig. 2.2a–c). The irregular structure of the lid loop is stabilized by the two consecutive conserved proline residues near the lid base, Pro463 and Pro464, and by multiple specific polar and hydrophobic interactions between conserved side chains and the barrel wall. The contact between the lid tip and the barrel wall is formed by two sequence motifs that are highly conserved in the entire Omp85 family (Delattre *et al.* 2010): Arg477 from the (I/V)RG(Y/F) motif (residues 476–479) in the L6 lid engages in a salt bridge with Asp521 and forms cation-π interactions with Phe519 from the (F/G)xDxG motif (residues 519–523) in the barrel wall on strand 13. In addition, Glu505 of strand 12, Arg543 of strand 14 and Asp554 of strand 15 are engaged in a salt-bridge network around the tip of the lid (Fig. 2.2c). Intriguingly, the two sequence motifs are not in close contact in the FhaC structure, but their direct interaction observed here explains their evolutionary co-conservation and highlights the resulting ‘lid lock’ as a structural feature of central importance.

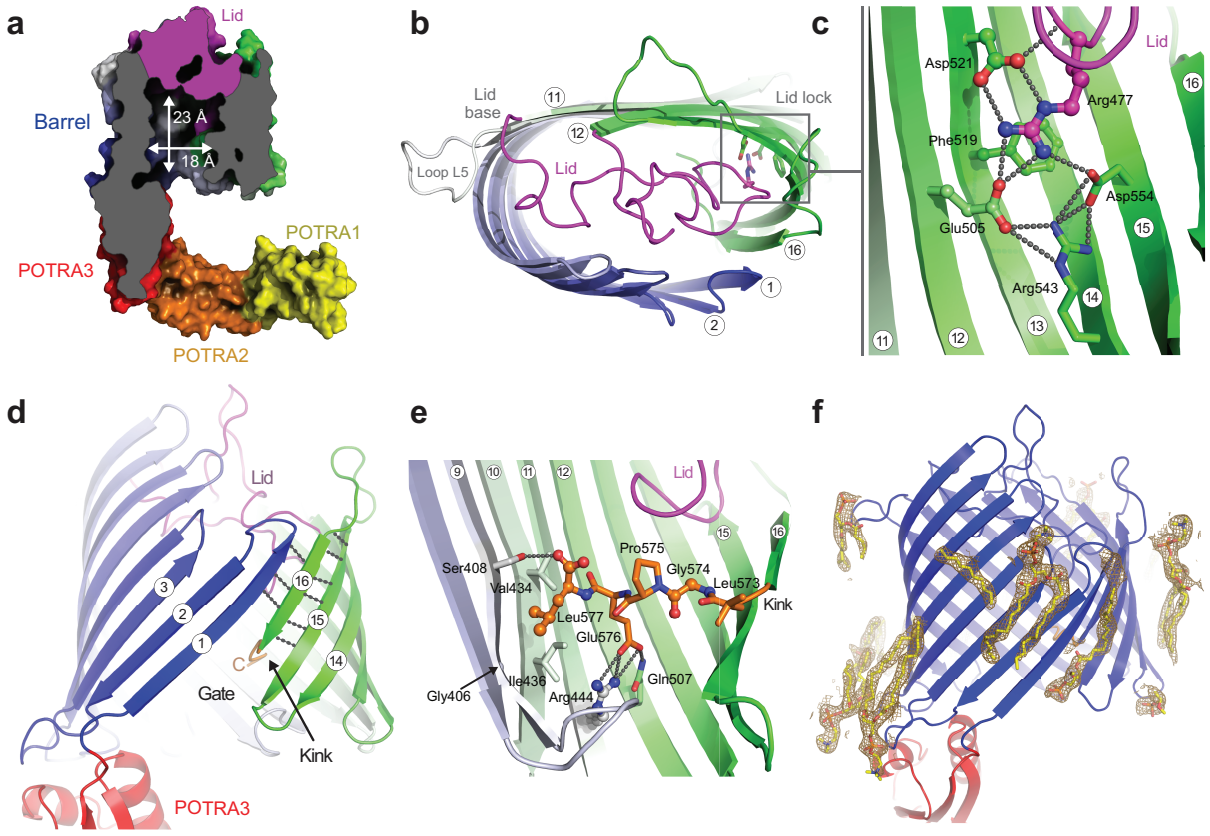

Figure 2.2 The closed lid and the lateral gate of TamA.
(**a**) Cross-sectional view. Loop L6 (magenta) acts as a lid at the extracellular face (coloring as in Fig. 2.1 but with blue-white-green color gradient from N- to C-terminus for the barrel). (**b**) Top view of TamA. The lid folds into an irregular structure spanning the full barrel diameter. (**c**) Close-up view of the lid lock region. Conserved residues are shown as sticks and highly conserved residues additionally with spheres. (**d**) Side view of the TamA structure. The C-terminus (orange) of TamA kinks into the barrel, creating a gate to the lipid phase and a weak interstrand contact between strands 16 and 1. (**e**) Close-up view of the C-terminal segment and part of the TamA barrel. Spheres denote highly conserved residues. (**f**) Structure of TamA in ribbon representation. Additional $2F_o–F_c$ electron density map is shown at 1σ contour level around lipid molecules modeled as 1,2-dimyristoyl-sn-glycero-3-phosphocholine (DMPC) fragments (stick representation).

A second highly unusual structural feature is located at the C-terminal strand 16 of the TamA barrel. This strand is not fully zipped up to strand 1 but forms an inward kink in the vicinity of the conserved lid lock (Fig. 2.2d). The kink is initiated with the highly conserved Gly574 and stabilized by a salt bridge between Glu576 and the conserved Arg444 of strand 11. The conserved Gly406 creates space for accommodating the terminal hydrophobic Leu577, and the hydroxyl group of Ser408 contacts the C-terminal carboxylate (Fig. 2.2e). As a consequence of the kink, strands 1 and 16 form a particular weak β-strand pair, with only three main chain hydrogen bonds between them, and a cleft opens between the periplasmic

ends of strands 1 and 15, near the POTRA3–barrel attachment site. In the crystal, electron density probably representing a lipid head group is observed in this cleft, thus suggesting that the cleft acts as an access gate for TamA substrates to the hydrophobic membrane phase (Fig. 2.2f).

Autotransporter biogenesis comprises two coupled events: insertion of the autotransporter β-barrel into the membrane and translocation of the passenger domain into the extracellular space (Pavlova *et al.* 2013). TamA has been implicated in translocation of the passenger domains of a subset of bacterial autotransporters (Selkrig *et al.* 2012). Substrate translocation across the outer membrane by Omp85 proteins has been well studied for FhaC with its soluble substrate protein FHA. Thereby, FhaC is able to translocate its substrate in the absence of any other proteins, thus indicating that the FhaC barrel forms the functional pore (Fan *et al.* 2012), although in the FhaC crystal structure this pore is blocked by the L6 loop (Clantin *et al.* 2007). TamA and FhaC share key conserved structural elements in the barrel domain, including the (I/V)RG(Y/F) and (F/G)xDxG motifs. They both use L6 for barrel closure, although it adopts somewhat different conformations in the two structures. Because the passenger domains of autotransporters are structurally similar to FHA, it appears most plausible that they are translocated through the central barrel pore of TamA. For translocation through FhaC, an opening of the pore is required, and indeed, conformational states with differential accessibility of L6 have been observed for FhaC, depending on its FHA substrate (Clantin *et al.* 2007, Guedin *et al.* 2000). On the basis of the conserved motifs in the L6 lid and the lock region, we assume that the TamA pore also opens during transport, and this could either be achieved by an opening of L6 itself or by structural changes creating a bypass around the lid.

Based on this model, the linker peptide that connects the passenger domain to the barrel domain in autotransporters will end up threaded through the TamA pore at the end of the translocation process. However, in the mature autotransporter, this linker segment spans the inside of the C-terminal barrel domain of the autotransporter (Pavlova *et al.* 2013, van den Berg 2010). For the resulting topology conflict, which notably also arises in autotransporter assembly by BamA, no satisfactory mechanistic solution has been found so far (Bernstein 2007, Sauri *et al.* 2012). The weak contact between strands 1 and 16 of TamA, also seen in the recently determined structure of the transmembrane domain of BamA (Noinaj *et al.* 2013), now opens the possibility for a transient lateral opening of the barrel, which would elegantly resolve this conflict. Importantly, the release of the linker from TamA must occur before completion of the autotransporter barrel assembly, because a lateral insertion into the fully assembled autotransporter barrel is unlikely. At first sight, this transfer could be achieved by diffusion of the linker segment through the lipid phase to the nearby barrel-folding intermediate. A second, intriguing possibility is a mechanism that couples passenger-

domain translocation and barrel-domain membrane insertion by using a hybrid β-barrel as an intermediate step (Fig. 2.3). In this scenario, substrate β-strands would use the gate to integrate into the TamA barrel between the loosely connected strands 1 and 16. The resulting hybrid barrel would provide a wide pore for passenger-domain translocation and would also allow a direct transfer of the linker segment to the autotransporter β-domain. Correct folding of the substrate barrel would be coordinated by the strands of TamA, which would serve as a structural template. A final fission event would separate the two barrels, release the fully assembled substrate laterally into the membrane and return TamA into its original state. Importantly, such a hybrid barrel-formation mechanism would not only explain Omp85-dependent autotransporter folding but also be compatible with Omp85-dependent OMP assembly. It could even, with slight variations, serve as a recognition mode for the large β-strand signature domains in Omp85 two-partner secretion-system substrates. The pronounced conservation of key structural features in TamA, BamA and FhaC identified here makes it tempting to speculate that lateral opening and hybrid-barrel formation could be of mechanistic relevance in the entire Omp85 family.

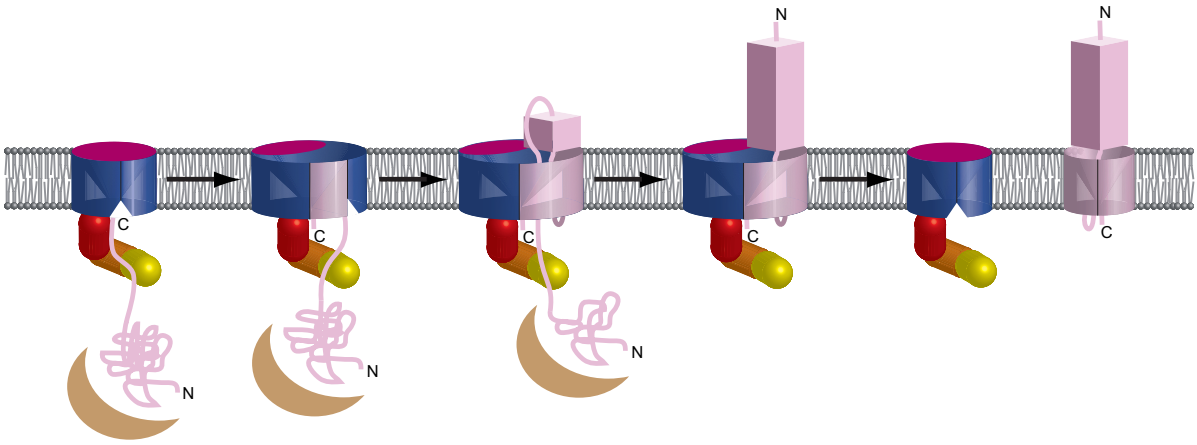

Figure 2.3 Proposed mechanism for substrate assembly through hybrid-barrel formation.
A delivery factor (brown) shuttles an unfolded autotransporter (light pink) to TamA (blue), which is closed by the L6 lid (magenta). Initial contact is made at the POTRA domains (yellow, orange and red). Subsequently, a hybrid barrel is formed by insertion of substrate β-strands through the gate region between strands 1 and 16 of the TamA barrel. Barrel expansion results in pore opening, and the passenger domain protrudes through the hybrid barrel. A fission mechanism concludes the assembly and releases the autotransporter into the membrane.

2.4. Methods

2.4.1. Plasmid construction

Full-length *E. coli* TamA was cloned into a pET22b vector (Novagen) by standard cloning methods. Briefly, the *pelB* signal sequence was removed from the pET22b vector and replaced by a *malE* signal sequence, by use of the oligonucleotides sigseq_down (5'-ATAGGAATTCCATATGAAAATAAAAACAGGTGCACGCATCCTCGCATTATCCGCATTAAC GACG-3') and sigseq_up (5'-GAGCGCATGCCATGGCGAGAGCCGAGGCGGAAAACATC ATCGTCGTTAATGCGGATAATGCGAGG-3') and the restriction enzymes NdeI and NcoI. DNA for a hexahistidine tag followed by a cleavage site for TEV protease was produced by annealing of the oligonucleotides histev_down (5'-CATGGCCCACCACCACCACCACCACG AGAATCTGTATTTCCAGGG-3') and histev_up (5'-AATTCCCTGGAAATACAGATTCTCGT GGTGGTGGTGGTGGTGGGC-3') and use of the restriction enzymes NcoI and EcoRI for insertion into the vector. Genomic *tamA* DNA from *E. coli* DH10β lacking the signal sequence–encoding nucleotides 1–63 and containing the stop codon was amplified by PCR with the oligonucleotides tama_down (5'-GGAATTCAAGCGAACGTCCGTCTACAGGTCG -3') and tama_up (5'-CCGCTCGAGTCATAATTCTGGCCCCAGACCGATG-3'), and the restriction enzymes EcoRI and XhoI were used to yield a plasmid for overexpression of full-length TamA. For the expression of a construct comprising the three POTRA domains of TamA and the residues corresponding to the first strand of the β-barrel (aa 22–275), the gene fragment was PCR amplified from *E. coli* K12 and cloned into the expression plasmid pET29a through the NdeI and XhoI restriction sites, thus linking the protein to a C-terminal hexahistidine tag.

2.4.2. Expression and purification

Chemically competent *E. coli* BL21(λ DE3)-omp3 cells were transformed with the TamA expression plasmid. After growth of cells in LB medium at 37 °C to an OD_{600} of 0.8, the temperature was decreased to 20 °C. After 2 h, expression of TamA was induced by addition of 0.1 mM IPTG. Expression continued overnight before cells were harvested, resuspended in 25 mM NaPi, pH 7.5, and 150 mM NaCl and lysed.

Unbroken cells and cell debris were pelleted for 10 min at 10,000*g*, and the supernatant containing membrane vesicles was centrifuged for 1 h at 100,000*g*. The membrane pellet was resuspended in 25 mM NaPi, pH 7.5, 150 mM NaCl and 3% β-OG. The insoluble fraction was pelleted for 1 h at 100,000*g* and 4 °C, and the supernatant containing solubilized TamA was used for all further procedures. Further purification steps were performed at room temperature.

Solubilized TamA including 10 mM imidazole was loaded onto a HisTrap FF column (GE

Healthcare), washed with 25 mM NaPi, pH 7.5, 150 mM NaCl, 0.8% β-OG and 10 mM imidazole, and eluted with a gradient from 10 mM to 500 mM imidazole. Eluted TamA fractions were pooled and diluted 1:3 with 25 mM NaPi, pH 7.0, and 0.8% β-OG before being loaded onto a MacroPrep High S (Bio-Rad) column. After the column was washed with 25 mM NaPi, pH 7.0, 50 mM NaCl and 0.8% β-OG, the protein was eluted with a gradient from 50 mM to 1 M NaCl in the same buffer. Eluted TamA fractions were pooled. For overnight digest at 15 °C with TEV protease, 5 mM β-mercaptoethanol was added to the protein solution. Digested protein was subjected again to a HisTrap FF column, and the flow through containing cleaved protein without His6-tag or His6-tagged TEV protease was concentrated in Amicon Ultra units (Millipore). TamA was gel-filtered on a Superdex 75 column (GE Healthcare) in 25 mM NaPi, pH 7.5, 150 mM NaCl and 0.8% β-OG, and eluted TamA fractions were analyzed by SDS-PAGE, pooled and concentrated to 12.5–25 mg mL^{-1}. Purified TamA was dialyzed overnight at 10 °C in 3.5-kDa-cutoff Slide-A-Lyzer cassettes (Pierce) against 80 mL 20 mM Tris-HCl, pH 7.5, 150 mM NaCl and 0.8% β-OG and again for 5 h against fresh buffer. Finally, the protein concentration was set to 12.5 mg mL^{-1} with dialysis buffer. The sample used for crystallization contained 2% β-OG, as determined by NMR spectroscopy. TamA yields were ~0.4 mg purified protein per 1 L culture.

The construct of the three TamA POTRA domains was overproduced in *E. coli* BL21(λ DE3) pRIL pL1SL2 (Betancor *et al.* 2008). After growth of cells in Terrific broth medium at 37 °C to an OD_{600} of 1, temperature was decreased to 20 °C, and protein expression was induced by the addition 0.1 mM IPTG overnight. After lysis in 50 mM HEPES, pH 7.4, 500 mM NaCl and 40 mM imidazole, the lysate was centrifuged and the protein in the supernatant purified by metal-chelate affinity (elution with 250 mM imidazole) and size-exclusion chromatography in 20 mM HEPES, pH 7.4, 250 mM NaCl, 5% glycerol and 5 mM DTT on a Superdex 75 column (GE Healthcare). The protein-containing fractions were pooled and concentrated in Amicon Ultra units (Millipore). Yields were ~20 mg purified protein per 1 L culture.

2.4.3. Crystallization

Crystallization of TamA was performed in bicelles composed of DMPC and CHAPSO. The bicelle stock solution consisted of 40% (w/w) bicelle mixture in H_2O with a molar ratio of DMPC to CHAPSO of 2.43:1. TamA was mixed 4:1 with the bicelle stock solution and incubated for at least half an hour at 4 °C before crystallization drops were set up with the sitting-drop method with a ratio of protein solution to reservoir of 1:2. After incubation at 4 °C for 5–10 min, the crystallization plates were transferred to 20 °C. Initial plate-like crystals were obtained in 0.1 M imidazole, pH 6, and 0.6 M sodium acetate after one week and used

for seed stock preparation. Well-diffracting plate-like crystals were obtained in 0.1 M imidazole and 1.2 M sodium acetate with the following seeding approach: appropriately concentrated seeds in mother liquor were added in a 1:9 ratio to TamA in bicelles before crystallization was set up as described above. Crystals were frozen with perfluoropolyether cryo-oil as cryoprotectant.

The periplasmic domain of TamA was crystallized by vapor diffusion with the sitting-drop method at 20 °C. The protein crystallized with several organic acids within a few days. The best crystals were grown from 15% PEG 3350, 0.1 M di-Na tartrate and 0.1 M HEPES, pH 7.5. The crystals were frozen after a gradual increase (5% steps) of the ethylene glycol concentration to 20% (v/v) over 2 h.

2.4.4. Data collection, molecular replacement and refinement

Diffraction data were collected at the Swiss Light Source on beamline PXIII at 100 K for full-length TamA and for the POTRA1–3 fragment and processed with XDS (Kabsch 2010). The structure of the POTRA domains was solved by SIRAS phasing with sodium iodide. The derivative was prepared by incubation of the crystals for 1 h with 300 mM NaI dissolved in harvesting buffer. Iodide sites were localized with SHELXD (Sheldrick 2010). Initial phases were calculated with Phaser (McCoy *et al.* 2007), and the initial model was built in space group $P4_32_12$ by wARP (Langer *et al.* 2008) with one molecule per asymmetric unit. Model building and structure refinement were performed with Coot (Emsley and Cowtan 2004) and PHENIX (Adams *et al.* 2002) at 1.84 Å resolution, yielding R_{work}/R_{free} of 0.17/0.20. The model starts at residue 25, the fourth residue after the native signal sequence, and misses residues 84–92, which are part of the loop between β-strands 1 and 2 of POTRA1, owing to weak electron density. The final model contains 95% of the residues in favored Ramachandran regions and 0.4% outliers.

For full-length TamA, molecular replacement was performed with Phaser in space group $P2_12_12$, with one molecule per asymmetric unit and a solvent content of 74%. TamA POTRA domain structure and a polyalanine β-barrel without loops from the FhaC structure (PDB entry 2QDZ (Clantin *et al.* 2007)) were used as search models. Initial model building was done automatically by ARP/wARP, and manual rebuilding and ligand modeling were done in Coot. Additionally, SAD data with a resolution of 4 Å for selenomethionine-labeled full-length protein was collected at a wavelength of 0.9794 Å and processed with XDS. Resulting anomalous difference maps confirmed methionine positions. Refinement was carried out with PHENIX against native data at 2.25 Å resolution, yielding R_{work}/R_{free} of 0.19/0.22. The model starts at residue 25, the fourth residue after the native signal sequence, and misses residues 84–92, which are part of the loop between β-strands 1 and 2 of POTRA1. Increased flexibility

of POTRA3 and around Gly574-Pro575 in the C-terminal region is indicated by increased temperature factors (Supplementary Fig. 2.4). The final model contains 95% of the residues in favored Ramachandran regions and 0.18% outliers.

2.4.5. Mapping of conserved regions

To map evolutionary conservation, 11 orthologous TamA sequences from different organisms were selected with pairwise identities between 25% and 33% (NCBI accession codes P0ADE4.1, WP_010374432.1, YP_006917734.1, YP_005378779.1, WP_006914415.1, WP_006956461.1, WP_007639592.1, YP_006416500, YP_007468392.1, WP_008316497.1 and YP_006721763.1). The sequences were aligned with Clustal Omega (Goujon *et al.* 2010, Sievers *et al.* 2011) and manual adjustments based on known secondary structure information. Ten orthologous BamA sequences with pairwise identities between 19% and 36% were aligned separately (NCBI codes YP_002998039.1, YP_001121414.1, WP_003783125.1, YP_001219350.1, WP_010501263.1, YP_865762.1, YP_007459313.1, YP_004865655.1, YP_002549812.1 and WP_008996841.1), and ten sequences of FhaC homologs with pairwise identities between 18% and 35% were aligned separately (AAB30624.1, YP_335961.1, WP_005764711.1, YP_003741556.1, WP_002831157.1, YP_006646915.1, YP_004122309.1, WP_008291755.1, WP_005980414.1 and YP_003307097.1).

The three resulting alignments were aligned as profiles with Clustal Omega and adjusted manually. The final alignment was used to create an evolutionary tree (Supplementary Fig. 2.1) and as input for AL2CO (Pei and Grishin 2001) to map conservation onto the *E. coli* TamA structure. To obtain a complete model of TamA for visualization of conservation, one loop of POTRA1 and the N-terminus of POTRA1 were inserted by modeling.

2.5. Accession codes

Coordinates and structure factors for full-length TamA and for TamA POTRA1–3 have been deposited in the Protein Data Bank under accession codes 4C00 and 4BZA, respectively.

2.6. Author contributions

S.H. and T.M. designed the study and guided the research experiments. F.G., F.Z., R.P.J. and B.M.B. carried out the experiments. All authors analyzed data. F.G., S.H. and T.M. wrote the paper.

2.7. Acknowledgements

Crystallographic experiments were performed at PXIII (Swiss Light Source, Paul Scherrer Institute, Switzerland). We thank M. Wang and V. Olieric for support at the beamline, T. Schirmer for discussion and L. Betancor and P.F. Leadlay (University of Cambridge) for the pL1SL2 plasmid. This work was supported by the Swiss National Science Foundation (Grant PP00P3_128419 to S.H.) and the European Research Council (FP7 contract MOMP 281764 to S.H.). F.G. acknowledges a fellowship by the Werner-Siemens Foundation.

2.8. Supplement

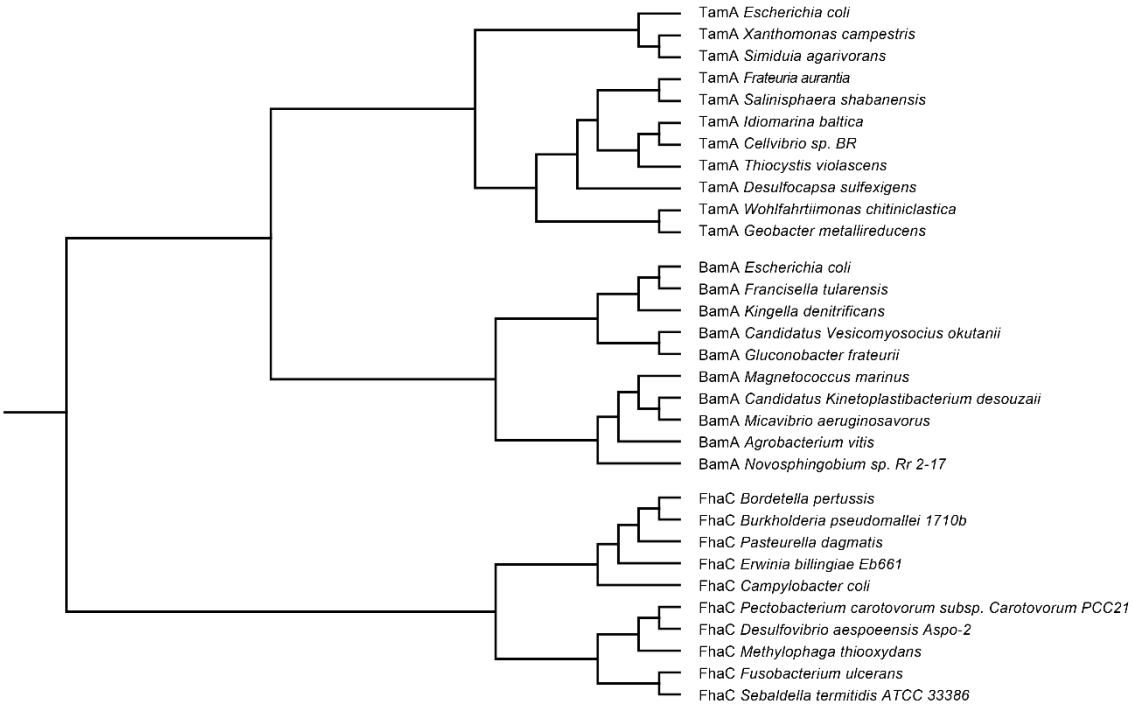

Supplementary Figure 2.1 Evolutionary tree for 11 TamA, 10 BamA and 10 FhaC orthologues. Protein and species names are indicated.

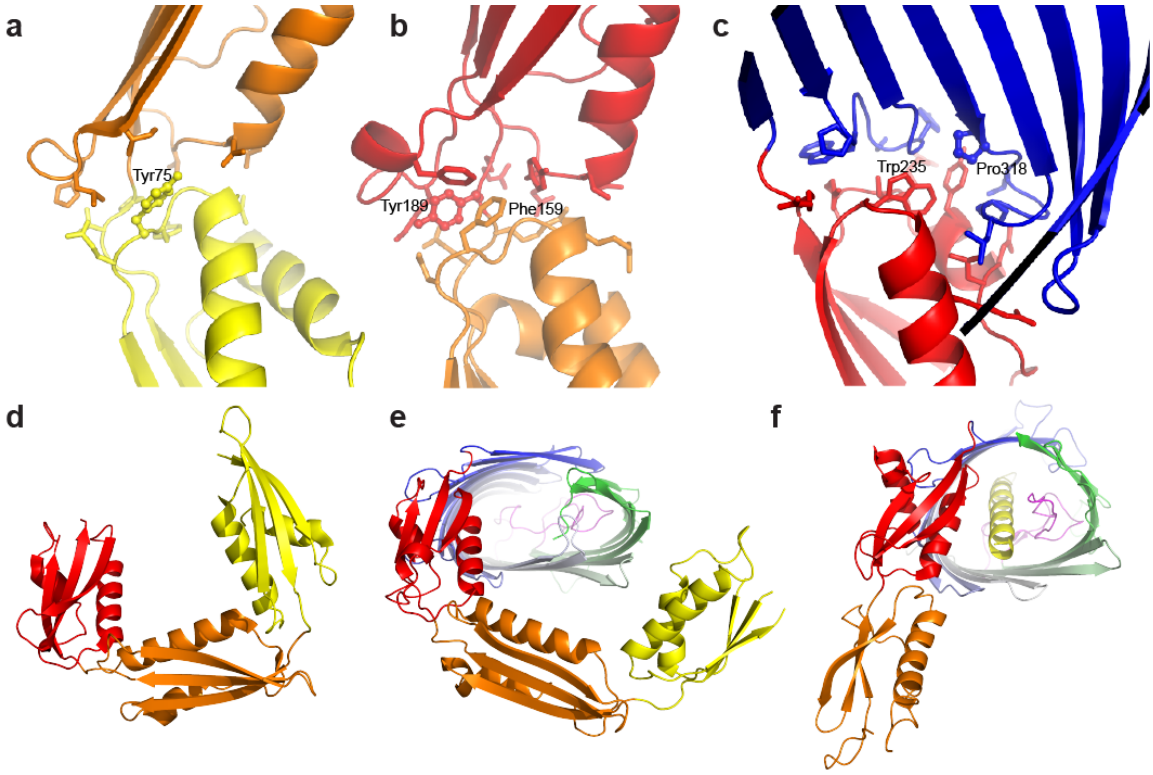

Supplementary Figure 2.2 Interfaces between the TamA domains and structural comparison of BamA, TamA and FhaC POTRA domains.

(**a**) Interface between POTRA1 (yellow) and POTRA2 (orange). (**b**) Interface between POTRA2 (orange) and POTRA3 (red). (**c**) Interface between POTRA3 (red) and the barrel (blue). The conserved residues Y75, Y189 and P318 are shown in ball-and-stick representation. Additional aromatic residues that are part of the interfaces are indicated. The core of the interfaces is dominated by hydrophobic interactions, surrounded by polar interactions at the surface. (**d**) Model of BamA POTRA domains 3 to 5 (POTRA3: yellow, POTRA4: orange, POTRA5: red) by combining the structure of POTRA domains 4 and 5 (PDB entry 3Q6B (Zhang *et al.* 2011); similar conformation as in PDB entry 3OG5 (Gatzeva-Topalova *et al.* 2010)) with the structure of POTRA domains 3 and 4 (PDB entry 2QDF (Kim *et al.* 2007); similar conformation as in PDB entry 2QCZ (Kim *et al.* 2007) and PDB entry 3EFC (Gatzeva-Topalova *et al.* 2008)). The POTRA domains in this combined model adopt a C-shape. (**e**) Structure of TamA determined in this work. The POTRA domains of TamA (POTRA1: yellow, POTRA2: orange, POTRA3: red) are arranged in C-shape around the axis of the barrel (color gradient: blue – white – green from N- to C-terminus). The TamA barrel adopts a kidney shape. (**f**) Structure of FhaC (PDB entry 2QDZ (Clantin *et al.* 2007)). The orientation of POTRA1 (orange) of FhaC deviates significantly from the orientation of the corresponding POTRA2 of TamA. The FhaC barrel adopts a triangular shape.

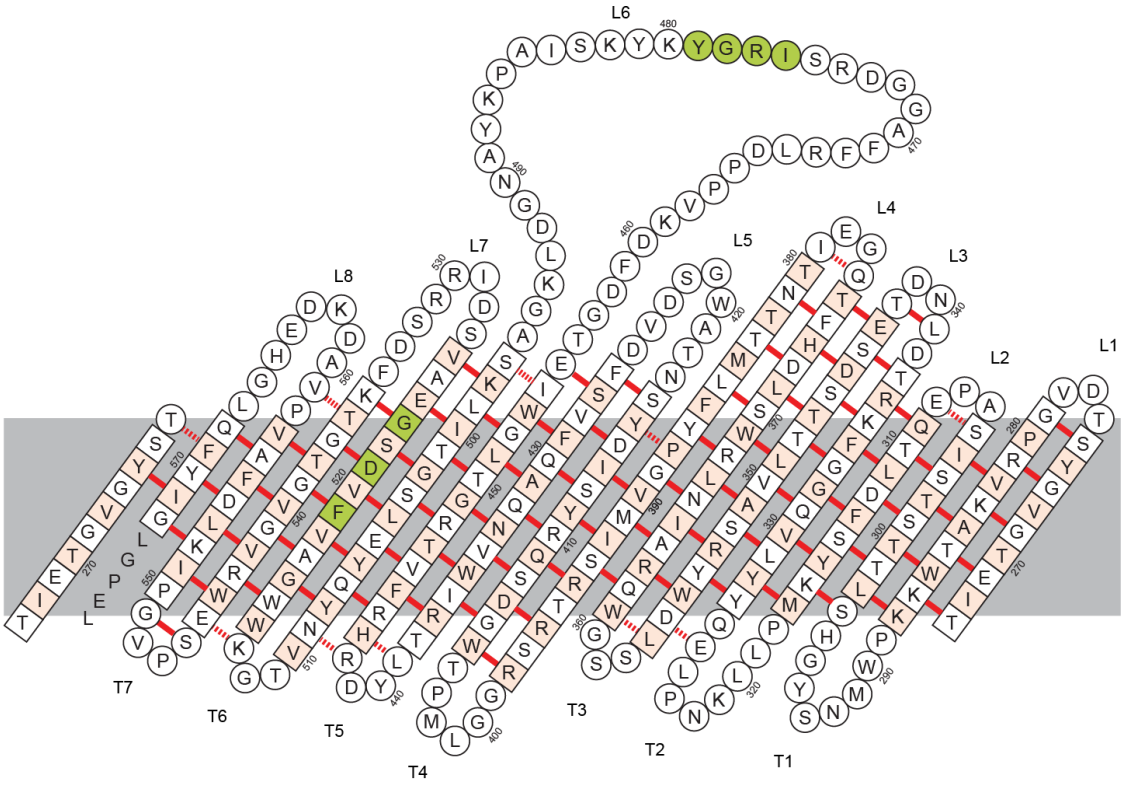

Supplementary Figure 2.3 2D representation of the TamA barrel topology as viewed from the barrel exterior.

Residues forming β-strands are indicated by rectangles, residues of loops and turns by circles. The side chains of orange residues point towards the membrane. The extracellular loops are numbered L1 to L8 from N- to C-terminus, the periplasmic turns are numbered T1 to T7. Interstrand backbone hydrogen bond pairs are indicated by red lines between the corresponding residues, single hydrogen bonds by red dotted lines. Strand 1 is repeated on the left hand side to show the hydrogen bonds that form to strand 16. The conserved motifs (I/V)RG(Y/F) (residues 476–479) and (F/G)xDxG (residues 519–523) are highlighted green.

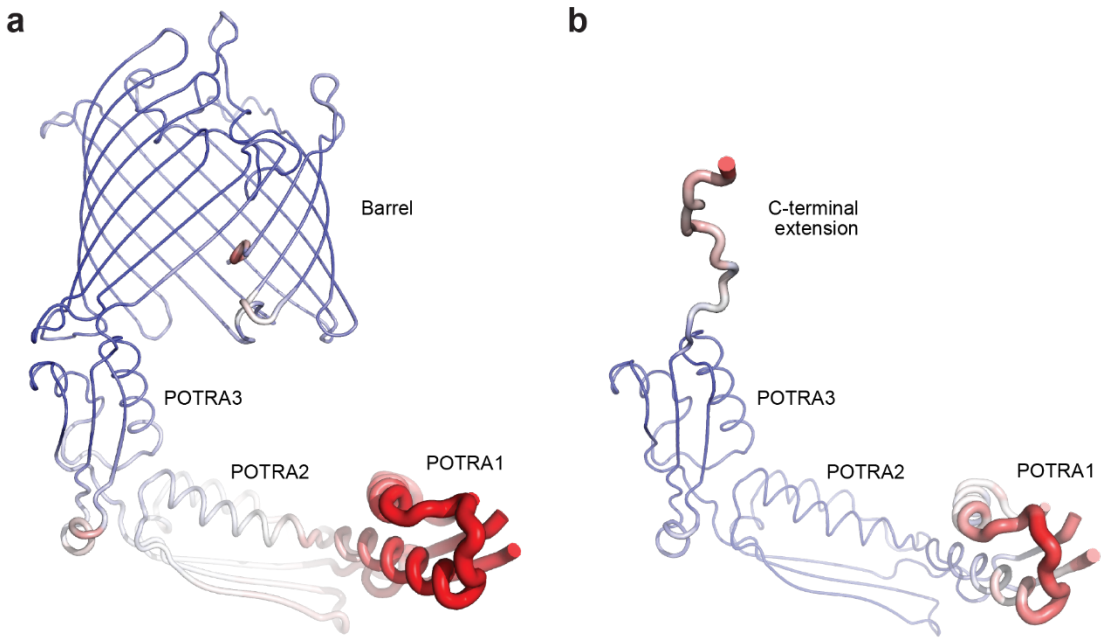

Supplementary Figure 2.4 Crystallographic temperature factor distribution.
The value of the temperature factors on a 1–200 Å^2 scale is indicated by putty cartoon representation (low values thin, high values thick) and color gradient (low values in blue via white to high values in red). (**a**) B-factor distribution in the full-length TamA structure and (**b**) in the structure of the isolated POTRA domains fragment comprising the region corresponding to the first β-strand of the TamA-barrel in a non-β-strand conformation.

Supplementary Table 2.1 Data collection and refinement statistics.

	TamA full-length	TamA POTRA1–3
Data collection		
Space group	P 21 21 2	P 43 21 2
Cell dimensions		
a, *b*, *c* (Å)	77.47, 261.06, 57.84	83.05, 83.05, 150.66
α, β, γ (°)	90, 90, 90	90, 90, 90
Resolution (Å)	74.27 – 2.25 (2.33 – 2.25) *	42.97 – 1.84 (1.95 – 1.84)
R_{merge}	0.071 (0.854)	0.047 (1.731)
$I / \sigma I$	20.74 (2.39)	31.35 (1.99)
Completeness (%)	98.4 (94.3)	99.8 (99.1)
Redundancy	7.3 (7.0)	13.0 (12.5)
Refinement		
Resolution (Å)	74.27 – 2.25	42.97 – 1.84
No. reflections	55995	46484
R_{work} / R_{free}	0.190 / 0.217	0.173 / 0.202
No. atoms	5043	2287
Protein	4389	1989
Ligand/ion	428	8
Water	226	290
B-factors		
Protein	76.77	71.25
Ligand/ion	90.10	80.85
Water	56.38	61.84
R.m.s. deviations		
Bond lengths (Å)	0.003	0.018
Bond angles (°)	0.96	1.46

*Values in parentheses are for highest-resolution shell.

CHAPTER 3:

Purification and Bicelle Crystallization for Structure Determination of the *E. coli* Outer Membrane Protein TamA

Reproduced from:

Methods in Molecular Biology, 1329:259-270; October 2015

Purification and Bicelle Crystallization for Structure Determination of the E. coli Outer Membrane Protein TamA.

Fabian Gruss, Sebastian Hiller, and Timm Maier

in

The BAM Complex

Methods and Protocols

Editors: Susan Buchanan and Nicholas Noinaj

DOI 10.1007/978-1-4939-2871-2_20

Print ISBN 978-1-4939-2870-5

Online ISBN 978-1-4939-2871-2

With permission of Springer Science+Business Media

3.1. Abstract

TamA is an Omp85 protein involved in autotransporter assembly in the outer membrane of *Escherichia coli*. It comprises a C-terminal 16-stranded transmembrane β-barrel as well as three periplasmic POTRA domains, and is a challenging target for structure determination. Here, we present a method for crystal structure determination of TamA, including recombinant expression in *E. coli*, detergent extraction, chromatographic purification, and bicelle crystallization in combination with seeding. As a result, crystals in space group $P2_12_12$ are obtained, which diffract to 2.3 Å resolution. This protocol also serves as a template for structure determination of other outer membrane proteins, in particular of the Omp85 family.

3.2. Introduction

The insertase proteins of the Omp85 family are responsible for the assembly of β-barrel proteins in the outer membrane of Gram-negative bacteria, mitochondria, and chloroplasts (Chacinska *et al.* 2009, Kim *et al.* 2007, Walther *et al.* 2009). Omp85 insertases comprise a 16-stranded C-terminal transmembrane β-barrel and between one and five attached periplasmic POTRA domains (Clantin *et al.* 2007, Gruss *et al.* 2013, Noinaj *et al.* 2013), which are involved in initial substrate interaction via β-strand augmentation (Delattre *et al.* 2011). The β-barrel domain is characterized by an unusually weak lateral connection between the N-terminal and C-terminal strand. The latter strand is not fully zipped up but kinks to the inside of the barrel, thus creating a gate to the lipid phase of the membrane (Gruss *et al.* 2013, Noinaj *et al.* 2013).

TamA and BamA are the only Omp85 proteins in *E. coli* K12. BamA is the core subunit of the general β-barrel assembly machinery (BAM) (Kim *et al.* 2007). TamA is more specialized and involved in the biogenesis of a subset of autotransporters (Selkrig *et al.* 2012, Stegmeier *et al.* 2007), which typically consist of a 12-stranded membrane-embedded β-barrel linked to a large extracellular passenger domain (Dautin and Bernstein 2007, van den Berg 2010).

For structure determination, TamA is recombinantly expressed into the outer membrane of its native host *E. coli*, using a pET vector that provides an N-terminal *malE* signal sequence for periplasmic targeting, followed by a hexahistidine purification (Hs6-) tag and a TEV protease cleavage site preceding the insertion site for the coding sequence of mature TamA without its native export signal sequence. TamA is overexpressed in a partially OMP-deficient *E. coli* strain and extracted from membrane pellets using the mild detergent β-octylglucoside (β-OG). Immobilized metal affinity chromatography (IMAC) via the His6-tag is employed for initial purification, followed by cation-exchange chromatography (CIEX) for buffer exchange for subsequent TEV cleavage of the His6-tag. A second IMAC step removes

TEV protease and uncleaved TamA. Finally, the cleaved protein is subjected to size-exclusion chromatography (SEC), yielding monodisperse monomeric TamA of high purity as determined by SDS-polyacrylamide gel electrophoresis (SDS-PAGE). After buffer exchange and detergent concentration equilibration via dialysis, the protein is integrated into bicelles by mixing it with an aqueous solution of preformed DMPC/CHAPSO bicelles. The mixture is used directly for crystallization screening and optimization. Crystals diffracting to high resolution are obtained by adding seeds prepared from lower quality crystals grown in similar conditions to the protein-bicelle mixture prior to crystallization setup. This seeding strategy is generally applicable to bicelle crystallization of other membrane proteins.

3.3. Materials

3.3.1. Plasmid construction

1. Vector: pET22b (Novagen).
2. Cloning strain and genomic DNA source: *E. coli* DH10B.
3. Oligonucleotides:
   sigseq_down: 5′-ATAGGAATTCCATATGAAAATAAAAACAGGTGCACGCATCCTCGCATTATCCGCATTAACGACG-3′
   sigseq_up: 5′-GAGCGCATGCCATGGCGAGAGCCGAGGCGGAAAACATCATCGTCGTTAATGCGGATAATGCGAGG-3′
   histev_down: 5′-CATGGCCCACCACCACCACCACCACGAGAATCTGTATTTCCAGGG-3′
   histev_up: 5′-AATTCCCTGGAAATACAGATTCTCGTGGTGGTGGTGGTGGTGGGC-3′
   tama_down: 5′-GGAATTCAAGCGAACGTCCGTCTACAGGTCG-3′
   tama_up: 5′-CCGCTCGAGTCATAATTCTGGCCCCAGACCGATG-3′
4. DNA polymerase for PCR amplification.
5. Restriction endonucleases: NdeI, NcoI, EcoRI, XhoI (New England BioLabs).
6. Ligation enzyme: T4 DNA ligase (New England BioLabs).

3.3.2. Expression

1. Expression strain: *E. coli* BL21(λ DE3)omp3 (Prilipov *et al.* 1998).
2. LB medium (400 mL) for pre-cultures.
3. LB medium (18 L) for main cultures.
4. Flasks (4 x 500 mL) for pre-cultures.
5. Baffled flasks (12 x 5 L) for main cultures.
6. Ampicillin.
7. Isopropyl β-d-thiogalactopyranoside (IPTG).

3.3.3. Purification

1. Stock solutions for buffer preparations:
   (a) 500 mM Na_2HPO_4.
   (b) 500 mM NaH_2PO_4.
   (c) 5 M NaCl.
2. Lysis buffer (500 mL): 25 mM NaPi, pH 7.5 (86.6% Na_2HPO_4, 13.4% NaH_2PO_4), 150 mM NaCl (see Note 1).
3. High-pressure homogenizer (*e.g.*, Microfluidizer by Microfluidics).
4. Extraction buffer (250 mL): 25 mM NaPi, pH 7.5, 150 mM NaCl, 3% β-OG (n-octyl-β-d-glucopyranoside, >99% chemical purity and >98% β-anomer purity, Anatrace) (see Note 1).
5. High-performance liquid chromatography system (*e.g.*, Äkta by GE Healthcare, NGC by Bio-Rad).
6. HisTrap FF column (5 mL) (GE Healthcare).
7. Immobilized metal affinity chromatography (IMAC) buffers (see Note 1):
   (a) A (250 mL): 25 mM NaPi, pH 7.5, 150 mM NaCl, 0.8% β-OG.
   (b) B (150 mL): 25 mM NaPi, pH 7.5, 150 mM NaCl, 0.8% β-OG, 500 mM imidazole.
8. CIEX (cation exchange) column: 6 mL column with MacroPrep High S resin (Bio-Rad).
9. CIEX buffers (see Note 1):
   (a) Dilution buffer (150 mL): 25 mM NaPi, pH 6.9 (53.3% Na_2HPO_4, 46.7% NaH_2PO_4), 0.8% β-OG.
   (b) A (300 mL): 25 mM NaPi, pH 7.0, 50 mM NaCl, 0.8% β-OG.
   (c) B (200 mL): 25 mM NaPi, pH 7.0, 1 M NaCl, 0.8% β-OG.
10. TEV protease (His6-tagged) (Addgene plasmid 8827 (Kapust *et al.* 2001)).
11. β-Mercaptoethanol.
12. Syringe filters (0.45 μm) (PTFE based for particle removal).
13. Superdex 75 16/60 column (GE Healthcare).
14. Size-exclusion chromatography (SEC) buffer (400 mL) (see Note 1): 25 mM NaPi, pH 7.5, 150 mM NaCl, 0.8% β-OG.
15. Concentrator: Amicon Ultra unit 30 kDa c/o (Millipore).
16. Slide-A-Lyzer cassette, 3.5 kDa c/o (Pierce).
17. Dialysis buffer (200 mL): 20 mM Tris–HCl, pH 7.5 (adjusted at 10 °C), 150 mM NaCl, 0.8% β-OG.

3.3.4. Crystallization

1. 1,2-Dimyristoyl-sn-glycero-3-phosphocholine (DMPC, Anatrace).
2. 3-[(3-Cholamidopropyl)dimethylammonio]-2-hydroxy-1-propanesulfonate (CHAPSO, Anatrace).
3. Vortex mixer.
4. Crystallization screens: MembFac (Hampton Research), MemGold (Molecular Dimensions), MemStart & MemSys (Molecular Dimensions).
5. Crystallization solutions: Initial crystals: 0.1 M imidazole pH 6, 0.6 M Na-acetate; crystals with seeding: 0.1 M imidazole pH 6, 1.2 M Na-acetate.
6. Crystallization plates: MRC 2 Well (Swissci, Hampton Research).
7. Crystallization robot (*e.g.*, OryxNano by Douglas Instruments, optional but recommended).
8. Cryoprotectant: Perfluoropolyether oil (dried, Hampton Research).

3.3.5. Data processing and model building software

1. XDS (Kabsch 2010).
2. CCP4 (Winn *et al.* 2011).
3. PHENIX (Adams *et al.* 2010).
4. COOT (Emsley and Cowtan 2004).

3.4. Methods

3.4.1. Plasmid construction

1. Anneal the oligonucleotides sigseq_down and sigseq_up to obtain the *malE* signal sequence DNA.
2. Digest individually the *malE* signal sequence DNA and the pET22b vector using NdeI and NcoI restriction enzymes to remove the *pelB* signal sequence from the vector and purify digested DNA via agarose gel electrophoresis (see Note 2).
3. Ligate the purified DNA into the pET22b vector using T4 DNA ligase.
4. Transform the ligation product into electrocompetent *E. coli* DH10B, and plate out and select positive colonies for plasmid purification to obtain the pET22b-malEss vector (Fig. 3.1a).
5. Repeat steps 1–4 using the oligonucleotides histev_down and histev_up, the pET22b-malEss vector obtained from step 4 and NcoI and EcoRI restriction enzymes to obtain the pET22b-malEss-his6-tev vector containing the *malE* signal sequence followed by a His6-tag and a cleavage site for TEV protease (Fig. 3.1b).
6. Amplify genomic *tamA* DNA without the *tamA* signal sequence from an *E. coli* K12 strain

(*e.g.*, DH10β) using oligonucleotides tama_down and tama_up and purify the PCR product via agarose gel electrophoresis.

7. Repeat steps 2–4 using the *tamA* PCR product from step 6, the pET22b-malEss-his6-tev vector obtained from step 5, and EcoRI and XhoI restriction enzymes to obtain the final TamA expression vector containing the *malE* signal sequence followed by a His6-tag and a cleavage site for TEV protease followed by *tamA* (Fig. 3.1c).

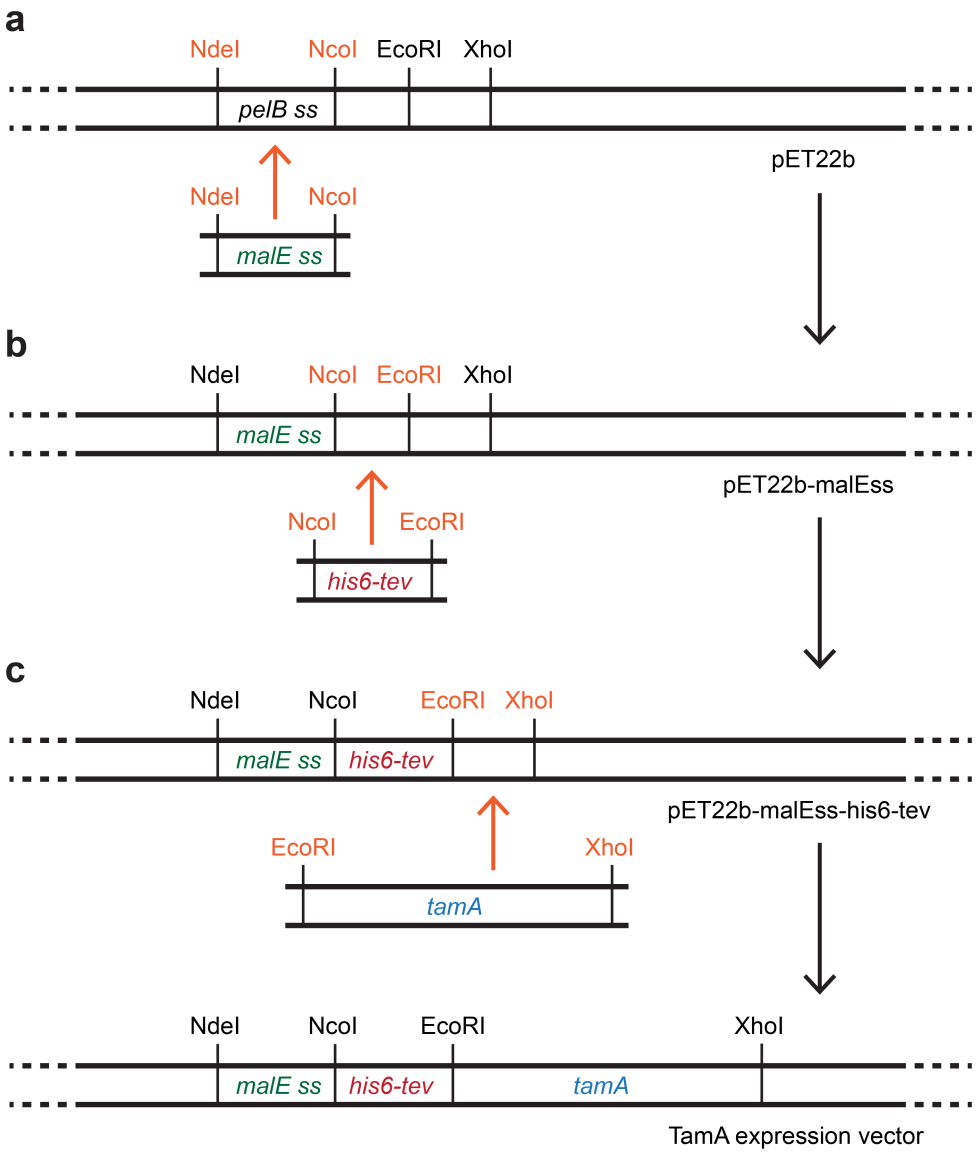

Figure 3.1 Cloning strategy for the TamA expression vector.
(**a**) In the first step, the *pelB* signal sequence of the pET22b vector is replaced by the *malE* signal sequence. (**b**) In the second step, DNA coding for a His6-tag followed by a cleavage site for TEV protease is put 3′ of the signal sequence. (**c**) Last, the *tamA* DNA without its own signal sequence is inserted 3′ of the TEV site.

3.4.2. Expression

1. Transform chemically competent *E. coli* BL21(λ DE3)omp3 cells (Prilipov *et al.* 1998) with the TamA expression vector obtained from Subheading 3.4.1. Inoculate 4 x 100 mL LB medium containing 100 mg L^{-1} ampicillin with the transformed cells and grow overnight by shaking at 37 °C.
2. Inoculate 12 x 1.5 L LB medium in baffled 5 L flasks containing 100 mg L^{-1} ampicillin with the overnight cultures from step 1 to an OD_{600} (optical density at 600 nm) of around 0.06 and grow by shaking at 100 rpm and 37 °C.
3. When the cultures reach OD_{600} = 0.8 set temperature to 20 °C and continue shaking the cells for 2 h before inducing protein expression by addition of IPTG to a final concentration of 0.1 mM.
4. Continue shaking at 20 °C for 18 h before harvesting. The obtained bacterial pellet is used directly or stored at −80 °C (see Note 3).

3.4.3. Purification

1. Resuspend the bacterial pellet obtained from Subheading 3.4.2 in 450 mL lysis buffer and lyse the cells by processing the suspension twice with the microfluidizer (see Note 4). Centrifuge for 10 min at 10,000*g* and 4 °C to remove inclusion bodies and cell debris. Centrifuge the supernatant containing soluble protein and membrane vesicles for 1 h at 100,000*g* and 4 °C to pellet membrane vesicles containing TamA. Remove the supernatant, and gently wash the pellet three times using lysis buffer.
2. Add 250 mL extraction buffer to the membrane pellet and stir overnight at 10 °C to extract TamA. Centrifuge the resuspended membranes for 1 h at 100,000*g* and 10 °C to pellet the detergent-insoluble components. Harvest the supernatant containing solubilized TamA.

   All the following steps should be performed at temperatures between 10 and 15 °C, because the detergent-solubilized protein solution tends to precipitate reversibly at low temperatures. Chromatographic purification steps are carried out at room temperature (see Note 5).
3. Add 4% v/v IMAC buffer B to the protein solution to adjust the imidazole concentration to approx. 20 mM. Load this solution onto a 5 mL or larger HisTrap FF column equilibrated with IMAC buffer A (see Note 6). Wash the column with a mixture of 96% IMAC buffer A / 4% IMAC buffer B until the A_{280} reaches a stable baseline (typically 5–6 column volumes) and collect the flow-through. Elute the bound protein with a linear gradient from 4 to 100% IMAC buffer B in 5 column volumes. When using a 5 mL column, repeat this step from column loading to elution using the flow-through of the first loading step to increase the

yield by capturing remaining unbound protein.

4. Pool the fractions of the elution peak (resp. peaks if using a 5 mL HisTrap FF column) to obtain about 30–40 mL total volume of elution fractions containing TamA. Slowly add three times the volume of dilution buffer to adjust ionic strength for CIEX (cation exchange).
5. Load the protein solution onto a 6 mL MacroPrep High S column, equilibrated with CIEX buffer A. Wash the column with CIEX buffer A until the A_{280} reaches a stable baseline. Elute the protein with a linear gradient from 0 to 100% CIEX buffer B in 100 mL volume. Pool peak fractions to obtain a total volume of 30–50 mL (Fig. 3.2a).
6. Add 5 mM β-mercaptoethanol to the solution before adding about 1 mg of His6-tagged TEV protease. Digest the protein overnight. The digested protein solution may appear slightly cloudy due to precipitation. Centrifuge or filtrate to remove the precipitate.
7. Load the solution onto a HisTrap FF 5 mL column, equilibrated with IMAC buffer A without imidazole. Collect the flow-through containing cleaved TamA and concentrate it with 30 kDa c/o centrifugal concentrator units to a volume of 1 mL. At this step, TamA should be essentially pure (Fig. 3.2b).
8. Load the protein onto a Superdex 75 16/60 column, equilibrated with SEC buffer, collect the peak fractions to obtain about 10 mL total volume, and concentrate it with 30 kDa c/o centrifugal units to a concentration of 15–20 mg mL^{-1} and about 0.5 mL volume (Fig. 3.3).
9. Dialyze the protein solution overnight against 80 mL dialysis buffer in a 3.5 kDa c/o Slide-A-Lyzer cassette. Dialyze it again against 80 mL fresh dialysis buffer for 5 h. Adjust the protein concentration to 12.5 mg mL^{-1} by adding the appropriate volume of dialysis buffer to obtain the final protein sample for crystallization. Typical yields of purified TamA are in the range of 5–10 mg from an 18 L LB culture.

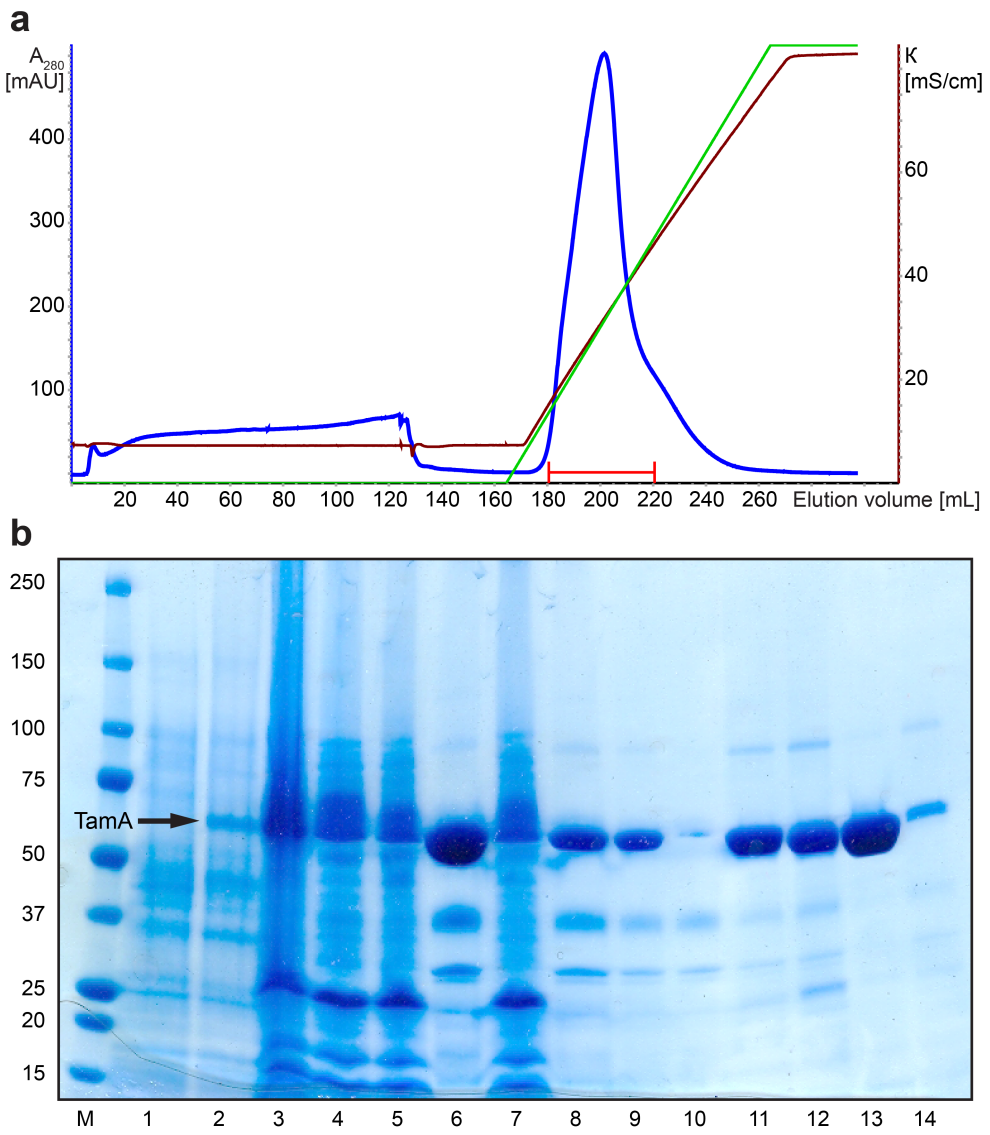

Figure 3.2 CIEX chromatogram and SDS-PAGE analysis of TamA purification.
(**a**) Chromatogram of CIEX chromatography. Blue curve: absorbance at 280 nm; green curve: buffer B concentration; brown curve: conductivity; the red line indicates pooled fractions. (**b**) SDS-PAGE analysis of TamA expression and purification. Lane M shows a molecular weight standard and molecular weights in kDa for the bands are indicated on the left-hand side. Lane 1: *E. coli* expression cells before induction with IPTG; lane 2: *E. coli* expression cells after induction and growth overnight; lane 3: membrane pellet containing TamA suspended with extraction buffer; lane 4: supernatant after ultracentrifugation of the suspension; lane 5: first load onto HisTrap FF 5 mL column, flow-through; lane 6: pooled peak fractions of first HisTrap elution; lane 7: second load onto HisTrap FF 5 mL column, flow-through; lane 8: pooled peak fractions of second HisTrap elution; lane 9: Macroprep High S column load; lane 10: Macroprep High S flowthrough; lane 11: MacroPrep High S pooled peak fractions; lane 12: TamA after TEV digest; lane 13: flow-through of HisTrap FF 5 mL column after TEV digest, containing TamA without His6-tag; lane 14: elution from the HisTrap FF 5 mL column with 500 mM imidazole, containing TamA with non-cleaved His6-tag and His6-tagged TEV protease.

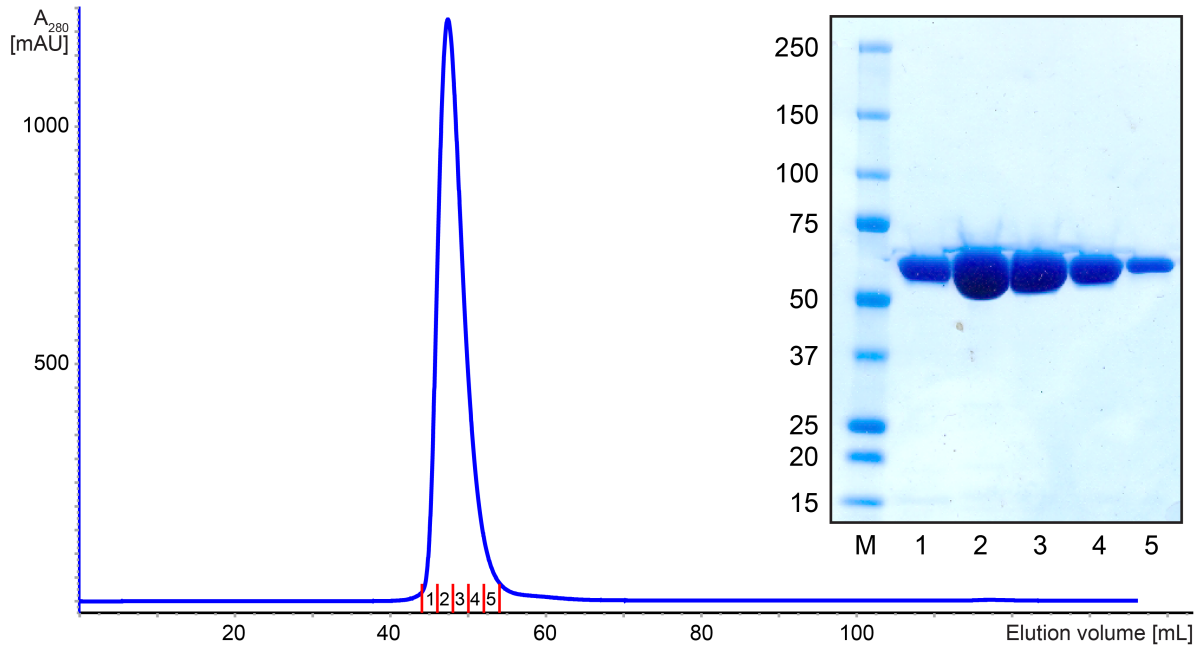

Figure 3.3 Size-exclusion chromatogram and SDS-PAGE analysis of peak fractions.
Blue curve: absorbance at 280 nm; red lines indicate pooled fractions. Lane M shows a molecular weight standard and molecular weights in kDa for the bands are indicated on the left-hand side. Lanes 1–5: SEC fractions 1–5.

3.4.4. Crystallization

1. To prepare 500 µL 40% w/w bicelle stock solution composed of DMPC and CHAPSO in a molar ratio of 2.43:1, weigh out 144.6 mg DMPC in a 1.5 mL vial, and add 55.4 mg CHAPSO on top. Cover it with 300 µL H_2O. Mount the 1.5 mL vial on a vortex mixer and vortex overnight at 4 °C to dissolve the bicelle mixture. If it has not dissolved completely, apply a few cycles of heating to 50 °C, cooling on ice, vortexing, and freezing (Ujwal and Bowie 2011) until the solution is homogenous and clear. You can store the bicelle solution at −20 °C or keep it at 4 °C for immediate use.
2. To prepare a solution of TamA in 8% bicelles (see Note 7), add one-fourth the volume bicelle stock solution to TamA solution (*e.g.*, add 50 µl bicelle stock to 200 µl TamA), mix by pipetting up and down, and incubate for at least 30 min at 4 °C. Do not store this solution on ice as a phase transition may occur resulting in a cloudy inhomogeneous sample (see Note 8).
3. Setting up crystallization plates must be performed at 4 °C either using a robot (*e.g.* OryxNano) or manually. Pipette the crystallization solution on top of the protein-bicelle mixture or add both at the same time when using an OryxNano robot. After pipetting, immediately seal the crystallization plates and keep at 4 °C for 10 min before shifting to 20 °C. Initial crystallization trials may be set up using the sitting-drop vapor diffusion

method with commercial membrane protein crystallization screens (*e.g.*, MembFac, MemStart & MemSys, MemGold). Initial plate-like crystals for seeding can be obtained in 0.1 M imidazole pH 6 and 0.6 M sodium acetate with a ratio of protein to reservoir solution in the drop of 1:2 after about 1 week.

4. Seed preparation: Prepare a solution resembling the mother liquor of the crystals: Mix dialysis buffer in a 4:1 ratio with bicelle stock solution and mix the resulting solution in a 1:2 ratio with 0.1 M imidazole pH 6 and 0.6 M sodium acetate. Transfer crystals into a 1.5 mL vial containing 50–100 µL mother liquor solution using a loop or a pipette. Pipette up and down to crush crystals. Finally, vortex for 1 min. Prepare a dilution of the seed stock of 1:10 by mixing part of the seed solution 1:9 with mother liquor solution. Repeat to obtain a dilution series of 1:1, 1:10, 1:100, 1:1000, 1:10,000, and 1:100,000 (see Note 9).
5. To grow high-quality crystals, prepare TamA-bicelle solutions of different protein concentrations (*e.g.*, 5–10 mg mL^{-1} in 1 mg mL^{-1} steps) by diluting the TamA solution with dialysis buffer before mixing with bicelle stock solution. Split each TamA-bicelle mixture into 6 parts and add one-ninth the volume of each of the seed stocks (*e.g.*, add 1 µl 1:1000 seed stock to 9 µl TamA in bicelles with a protein concentration of 6 mg mL^{-1}). Set up a 2D-grid screen of protein concentration versus seed dilution using 0.1 M imidazole pH 6 and 1.2 M sodium acetate as reservoir solution and set up drops as before, mixing the TamA-bicelle / seed solutions in a 1:2 ratio with reservoir solution. The seed stocks can be frozen in liquid nitrogen and stored at −80 °C to later reproduce conditions producing optimal crystals (see Note 9) (Fig. 3.4).
6. To freeze crystals, cover the respective drop with perfluoropolyether oil for cryo-protection before fishing crystals with a loop, moving them through the oil layer and immediately vitrifying them in liquid nitrogen.

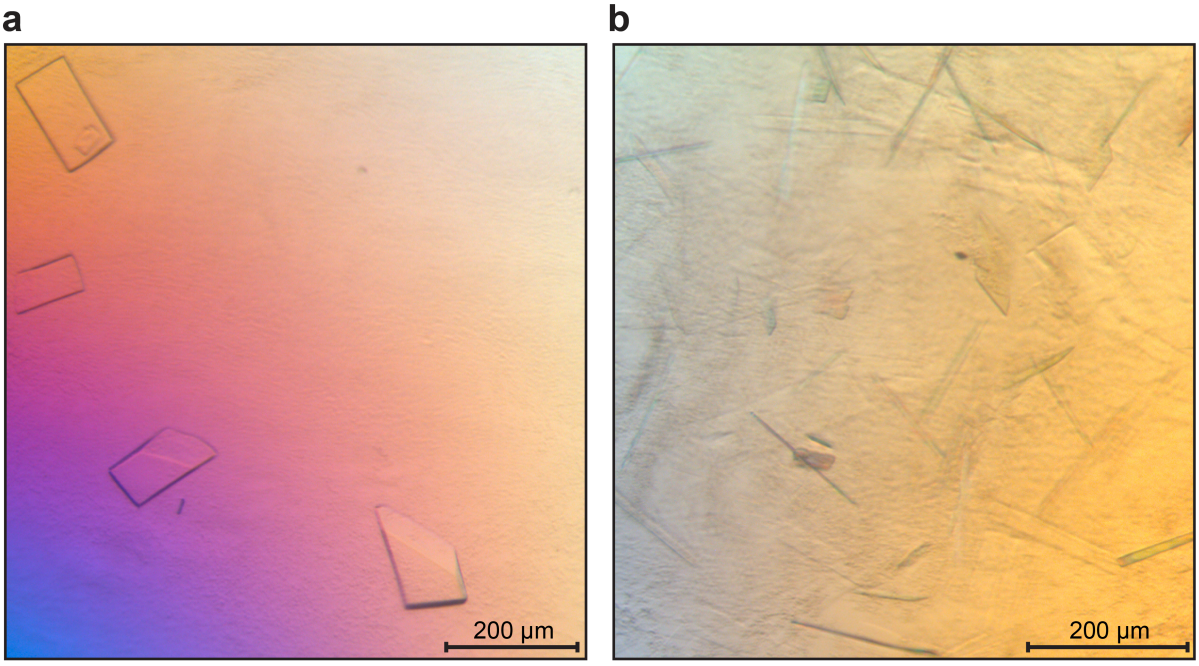

Figure 3.4 TamA bicelle crystallization with seeding.
(**a**) Crystals grown using TamA in a concentration of 7 mg mL^{-1} and a 1:1000 diluted seed stock, which diffracted to a resolution of 2.25 Å. (**b**) Lower quality crystals grown using TamA in a concentration of 8 mg mL^{-1} and a 1:100 diluted seed stock.

3.4.5. Data processing and model building

1. Diffraction data can be processed using standard programs, *e.g.*, XDS (Kabsch 2010). The space group should be $P2_12_12$ with unit cell axis dimensions of a = 77.5 Å, b = 261.1 Å, c = 57.8 Å, and α = β = γ = 90°.
2. Initially, phases could be solved by molecular replacement with the CCP4 program Phaser (McCoy *et al.* 2007, Winn *et al.* 2011) using the separately solved structure of the POTRA domains of TamA (PDB entry 4BZA (Gruss *et al.* 2013)) and the barrel of FhaC (PDB entry 2QDZ (Clantin *et al.* 2007)).
3. Model building and refinement can be done using the programs COOT (Emsley and Cowtan 2004) and PHENIX (Adams *et al.* 2010), respectively. The TamA crystal structure is provided under the PDB entry 4C00 (Gruss *et al.* 2013).

3.5. Notes

1. The pH of NaPi buffers can be adjusted at room temperature by mixing Na_2HPO_4 and NaH_2PO_4 stock solutions in appropriate ratios to obtain near-final values and fine-tuning by addition of HCl or NaOH to the buffer solutions containing all ingredients.
2. It is possible that the *pelB* signal in the pET22b vector can also be used for expression

and does not need to be replaced by the *malE* signal sequence.

3. After induction of expression and overnight growth, the bacterial pellet appears partially lysed, which has no detectable effect on protein quality.
4. French pressure cell and sonication may be suitable alternative lysis methods.
5. When keeping TamA below 4 °C it may aggregate. This aggregation is reversible upon shifting to 4 °C again.
6. The choice of the IMAC resin material may affect yield and purity.
7. The β-OG concentration of final TamA samples before mixing with bicelles is measured by NMR spectroscopy and may be adjusted to 2.0%.
8. It is recommended to keep the TamA-bicelle mixture at 4 °C. Neither put it on ice nor warm it up as phase transitions occur, which may affect sample quality. Phase transitions are usually reversible but for a warmed-up sample it may take hours or even days until the solution turns clear again at 4 °C.
9. Seed dilution series and crystal growth testing have to be repeated each time a new seed stock is prepared as the concentration of seeds differs between preparations. For these 2D-grid screens manual setup may be necessary as different protein solutions are used.

CHAPTER 4:

Interactions of TamA and TamB

4.1. Abstract

TamB is a large protein of 140 kDa, forming the TAM complex together with the outer membrane protein TamA, which is involved in autotransporter assembly. TamB presumably contains an N-terminal transmembrane α-helix inserted in the inner membrane, while the remaining β-sheet-rich structure is located in the periplasm. Here, we characterize the interaction of TamB and TamA theoretically and experimentally. The existence of interaction between TamB and the POTRA domains of TamA is demonstrated by analytical size exclusion chromatography (SEC) as well as isothermal titration calorimetry (ITC) and the binding sites are mapped using computational co-evolution analysis. In addition, co-evolution hints to a second binding site of TamB at the TamA barrel. These data provide exciting new insights into the TAM architecture.

4.2. Introduction

Many Gram-negative bacteria possess an operon encoding for the proteins TamA and TamB, which together form the TAM complex (Heinz and Lithgow 2014, Selkrig *et al.* 2012, Stegmeier *et al.* 2007). This complex was shown to be involved in the assembly of a subset of autotransporter proteins (Selkrig *et al.* 2012), which often mediate bacterial virulence (van Ulsen *et al.* 2014). Whereas the 65 kDa Omp85 protein TamA consists of an outer membrane embedded β-barrel and three N-terminal periplasmic POTRA domains (Gruss *et al.* 2013), the 140 kDa TamB is presumably tethered to the inner membrane via an N-terminal α-helix. The rest of TamB is located to the periplasm (Selkrig *et al.* 2015, Selkrig *et al.* 2012, Shen *et al.* 2014). A C-terminal region of TamB interacts with the TamA POTRA domains and therefore the TAM complex is assumed to span the whole periplasm from inner to outer membrane (Selkrig *et al.* 2015, Shen *et al.* 2014).

Crystal structure determinations of TamA (Gruss *et al.* 2013) and the general OMP insertase BamA (Noinaj *et al.* 2013) revealed insights into the OMP assembly mechanism: Presumably, unfolded substrate OMP substrates integrate their β-barrel into the Omp85 barrel between the loosely connected terminal strands 1 and 16 (Estrada Mallarino *et al.* 2015, Gruss *et al.* 2013, Noinaj *et al.* 2014). Necessity of opening between these two strands was demonstrated by crosslinking experiments *in vivo* (Noinaj *et al.* 2014).

The structure of TamB is unknown, but predicted to be rich in β-strands (Heinz *et al.* 2015). Noteworthy, the very C-terminus of TamB resembles the β-signal found in the last transmembrane strand of OMPs, which is crucial for their assembly (Struyvé *et al.* 1991). The functional involvement of TamB, however, has largely remained elusive. It was demonstrated that TamA and TamB knock out mutants show similar phenotypes in *E. coli*,

including growth defects, decreased cell adhesion, and accumulation of autotransporter proteins in the periplasm (Selkrig *et al.* 2012). In addition, the presence of TamB reduces autotransporter assembly *in vitro* (Shen *et al.* 2014), together suggesting an essential regulatory role for TamB.

4.3. Results

4.3.1. Analytical size exclusion chromatography

To confirm previously published results demonstrating binding of TamB to TamA and TamA POTRA domains only (Selkrig *et al.* 2015, Selkrig *et al.* 2012, Shen *et al.* 2014), separately purified TamB and TamA POTRA domains 1–3 were incubated and subjected to SEC. Three runs were performed, each with a total sample volume of about 85 µl. The first sample contained only TamB at a concentration of 32 µM, the second sample only TamA POTRA domains at a concentration of 159 µM and the last sample TamB and TamA POTRA domains mixed at the same concentrations as in the individual runs, leaving the POTRA domains in about fivefold molar excess over TamB.

Whereas the A_{280} profiles of the SEC runs in presence of 0.05% DDM do not allow unambiguous conclusions about protein co-migration, SDS-PAGE analysis of the eluted fractions demonstrates a clear co-migration of TamA POTRA domains with TamB. From an inspection of the band sizes and intensities, a 1:1 molar ratio in the co-migrating fractions seems plausible (Fig. 4.1).

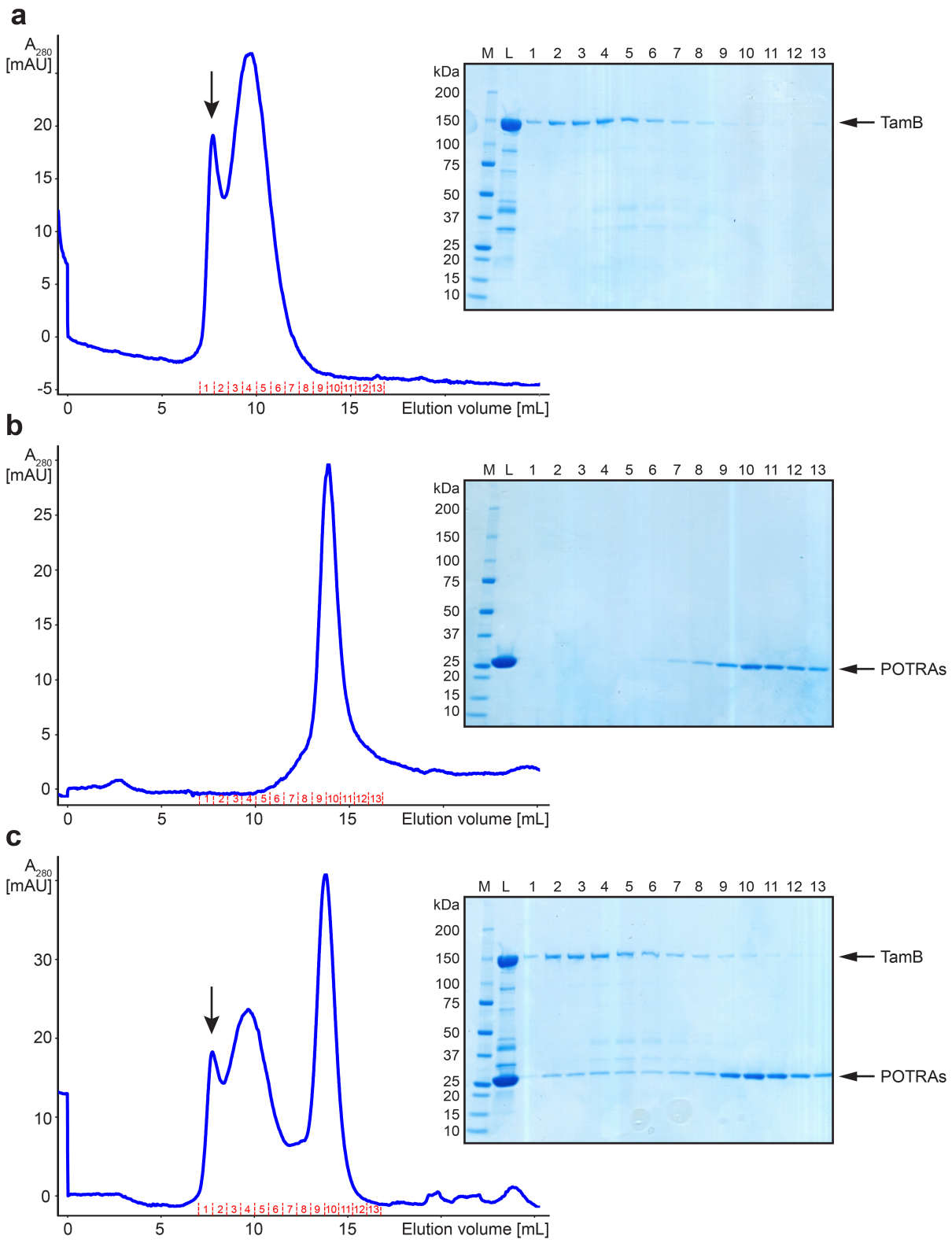

Figure 4.1 SEC runs of TamB and TamA POTRA domains.

A_{280} profiles for the Superose 12 10/300 GL SEC runs and SDS-PAGE analysis of the respective column load (L) and individual fractions (1–13, as indicated) is shown for (**a**) 32 µM TamB, (**b**) 159 µM TamA POTRA domains, and (**c**) 32 µM TamB + 159 µM TamA POTRA domains. M = molecular weight marker. The position of void volume peaks is indicated by an arrow.

4.3.2. Isothermal titration calorimetry

The binding interaction between TamB and TamA POTRA domains was further characterized by ITC. Purified TamB, TamA POTRA domains 1–3 and POTRA domain 1 samples (Fig. 4.2) had the same buffer composition for the ITC measurements. The DDM detergent concentration was 0.05% in the POTRA domains samples and 0.1% in the TamB and control samples, as determined by refractive index measurements. TamB was used at a concentration of 5 μM and POTRA domains at concentrations of 35 or 50 μM for ITC experiments (Fig. 4.3).

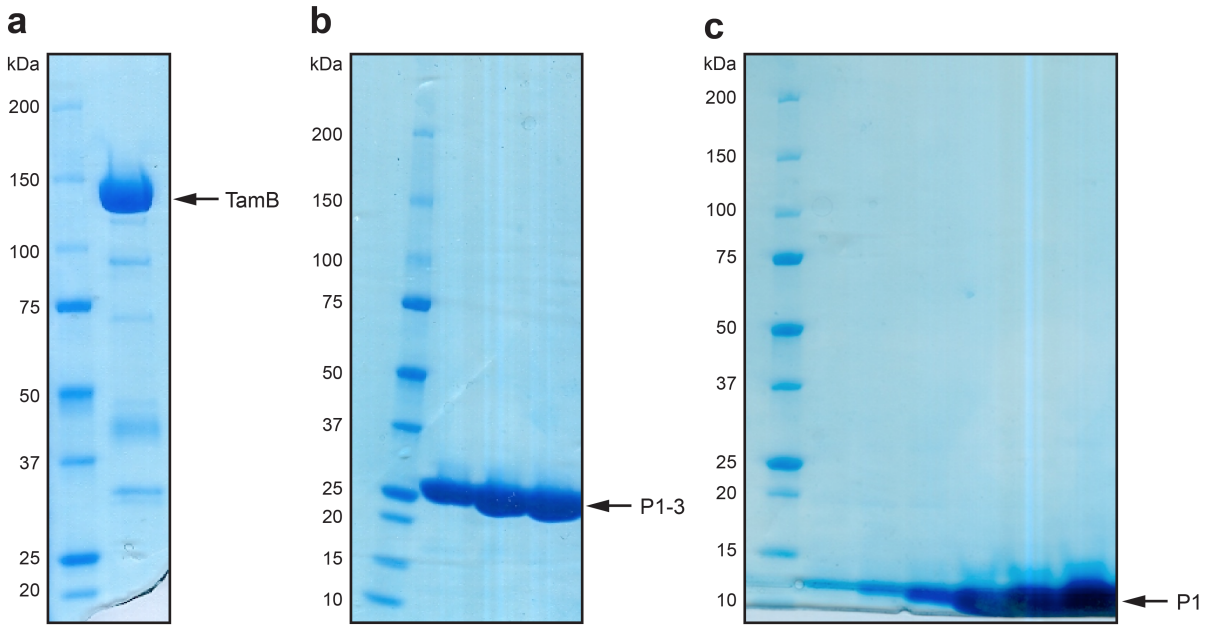

Figure 4.2 SDS-PAGE analysis of purified proteins used for ITC.
Each SDS-PAGE includes a molecular weight marker and shows purified protein for (**a**) TamB in DDM micelles, (**b**) TamA POTRA domains 1–3, and (**c**) TamA POTRA domain 1 after final SEC purification.

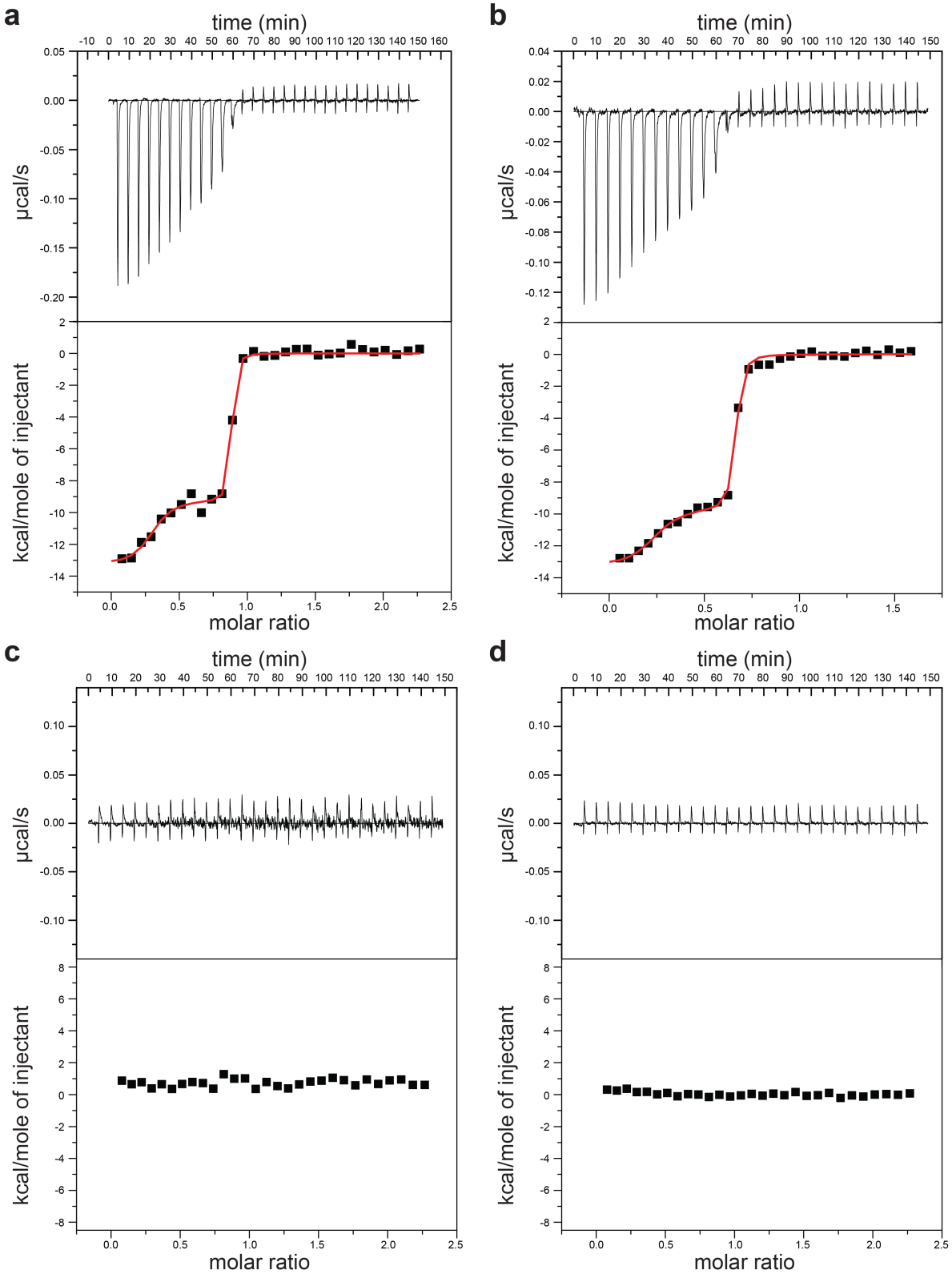

Figure 4.3 ITC measurements of TamB and TamA POTRA domain constructs.
Raw data and processed data with fitted curves are shown for (**a**) TamA POTRA1–3 at 50 µM titrated to TamB, (**b**) TamA POTRA1–3 at 35 µM titrated to TamB, (**c**) TamA POTRA1 at 50 µM titrated to TamB, and (**d**) TamA POTRA1–3 at 50 µM titrated to buffer. The buffer in TamA POTRA samples contained 0.05% DDM, in TamB samples and the control 0.1% DDM.

TamB binding can be observed only for TamA POTRA domains 1–3. For data analysis, curve fitting with a two-sets-of-sites model in the Origin 7 software (OriginLab, Northamton, MA, USA) was applied. The calculated values for enthalpy (ΔH), number of binding sites (N), dissociation constant (K_D) and entropy change (ΔS) for both measurements of TamB in combination with TamA POTRA domains 1–3 are listed in Table 4.1. In both experiments the determined K_D values are of similar magnitude in the pM or nM range for the first and second transitions, respectively, but have high errors. This uncertainty is plausibly based on the two transitions being not well separated, which leads to a missing baseline between them, as well as a missing baseline before the first transition and too few data points in the second transition. As a consequence of the large difference between the concentration of TamB in the cell and the determined K_D values for the single transitions, the calculated C-values, which are a measure of the steepness of the sigmoidal curves, are in the unwanted range of > 500 (Turnbull and Daranas 2003). The data clearly show that there are two binding transitions. However, the derived numerical thermodynamic data are highly dependent on the choice of data model. Besides the two-sets-of-sites model also more complex models, *e.g.* involving cooperativity, may be possible for the TamB – TamA POTRAs binding, but the correct model cannot be inferred from the ITC data.

Table 4.1 ITC measurements of TamB and TamA POTRA domains 1–3.

c(TamB) (μM)	5		5	
c(POTRAs) (μM)	50		35	
	1st transition	2nd transition	1st transition	2nd transition
ΔH (kcal mol^{-1})	-13.4 ± 0.5	-9.2 ± 0.3	-13.4 ± 0.6	-9.6 ± 0.3
ΔS (cal mol^{-1} deg^{-1})*	-0.3	7.2	-2.6	4.9
N (sites)*	0.28 ± 0.02	0.58 ± 0.02	0.22 ±0.02	0.42 ± 0.02
K_D (nM)*	0.06 ± 0.05	1.5 ± 1.4	0.18 ± 0.11	3.2 ± 1.2
C-value* (:= c(TamB) x K_D^{-1} x N)	2.4 x 10^5	1.9 x 10^4	4.3 x 10^4	5 x 10^3

*These data are approximations for a two-sets-of-sites model.

4.3.3. Co-evolution analysis

To investigate possible binding sites of TamA and TamB from a bioinformatics approach, co-evolution analysis using the Gremlin server was performed. Sufficiently many TamA – TamB DUF490 sequence pairs could be obtained to allow for the analysis of intermolecular co-evolution. Remarkably, four amino acid pairs with the highest interaction probabilities cluster in the sequence and are found in distinct regions of the two proteins: Residues

D1252, L1253, E1258 and F1259 from the very C-terminus of TamB form pair with residues R281, V272, T267 and I268, respectively, located at the N-terminus of the TamA barrel. Three of the TamA residues belong to strand 1 and one residue to strand 2. Additionally, two pairs of lower probability, yet still ranking 9th and 11th, D1248–S275 and A1250–S275 are found in the cluster as well, involving one additional residue from TamA barrel strand 1 (Table 4.2, "Cluster A" in Fig. 4.4). The ranks 5 to 7 are taken by the amino acid pairs V1007–K70, V1007–L168 and M1009–L172. The two residues involved from TamB are located approximately at quarter the DUF490 domain sequence. Residue 70 of TamA is located in POTRA domain 1 and residues 168 and 170 in POTRA domain 2 (Table 4.2, "Cluster B" in Fig. 4.4). Corresponding co-evolution analyses between any other region of TamB and full-length TamA do not reveal probable co-evolving amino acid pairs.

Table 4.2 Gremlin co-evolution scores of the eleven top-ranked intermolecular amino acid pairs.

Residue TamB	Residue TamA	Scaled Score*	Probability*	I_Probability*
D1252	R281	2.38	0.99	0.97
L1253	V272	2.30	0.99	0.96
E1258	T267	1.89	0.94	0.86
F1259	I268	1.83	0.93	0.84
V1007	K70	1.77	0.91	0.81
V1007	L168	1.59	0.84	0.69
M1009	L172	1.53	0.81	0.63
L1082	A556	1.39	0.71	0.50
D1248	S275	1.35	0.68	0.45
V1034	V260	1.32	0.66	0.42
A1250	S275	1.30	0.64	0.40

*As calculated by Gremlin (Ovchinnikov *et al.* 2014).

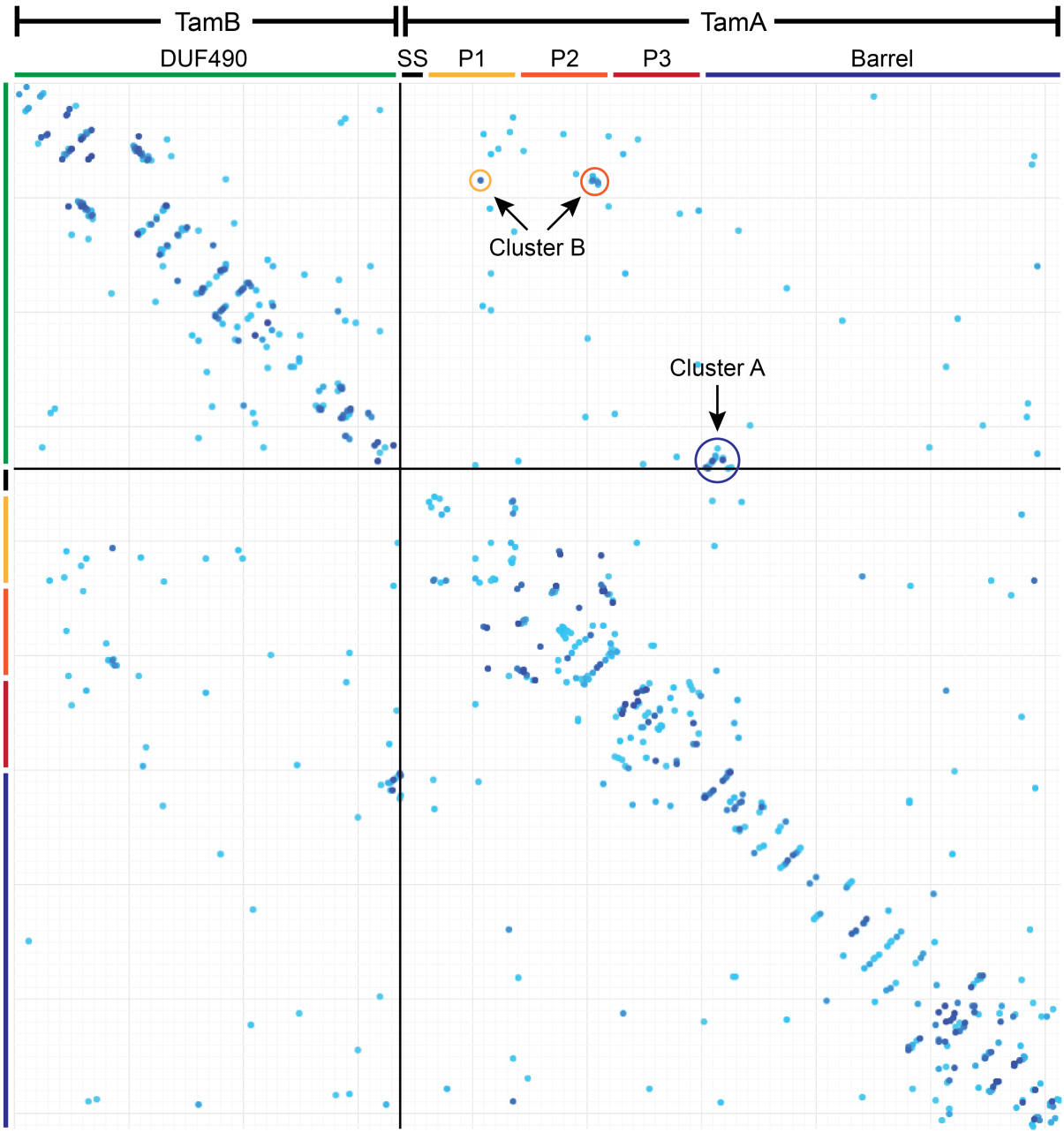

Figure 4.4 Co-evolution analysis of the TamB DUF490 domain and TamA.

Each large square represents 100 residues of the joined sequences TamB DUF490 – TamA as used for the multiple sequence alignment (MSA). The boundaries between the proteins in horizontal and vertical direction are indicated by black lines within the plot. The vertical and horizontal bars on the left-hand side and on top of the plot indicate the TamB DUF490 domain (“DUF490”, green), the TamA signal sequence (“SS”, black), TamA POTRA domain 1 (“P1”, yellow), TamA POTRA domain 2 (“P2”, orange), TamA POTRA domain 3 (“P3”, red), and the TamA barrel (“Barrel”, blue). Blue dots in the plot represent the amino acid pairs with the highest Gremlin scores. The darker the color of a dot, the higher the interaction probability. Intermolecular pairs of high interaction probability are encircled; “Cluster A” and “Cluster B” are indicated according to the text.

4.4. Discussion

4.4.1. Binding of TamB to TamA POTRA domains

TamA POTRA domains 1–3 bind strongly to TamB, with a very low dissociation constant, but TamA POTRA domain 1 alone does not bind TamB with detectable affinity. Furthermore, TamA POTRA domains have two distinct TamB binding modes. For both of these binding events the ITC measurements indicate that more than one TamB molecule bind to the POTRA domains. However, not all TamB molecules may be in a binding-competent state as implied by SEC profiles (Fig. 4.1). Therefore, the determined ratios represent upper limits and it cannot be excluded that binding occurs in a lower ratio, such as 1:1 for the second binding event.

The two binding modes observed in the ITC measurements are compatible with several scenarios. The most plausible model appears to be that initially an unfolded part at the C-terminus of TamB forms non-specific transient interactions via β-augmentation with all three POTRA domains under fast rearrangements. For such a binding mode, even a second TamB molecule may be involved, giving rise to the observed sub-stoichiometric ratio of POTRA domains to TamB molecules. The high affinity may therefore be an effect of avidity and the interactions would mainly involve hydrogen bonding. The second ITC transition would arise from specific binding of a presumably folded part of TamB DUF490 to a distinct site of the TamA POTRA domains. Moreover, folding of this part of the DUF490 domain may possibly be initiated by the transient initial binding. The specific binding sites of TamB and the TamA POTRA domains can be located using the results of the co-evolution analysis: Cluster B (Fig. 4.4) contains TamB residues V1007 and M1009 that interact with TamA residues K70, L168, L170, located at the hinge between POTRA domains 1 and 2 (Fig. 4.5a). The high amount of hydrophobic residues involved in interaction at these sites could be a possible explanation of the positive entropy change observed in the second transitions of the ITC measurements (Table 4.2). The involvement of residues L168 and L170 from POTRA domain 2 rationalizes the inability of POTRA domain 1 alone to bind TamB as observed by ITC. Importantly, this scenario would be in agreement with published data, showing that truncation of POTRA domain 1 also abolishes the TamA – TamB interaction (Selkrig *et al.* 2015).

4.4.2. Co-evolution suggests binding of the TamB C-terminus to the TamA barrel

The co-evolved residues in cluster A (Fig. 4.4) show that the C-terminus of TamB interacts with the TamA barrel in vicinity of strand 1. A structural explanation for this interaction would be an insertion of a hairpin from the TamB C-terminus between TamA strands 1 and 16

(Fig. 4.5), which would correspond to the first step of a hybrid barrel formation mechanism with an autotransporter substrate (Gruss *et al.* 2013).

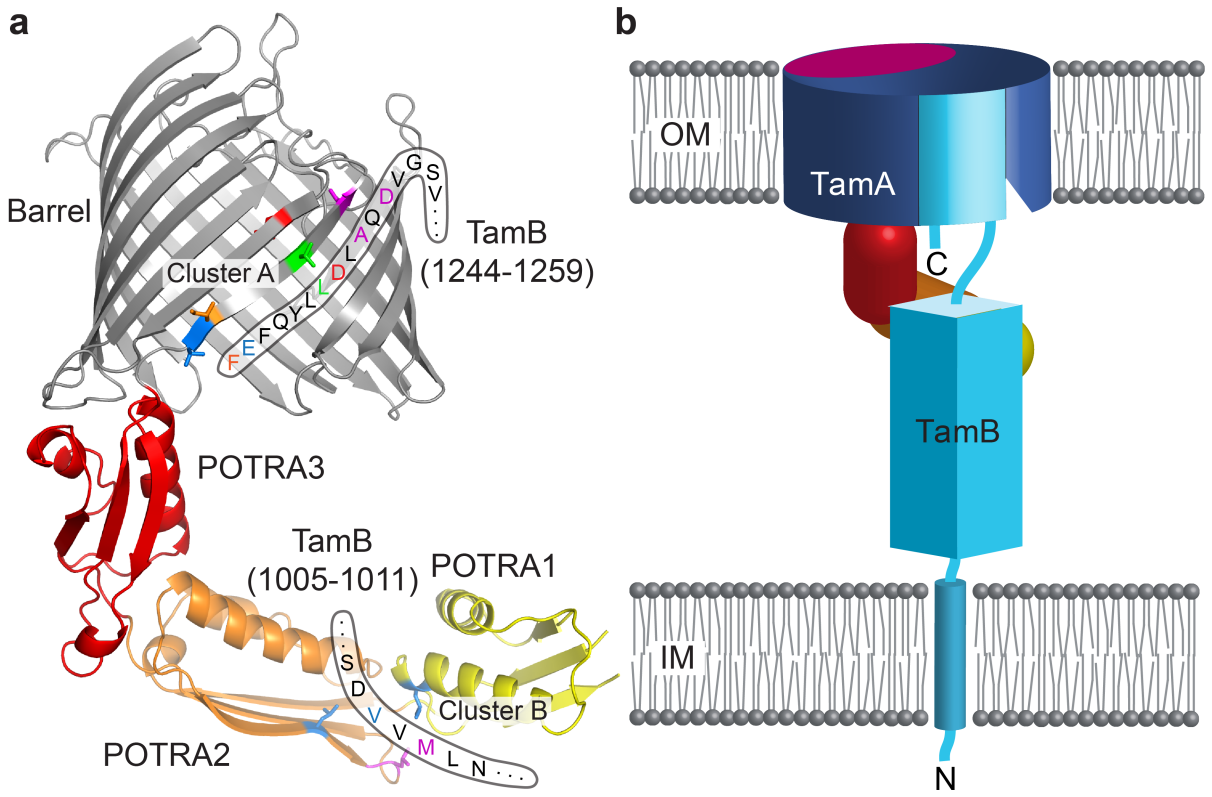

Figure 4.5 TamB – TamA interactions and a model for the TAM complex.
(**a**) Ribbon representation of TamA. The barrel is shown in grey, the POTRA domains in yellow – orange – red. Residues interacting with TamB, as suggested by co-evolution analysis, are colored and the side chains are shown as sticks. Segments of TamB, suggested to interact with TamA by co-evolution analysis, are shown next to TamA barrel strand 1 and POTRA domains 1 and 2. Residues in TamA and TamB that co-evolve are shown in the same color; "Cluster A" and "Cluster B" are indicated according to the text. (**b**) A possible model for the TAM complex. The C-terminus of TamB (cyan) would integrate into the TamA barrel (blue) between strands 1 and 16, while other residues of TamB are involved in interactions with the TamA POTRA domains (yellow – orange – red). The N-terminus of TamB spans the inner membrane as an α-helix.

Structurally, such an insertion is reasonable: Co-evolving residues in TamA include sidechains that head both to the membrane and the barrel interior. The side chains of the respective co-evolving residues in TamB would be located exactly next to the TamA side chains, if the C-terminus inserted as a strand into the TamA barrel with side chains alternatingly heading towards the barrel lumen and the membrane environment (Fig. 4.5a). Similar co-evolution between TamA strand 16 and the TamB C-terminus is not detected and, importantly, also for TamA strands 1 and 16 no intramolecular co-evolving residues are

found (Fig. 4.4). Therefore, the existence of co-evolving residues between TamA strand 16 and the TamB C-terminus is not necessarily expected. Since TamB is not a substrate of TamA and since it does not contain a predicted β-barrel, TamB could mediate a regulatory function for substrate selectivity by competing with incoming substrates for hairpin insertion into the TamA barrel.

The additional binding of TamB to the POTRA domains of TamA via cluster B (Fig. 4.4) may be important both for initial TamB hairpin insertion into the TamA barrel, since a TamA truncation variant lacking POTRA domain 1 fails to bind TamB (Selkrig *et al.* 2015), and during autotransporter substrate assembly: The autotransporter will displace the C-terminal TamB hairpin integrated into the TamA barrel when inserting its own β-barrel, but TamB can stay in proximity by interacting with the POTRA domains until the hybrid TamA – autotransporter barrel has disintegrated. The distance between the TamA POTRA binding site for TamB and the TamA barrel rim is about 4.5 nm, which could well be spanned by the ~250 residues between the two binding sites in TamB, if they adopted a β-helical structure.

MorC, the TamB homologue from *Aggregatibacter actinomycetemcomitans*, is important for the integrity of the cell envelope (Smith *et al.* 2015). The *E. coli* TAM complex in the proposed conformation where the C-terminus of TamB is bound to TamA and the N-terminal hydrophobic transmembrane helix is embedded in the IM (Fig. 4.5b) may thus plausibly also have a similar function in cell shape maintenance in addition to autotransporter biogenesis.

4.5. Methods

4.5.1. Plasmid construction

Full-length *E. coli* TamB was cloned into a pET21d vector (Novagen) by standard cloning methods. Briefly, the genomic *tamB* DNA was amplified from *E. coli* DH10β using the oligonucleotides 5'-CATGCCATGGCGAGTTTATGGAAAAAAATCAGCCTCGGCG-3' and 5'-CCGCTCGAGAAACTCGAACTGATAGAGCAAATCCAGTGC-3'. The empty vector and the PCR product were individually digested using restriction enzymes NcoI and XhoI (NEB). The digested vector and the *tamB* DNA were ligated using T4 DNA ligase (NEB) to yield the TamB expression vector. It encodes TamB in full-length with an additional Ala after the N-terminal Met and an additional sequence Leu-Glu followed by a His6-tag at the C-terminus.

E. coli TamA POTRA domains 1–3 and POTRA domain 1 alone were constructed similarly using oligonucleotides 5'-CATGCCATGGCGAACGTCCGTCTACAGGTCG-3' and 5'-CGGAATTCTCAGTGATGGTGATGGTGATGTGTTCGCGGCGAAACCACGCC-3' (POTRA1–3) resp. 5'-CGGAATTCTCAGTGATGGTGATGGTGATGCACGCCTGGCGTGA CTTTGGC-3' (POTRA1 alone) for PCR amplification from *E. coli* DH10β. The PCR products

and pET21d vector were digested using restriction enzymes NcoI and EcoRI. The digested DNA for TamA POTRA1 and TamA POTRA1–3 were ligated into pET21d to yield the POTRA1 and POTRA1–3 expression vectors. They encode TamA 21-102 resp. TamA 21-264 with an additional N-terminal Met and C-terminal His6-tag.

4.5.2. Expression and purification

TamA POTRA1–3 and TamA POTRA1 were expressed and purified according to the procedure described in Chapter 2.4.2 for a similar POTRA domains construct. Electrocompetent *E. coli* BL21(λ DE3) cells were transformed with the TamB expression plasmid. After growth of cells in LB medium at 37 °C to an OD_{600} of 0.4–0.6, the temperature was decreased to 20 °C. After 45 min to 1 h, expression of TamB was induced by addition of 0.1 mM IPTG. Expression continued overnight before cells were harvested, resuspended in 50 mM HEPES, pH 7.4, 150 mM NaCl and lysed.

Unbroken cells and cell debris were pelleted for 10 min at 10,000*g*, and the supernatant containing membrane vesicles was centrifuged for 1 h at 100,000*g*. The membrane pellet was resuspended in 50 mM HEPES, pH 7.4, 150 mM NaCl, 2% DDM, 5 mM β-mercaptoethanol (β-ME), 10% glycerol. The insoluble fraction was pelleted for 1 h at 100,000*g* and 4 °C, and the supernatant containing solubilized TamB was used for the further procedure.

Solubilized TamB including 10 mM imidazole was loaded onto a 5 mL HisTrap FF column (GE Healthcare), then washed with 20 mM HEPES, pH 7.4, 500 mM NaCl, 0.05% DDM, 10% glycerol, 5 mM β-ME and subsequently with 20 mM HEPES, pH 7.4, 150 mM NaCl, 0.05% DDM, 10% glycerol, 5 mM β-ME. TamB was eluted from the column with a gradient to 500 mM imidazole in the same buffer. Eluted TamB fractions were pooled and diluted 1:2 with 20 mM HEPES, pH 7.4, 10% glycerol and 0.05% DDM before being loaded onto a 6 mL column containing PL-SAX anion exchange resin (4000 Å, 10 µm, Agilent). After the column was washed with 20 mM HEPES, pH 7.4, 50 mM NaCl, 10% glycerol, 5 mM β-ME and 0.05% DDM, the protein was eluted with a gradient from 50 mM to 500 mM NaCl in the same buffer. Eluted TamB fractions were pooled. TamB sample was cleaned from aggregates by centrifugation before it was gel-filtered on a Superose 6 or 12 10/300 GL column (GE Healthcare) in 20 mM HEPES, pH 7.4, 150 mM NaCl, 5% glycerol, 5 mM DTT and 0.05% DDM. Eluted TamB fractions were analyzed by SDS-PAGE, then pooled, but avoiding fractions from the void volume peak, and finally concentrated to the desired concentration for the respective purpose with 30 kDa c/o centrifugal units.

4.5.3. Analytical size exclusion chromatography

For co-migration runs on a Superose 12 10/300 GL column (GE Healthcare), TamB was used at a concentration of 4.4 mg mL^{-1} (32 µM) and TamA POTRA1–3 at 4.5 mg mL^{-1} (159 µM). Runs were performed with either of the two proteins and both in combination in 20 mM HEPES pH 7.4, 150 mM NaCl, 5% glycerol, 0.05% DDM and 5 mM DTT.

4.5.4. Isothermal titration calorimetry

For ITC experiments the purified POTRA constructs were dialyzed in a volume ratio of at least 1:200 against 20 mM HEPES, pH 7.4, 150 mM NaCl, 5% glycerol, 5 mM DTT and 0.05% DDM, using dialysis cassettes with a MW c/o of 3 kDa. ITC measurements were performed at 10 °C using a VP-ITC MicroCalorimeter (Malvern). About 2 mL of TamB solution at a concentration of 5 µM was used for the 1.415 mL cell. TamA POTRA domain 1 and POTRA domains 1–3 were used at concentrations of 35 or 50 µM. The first compensation injection of 1 µl was excluded from the data processing. 29 more injections of 10 µl volume were performed each in 20 s and in intervals of 5 min. Data was evaluated with the ITC data analysis software Origin 7 (OriginLab, Northamton, MA, USA).

4.5.5. Co-evolution analysis

For co-evolution analysis of the C-terminal TamB DUF490 domain and full-length TamA, the Gremlin server (http://gremlin.bakerlab.org) was used (Ovchinnikov *et al.* 2014). The full-length *E. coli* TamA sequence and *E. coli* TamB residues 923-1259 were provided. To generate the multiple sequence alignment (MSA) HHblits was chosen, the E-values for both sequences were set to 10^{-2} and for each 8 iterations were performed. The minimal and maximal values for Δgene were set to 1 and 20, which means that sequence pairs are only considered for the MSA if the distance between the genes corresponding to the submitted protein sequences on a genome lies within these thresholds.

CHAPTER 5:

Conserved Omp85 Lid-Lock Structure and Substrate Recognition in FhaC

Reproduced from:

Nature Communications, 6:7452; June, 10th 2015

Conserved Omp85 lid-lock structure and substrate recognition in FhaC.

Timm Maier, Bernard Clantin, Fabian Gruss, Frédérique Dewitte, Anne-Sophie Delattre, Françoise Jacob-Dubuisson, Sebastian Hiller and Vincent Villeret

DOI 10.1038/ncomms8452

5.1. Abstract

Omp85 proteins mediate translocation of polypeptide substrates across and into cellular membranes. They share a common architecture comprising substrate-interacting POTRA domains, a C-terminal 16-stranded β-barrel pore and two signature motifs located on the inner barrel wall and at the tip of the extended L6 loop. The observation of two distinct conformations of the L6 loop in the available Omp85 structures previously suggested a functional role of conformational changes in L6 in the Omp85 mechanism. Here we present a 2.5 Å resolution structure of a variant of the Omp85 secretion protein FhaC, in which the two signature motifs interact tightly and form the conserved 'lid lock'. Reanalysis of previous structural data shows that L6 adopts the same, conserved resting state position in all available Omp85 structures. The FhaC variant structure further reveals a competitive mechanism for the regulation of substrate binding mediated by the linker to the N-terminal plug helix H1.

5.2. Introduction

Omp85 proteins, such as the general *Escherichia coli* insertase BamA and the mitochondrial Sam50, are responsible for the insertion of β-barrel membrane proteins into the outer membranes of Gram-negative bacteria, mitochondria and chloroplasts (Chacinska *et al.* 2009, Kim *et al.* 2007, Walther *et al.* 2009). In Gram-negative bacteria, Omp85 family members also act as translocases (TpsB) for the secretion of specific partner proteins (TpsA) across the outer membrane (Fan *et al.* 2012, Poole *et al.* 1988). Such two-partner-secretion (TPS) systems are commonly contributing to bacterial pathogenicity (Jacob-Dubuisson *et al.* 2001, Yen *et al.* 2002). One of the best-studied TPS systems comprises the translocase FhaC and its substrate filamentous hemagglutinin (FHA), which is functionally involved in virulence and biofilm formation in *Bordetella pertussis* (Serra *et al.* 2011). Crystallographic structure determination of FhaC has provided the first depiction of the general Omp85 architecture (Clantin *et al.* 2007). This architecture builds upon a C-terminal, membrane-integrated β-barrel with 16 strands and up to six N-terminal POTRA domains directly attached to it. In FhaC, the two POTRA domains are involved in substrate recognition (Delattre *et al.* 2011), while the barrel forms a translocation pore for FHA secretion (Baud *et al.* 2014). The FhaC pore in its crystallized state is plugged with an N-terminal helical extension, the H1 helix, which is absent in Omp85 insertases but generally found in TpsB transporters.

The mechanism of Omp85-mediated protein insertion had remained enigmatic until the recent structure determinations of bacterial BamA and TamA (Gruss *et al.* 2013, Ni *et al.*

2014, Noinaj *et al.* 2013). BamA and TamA are characterized by an unusually weak connection between their β-strands 1 and 16, which facilitates unzipping and inward kinking of strand 16. A lipid head group occupies the position of the displaced strand in the 2.3 Å crystal structure of TamA, demonstrating the formation of a gate towards the lipid phase (Gruss *et al.* 2013). Molecular dynamics simulations of BamA recognized a distorted lipid bilayer around the kink and suggest that the initial gate promotes further unzipping up to a complete lateral barrel opening (Noinaj *et al.* 2013). The functional requirement for unzipping of strands 1 and 16 was elegantly demonstrated for BamA by disulfide bond trapping (Noinaj *et al.* 2014).

The barrels of BamA and TamA are tightly closed on the extracellular side by a lid, which is mainly formed by the large extracellular loop L6. This arrangement brings the two most conserved sequence motifs in the entire Omp85 family in close contact. These motifs are located at the tip of L6, and in the central inner barrel wall, respectively (Delattre *et al.* 2010, Gruss *et al.* 2013, Jacob-Dubuisson *et al.* 2013, Noinaj *et al.* 2013). To emphasize the nature of the strong interactions between these two motifs and its role for the lid conformation, the emerging structural feature has been termed the 'lid lock' (Gruss *et al.* 2013). Despite the pronounced sequence conservation, the conformation of the L6 loops in the Omp85 insertases is drastically different from the one observed in the crystal structure of FhaC, where loop L6 reaches to the periplasmic face of the barrel (Clantin *et al.* 2007).

On the basis of the available structural insights, several models have been formulated for the Omp85 mechanism (van den Berg 2013), involving lateral gating (Gruss *et al.* 2013, Noinaj *et al.* 2013), hybrid barrel formation (Gruss *et al.* 2013, Kim *et al.* 2012), alteration of the lipid bilayer structure (Gessmann *et al.* 2014, Noinaj *et al.* 2013) and conformational switching of POTRA domains and the L6 lid loop for pore opening and substrate transport (Clantin *et al.* 2007, Noinaj *et al.* 2013). Here we present the 2.5 Å resolution structure of the FhaC variant (V169T,I176N), which is characterized by disrupted substrate recognition and referred to as '$FhaC_{DIS}$' (disruption). The data provide evidence for the general conservation of the L6 loop conformation, and thus a new perspective on the role of the lid-lock arrangement in pore opening and substrate translocation. The mutant structure resolves interactions of the H1 plug helix and its linker with the pore and the POTRA domains as a structural basis for the dynamic plugging mechanism of FhaC.

5.3. Results and Discussion

5.3.1. Intermolecular helix swap in the $FhaC_{DIS}$ crystal structure

$FhaC_{DIS}$ carries two point mutations, V169T and I176N, which locate to the POTRA2 domain and abolish the secretion activity of FhaC due to a disruption of POTRA2–substrate

interaction (Delattre *et al.* 2011). $FhaC_{DIS}$ was crystallized from micelles in space group $C222_1$, isomorphous to wild-type (WT) FhaC crystals, but with considerably better diffraction than previous WT- or mutant FhaC crystals (Clantin *et al.* 2007, Delattre *et al.* 2010). The structural model of $FhaC_{DIS}$ was refined to R_{work}/R_{free} of 21.7% / 25.9% at 2.5 Å resolution (Table 5.1). It comprises the N-terminal extension helix H1, connected via a 25-residue linker to two POTRA domains and a C-terminal 16-stranded β-barrel (Fig. 5.1a). In contrast to previous FhaC structures (Clantin *et al.* 2007, Delattre *et al.* 2010), the register of the H1 helix was unambiguously determined from side-chain electron density. The polypeptide linker between POTRA1 and helix H1 in $FhaC_{DIS}$ was found to be well ordered. Tracing of the linker revealed that in the current crystal structure two adjacent $FhaC_{DIS}$ molecules form an intermolecularly swapped dimer via exchange of their helices H1 (Fig. 5.1b,c).

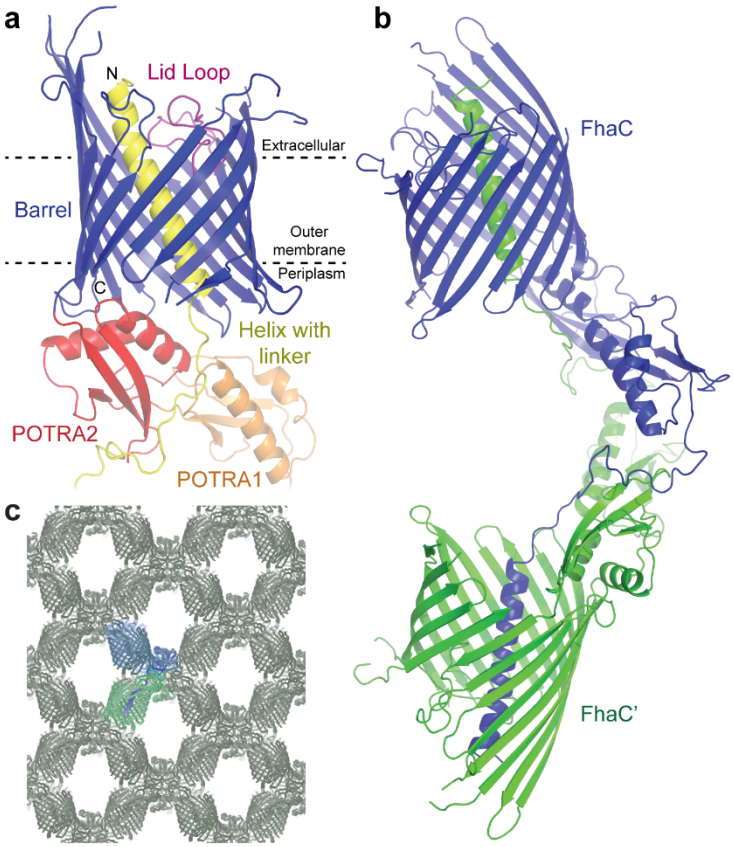

Figure 5.1 Structure and crystal packing of $FhaC_{DIS}$.
(**a**) Structural overview. Individual protein domains are colour-coded: Helix H1 with linker, yellow; POTRA1, orange; POTRA2, red; Barrel, blue; Lid Loop, magenta. (**b**) Formation of a swapped dimer in crystals of $FhaC_{DIS}$ by exchange of helix H1. The two crystallographically related protein molecules involved in swapping are coloured blue and green, respectively. (**c**) Crystal packing of $FhaC_{DIS}$. Two molecules equivalent to b are shown in the respective colours.

The $FhaC_{DIS}$ structure triggered a reanalysis of the previous 3.15 Å resolution WTFhaC data, which were reprocessed from raw images to 2.9 Å resolution using state-of-the-art techniques. Reinterpretation of the WTFhaC diffraction data on the basis of the $FhaC_{DIS}$ structure clearly revealed modelling ambiguities in the previous WTFhaC structure (PDB entry 2QDZ (Clantin *et al.* 2007), referred to as '$WTFhaC_{old}$') and yielded a revised model of WTFhaC (referred to as '$WTFhaC_{new}$').

Table 5.1 Data collection and refinement statistics.

	$WTFhaC_{new}$	$FhaC_{DIS}$
Data collection		
Space group	C 2 2 21	C 2 2 21
Cell dimensions		
a, *b*, *c* (Å)	108.60, 136.65, 112.27	106.38, 136.95, 110.97
α, β, γ (°)	90, 90, 90	90, 90, 90
Resolution (Å)	50 – 2.90 (2.95 – 2.90) *	50 – 2.50 (2.55 – 2.50)
R_{sym} or R_{merge}	0.090 (0.847)	0.057 (0.886)
I / σI	19.88 (3.28)	23.04 (2.13)
CC(1/2) (%)	99.8 (75.6)	99.9 (68.9)
Completeness (%)	98.8 (98.3)	99.7 (99.9)
Redundancy	10.90 (10.70)	4.91 (4.93)
Refinement		
Resolution (Å)	39.34 – 2.90	41.95 – 2.50
No. reflections	18626	28332
R_{work} / R_{free}	0.222 / 0.279	0.217 / 0.259
No. atoms	3731	4474
Protein	3726	4095
Ligand/ion	5	304
Water	-	75
B-factors		
Protein	91.4	78.9
Ligand/ion	78.8	77.6
Water	-	63.8
R.m.s. deviations		
Bond lengths (Å)	0.010	0.010
Bond angles (°)	1.09	1.08

*Values in parentheses are for highest-resolution shell.

5.3.2. Comparison of FhaC structural models: H1 linker and L6 loop

To clarify these differences, we compare the three structural models of WTFhaC$_{old}$, WTFhaC$_{new}$ and FhaC$_{DIS}$ in Fig. 5.2a–c. The structural models feature relevant differences in three regions: (i) The register of helix H1 in FhaC$_{DIS}$ and WTFhaC$_{new}$ is shifted by three residues relative to the partly modelled H1 helix of WTFhaC$_{old}$. (ii) The linker segment between POTRA1 and helix H1 (residues 33–58) is well-ordered in FhaC$_{DIS}$, but largely disordered in WTFhaC$_{old}$ and WTFhaC$_{new}$. Due to the isomorphous nature of the crystals, the intermolecular swap of helix H1 between two crystallographically related molecules of FhaC is also the most likely explanation for the WTFhaC crystal packing and therefore the assignments of helix H1 and the symmetry-related helix H1' have been swapped in WTFhaC$_{new}$ relative to WTFhaC$_{old}$. (iii) The positioning and structure of loop L6 and the adjacent strand is well-resolved in FhaC$_{DIS}$ in contrast to WTFhaC$_{old}$. FhaC$_{DIS}$ differs from WTFhaC$_{old}$ by a massive register shift in loop L6 and the following strand 12 and a concomitant change in the position of the tip of loop L6 by 17 Å (Fig. 5.2 and 5.3, Supplementary Fig. 5.1).

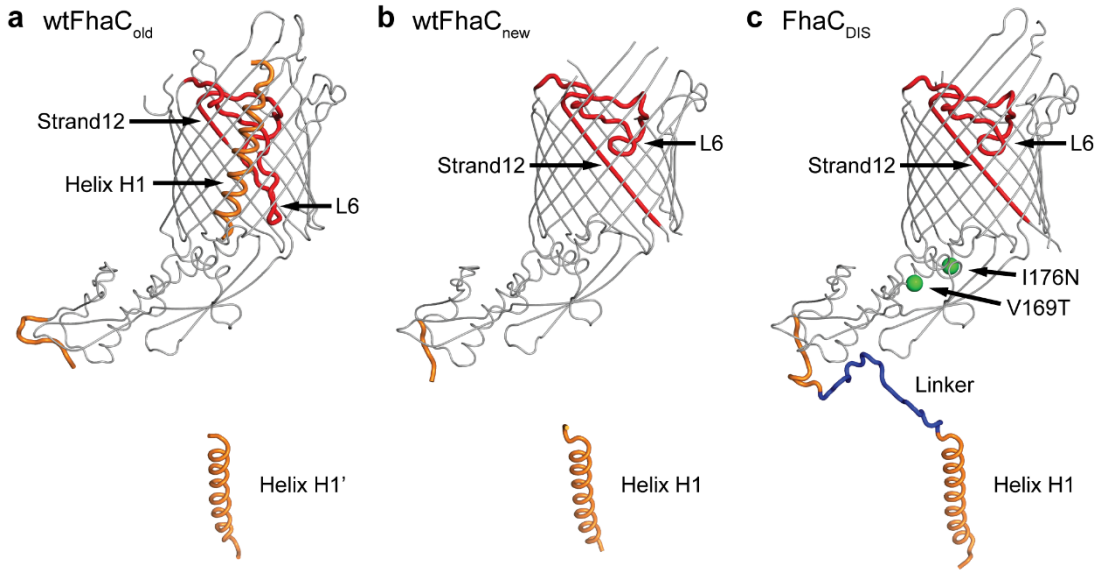

Figure 5.2 Overall comparison of FhaC$_{DIS}$ and WTFhaC structural models.
The structural models of (**a**) superseded WTFhaC$_{old}$, (**b**) WTFhaC$_{new}$ and (**c**) FhaC$_{DIS}$ are shown in backbone representation. Strand12 and lid loop L6 (red), helix H1 and its linker (orange, blue for the linker segment disordered in WTFhaC$_{new}$) are shown thick and in colour. For the superseded WTFhaC$_{old}$ structure, the symmetry-related helix H1' is shown to indicate that it has the same position as H1 in WTFhaC$_{new}$ and FhaC$_{DIS}$. For FhaC$_{DIS}$, the locations of the V169T and I176N mutations are indicated by green spheres.

In WTFhaC$_{old}$, loop L6 was depicted in a conformation, where its tip touches the periplasmic rim of the barrel (cyan conformation in Fig. 5.3a), but in the 2.5 Å resolution FhaC$_{DIS}$ structure the tip of loop L6 touches the inner side of the barrel wall at strand 13 (magenta conformation in Fig. 5.3a, Supplementary Fig. 5.2). In particular, this 'lid lock' conformation of loop L6 describes the WTFhaC data unambiguously better than the periplasmic conformation in WTFhaC$_{old}$, as directly evidenced by omit maps calculated for these two conformations against the respective data sets (Fig. 5.3b–e) and has thus been adopted in WTFhaC$_{new}$. We discuss the relevance of the L6 loop positioning for FhaC and Omp85 biology in general in the following.

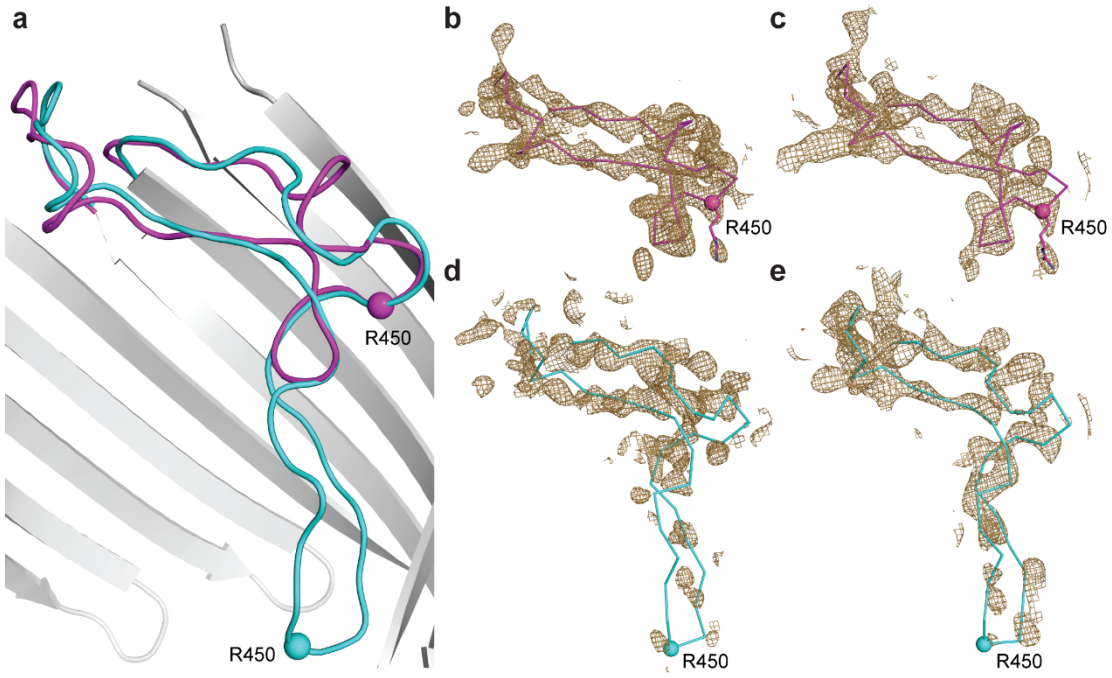

Figure 5.3 Comparison of L6 conformations in FhaC$_{DIS}$ and WTFhaC$_{old}$.
(**a**) Superposition of L6 loop conformations in the superseded WTFhaC$_{old}$ structure (cyan, PDB entry 2QDZ (Clantin *et al.* 2007)) and the FhaC$_{DIS}$ structure (magenta, PDB entry 4QL0; this work). Grey: The barrel of the FhaC$_{DIS}$ structure. (**b**–**e**) Simulated annealing composite omit maps for different combinations of structures and diffraction data. Maps are shown at 1.5σ contour level in a radius of 2.5 Å around atoms belonging to the L6 loop and are calculated based on (**b**) FhaC$_{DIS}$ model and the FhaC$_{DIS}$ diffraction data. (**c**) FhaC$_{DIS}$ model and WTFhaC diffraction data. (**d**) Superseded WTFhaC$_{old}$ model and FhaC$_{DIS}$ diffraction data. (**e**) Superseded WTFhaC$_{old}$ model and WTFhaC diffraction data.

5.3.3. A conserved lid-lock structure in the Omp85 family

In the WTFhaC$_{new}$ and the FhaC$_{DIS}$ structures, the two signature motifs (V/I)RG(Y/F) at the tip of the loop L6 and (F/G)xDxG in the inner barrel wall on strand 13 are in close spatial contact and interact directly via a salt bridge between the conserved central residues R450

and D492. This 'lid lock' formation is closely related to those previously found for TamA and BamA (Fig. 5.4a,b) (Gruss *et al.* 2013, Ni *et al.* 2014, Noinaj *et al.* 2013).

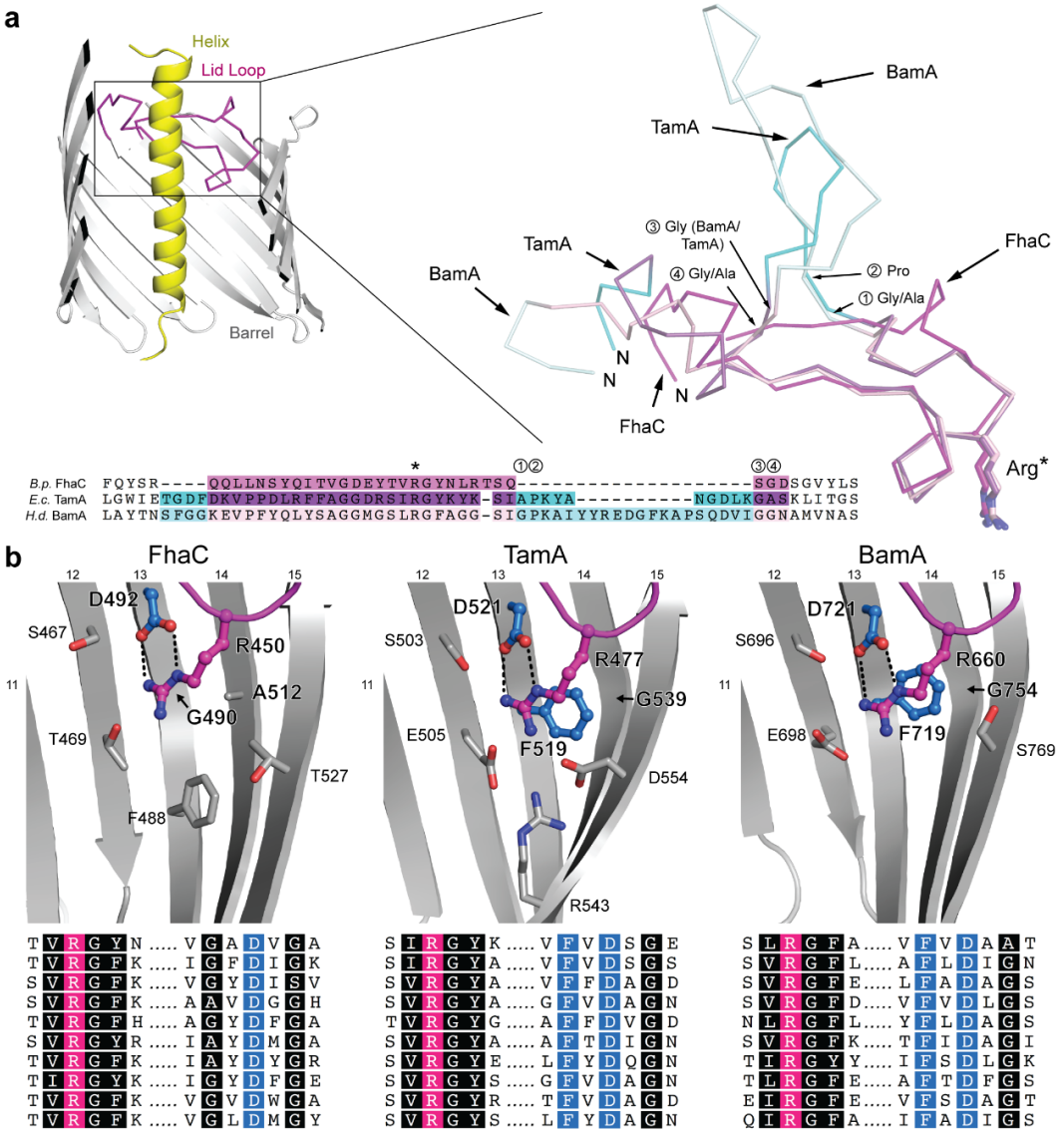

Figure 5.4 Conformation of loop L6 in the Omp85 family.

(**a**) Cross-section through FhaC and structural and sequence alignment of L6 in *B. pertussis* FhaC (PDB entry 4QL0; this work), *E. coli* TamA (PDB entry 4C00 (Gruss *et al.* 2013)) and *H. ducreyi* BamA (PDB entry 4K3C (Noinaj *et al.* 2013)). Yellow: helix, grey: barrel. Conserved regions of L6 are shown in magenta, purple and light magenta for FhaC, TamA and BamA, respectively; loop extensions in TamA and BamA in cyan and light cyan, respectively. (**b**) Variations in the signature motifs correlate to barrel shape alterations in FhaC (left), TamA (center) and *H. ducreyi* BamA (right). Loop L6 and the barrel are coloured magenta and grey, respectively. Selected side chains are shown as sticks, highly conserved residues as ball-and-stick. Lower panel: Sequence alignments of signature motifs for 10 representative members of the FhaC (TpsB), TamA and BamA families, respectively (see Methods). The conserved arginine of the (V/I)RG(Y/F) motif is highlighted by magenta, the conserved interacting aspartate and phenylalanine of the (G/F)xDxG by blue. Other motif residues are indicated in black.

Interestingly, the arrangement of the entire lid loop is not even affected by the presence of a variable insertion site in loop L6, which can incorporate up to 30 additional amino-acid residues in TamA and BamA. In *B. pertussis* FhaC, the insertion region contains only two residues, which structurally bridge the insertion point in the shortest possible way (Fig. 5.4a). In *Haemophilus ducreyi* BamA and *E. coli* TamA, the insertion site is flanked by glycine or alanine residues, which permit a sharp outward kinking of the entire insert region (Fig. 5.4a, Supplementary Fig. 5.3). In consequence, the entire conserved regions of the L6 loop adopt almost identical conformations as demonstrated by very low backbone rmsd values (FhaC:TamA: 1.21 Å, FhaC:BamA: 1.37 Å; insertions excluded). The L6 loop is thus structurally conserved in all structures of Omp85 known so far, including the BamA insertase and the FhaC translocase, strongly suggesting a general functional role of the 'lid lock' region for protein translocation and insertion in the entire Omp85 family.

5.3.4. Structural variations around the lid lock

A key difference between FhaC and BamA/TamA is the presence of the N-terminal helix H1 in FhaC, which plugs the FhaC pore by traversing the entire length of the barrel. Two structural adaptations of FhaC relative to BamA/TamA pave the way for complete insertion of H1: first, the loops L3 and L4 are opened up in FhaC, whereas they tightly interact with L6 to close the extracellular face of the barrel in BamA/TamA (Fig. 5.5a,b). Second, FhaC features a wider and rounder barrel shape, which enlarges the pore at the periplasmic face relative to the kidney-shaped structures of BamA and TamA.

The $FhaC_{DIS}$ and $WTFhaC_{new}$ structures indicate an involvement of the lid-lock motif on strand 13 in barrel shape determination: The sequence motif on strand 13 has the form FxDxG in TamA/BamA, but GxDxG in FhaC proteins (Fig. 5.4b). In TamA and BamA insertases, the central arginine of the (V/I)RG(Y/F) motif stacks on top of the phenylalanine residue of the FxDxG motif. This phenylalanine side chain bends towards a conserved glycine residue of neighboring strand 14 (G539/G754 in TamA/BamA). Accommodation of the phenylalanine side chain requires a pronounced bend in strand 14, which correlates with a strongly curved region of the barrel.

In contrast, FhaC features a glycine as the first residue in its GxDxG motif and additionally, strand 14 contains a conserved alanine (A512) at the adjacent position (Fig. 5.4b). These two adaptations in FhaC permit lid-lock formation without requiring a bend of strand 14. They may contribute to an inherently expanded barrel shape, which prepares FhaC for helix H1 insertion, although a contribution of the H1 insertion itself to barrel shape alterations cannot be ruled out. The FhaC structure describes an Omp85 conformation, in which a polypeptide – not a native substrate, but the H1 plug helix – can traverse an Omp85

pore without release of the conserved lid-lock structure.

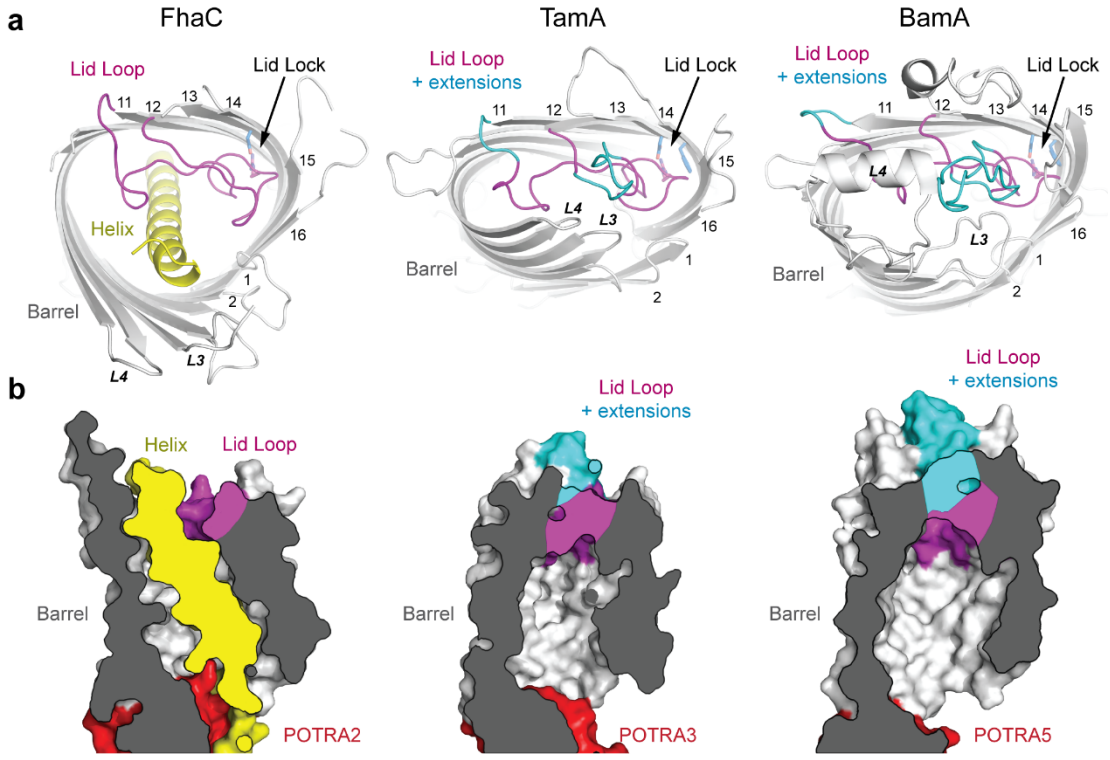

Figure 5.5 Barrel shape, lid lock and H1 helix insertion in FhaC.
(**a**) Top-view ribbon representation of the barrels of *B. pertussis* FhaC (left; PDB entry 4QL0; this work), *E. coli* TamA (center; PDB entry 4C00 (Gruss *et al.* 2013)) and *H. ducreyi* BamA (right; PDB entry 4K3C (Noinaj *et al.* 2013)). The β-barrels are shown grey, the helix of FhaC is shown yellow. Using the same colour code as in Fig. 5.4, conserved regions of loop L6 are shown in magenta, extensions of L6 in TamA and BamA relative to FhaC are shown in cyan. (**b**) Cross-sectional surface representation of the barrels of *B. pertussis* FhaC (left), *E. coli* TamA (center) and *H. ducreyi* BamA (right), in the same colour code. POTRA domains are shown in red.

5.3.5. Intermolecular swapping occurs in a defined linker region

Previous biochemical experiments have shown that the N-terminal helix H1 of FhaC acts as a dynamic plug, which spontaneously inserts into the barrel lumen of FhaC both in lipid vesicles and *in vivo* and occupies its central pore (Guérin *et al.* 2014). In the absence of substrates, helix H1 preferentially traverses the FhaC pore in a defined, rigid conformation and extends its N-terminus into the extracellular space, while blocking channel activity. On substrate transport it is released from the pore and is flexibly posed on the periplasmic face of the membrane in the vicinity of the POTRA domains (Guérin *et al.* 2014). The interaction mode of a swapped dimer in the crystal structure of $FhaC_{DIS}$ is not compatible with a native-like topology of the bacterial outer membrane (Fig. 5.1b,c). However, the unswapped form

would correspond to a state of H1, which has all characteristics of the resting, plugged state of FhaC.

From an inspection of the structure, we suggest that the swapping occurs in the 15 amino-acid region between residues 42 and 58 (Fig. 5.6), because all linker residues N-terminal to this segment remain in direct interaction with POTRA2 and all linker residues C-terminal to this segment remain in close contact to POTRA1 (Fig 5.6a,b). The role of residue 58 as a fixed anchor for the H1 linker agrees well with all available data: In reconstituted systems of FhaC transport, the mobility of residue 58 is not altered by substrate addition (Guérin *et al.* 2014) and in many FhaC-related TpsB proteins, residue 58 is mutated to a cysteine and presumably disulfide bonded to a nearby cysteine residue in POTRA1 (Guérin *et al.* 2014) (Supplementary Fig. 5.3).

In the crystallographic intermolecularly swapped dimer, the distance between the two ends of the segment 42–58 is only 21 Å, which is spanned by the 15-residue polypeptide segment in a crouched conformation. The corresponding distance for an intramolecular H1 – barrel interaction has a length of 39 Å, which could still be spanned by the 15-residue segment in a more extended conformation (Fig. 5.6a). Presumably, the shorter intermolecular swapping conformation was preferentially selected by crystal packing. The fact that the native membrane topology would readily prevent the existence of the swapped dimer configuration observed in the crystal, explains the lack of selective pressure on the linker segment to prevent such an arrangement.

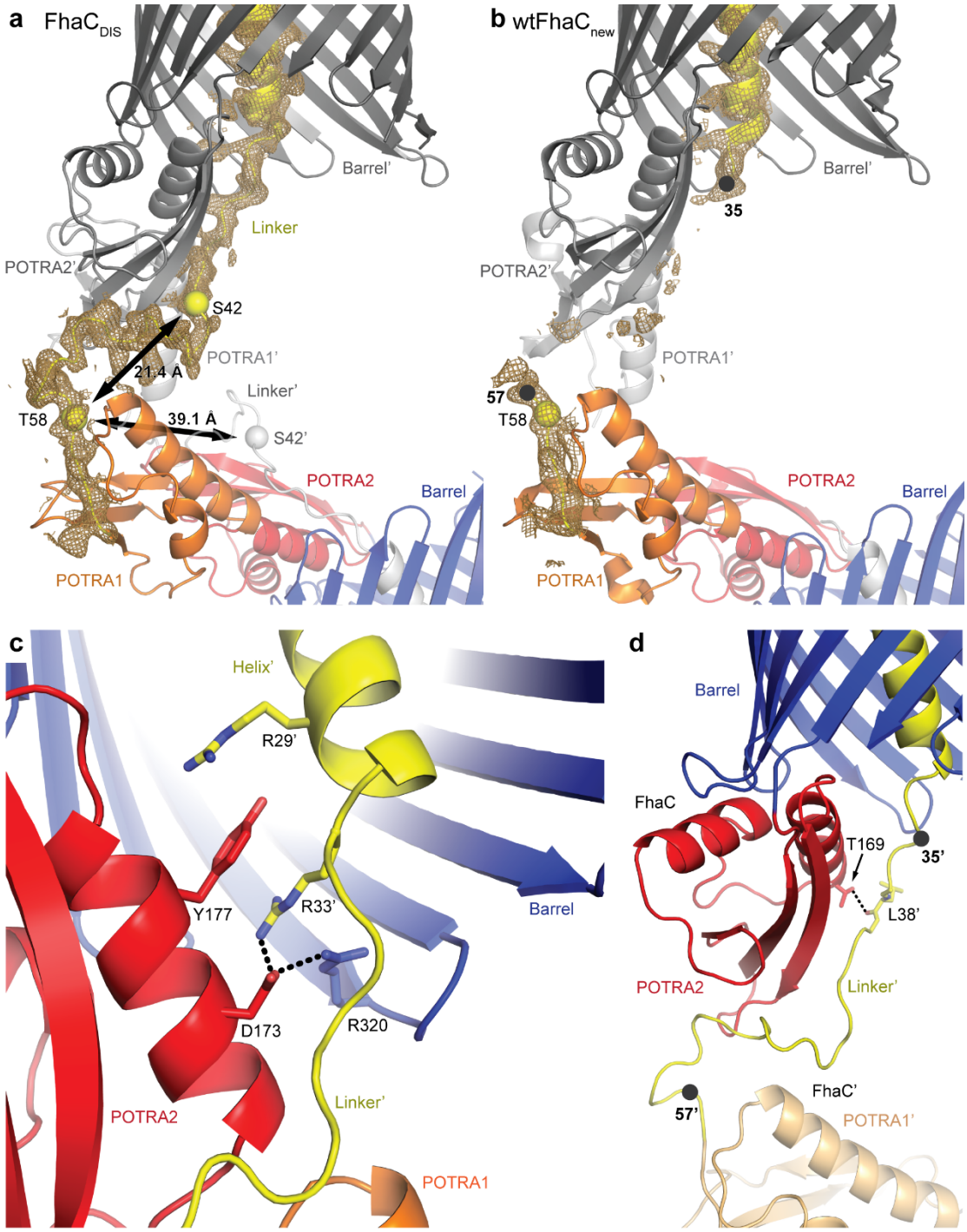

Figure 5.6 FhaC$_{DIS}$ linker and helix H1 interactions.

(**a**) $2F_oF_c$ map for FhaC$_{DIS}$ shown in a radius of 2.5 Å around atoms belonging to the linker (yellow) at 1σ contour level. Residues Ser42 and Thr58, which encompass the domain-swapping segment are shown as yellow spheres. (**b**) $2F_oF_c$ map for WTFhaC shown in the same region as for FhaC$_{DIS}$ at 1σ contour level. Residues 35 and 57, which encompass the disordered linker segment are shown as black spheres. (**c**) Interactions at the C-terminus of the helix including cation-π stacking and salt bridges. (**d**) Ribbon representation of the linker region in FhaC$_{DIS}$ showing the hydrogen bond between Leu38 and the mutated Thr169. For comparison, the linker region disordered in WTFhaC is indicated by black spheres for residues 35 and 57.

5.3.6. Competitive interplay of substrates and the H1 plug helix

The $FhaC_{DIS}$ structure, together with published biochemical and biophysical studies, rationalizes the plugging mechanism of TpsB proteins. The H1 helix comprising residues 1–32 shows numerous interactions with the barrel wall, including 5 salt bridges, 12 hydrogen bonds and a total interaction interface of 988 $Å^2$. Yet, this interaction interface almost completely lacks elements of side-chain interlocking, which would hinder a sliding of H1 along the barrel wall (Supplementary Fig. 5.4). The $FhaC_{DIS}$ structure now points to a key role of the N-terminal residues 29–38 for defining H1 interactions (Fig. 5.6c). In this segment, Arg33 is positioned by a salt bridge to Asp173, providing an interdigitation of side chains by stacking between Tyr177 of POTRA2 and Arg320 at the periplasmic rim of the barrel. Arg29 of the terminal winding of H1 may contribute to this interaction by stacking to the other face of Tyr177.

In $WTFhaC_{new}$, the polypeptide region 36–56 is disordered and thus remains structurally unresolved (Fig. 5.6a,b). In contrast, in $FhaC_{DIS}$ carrying the (V169T,I176N) double mutation, the full linker is ordered. In fact, Leu38, the third residue of the segment that is disordered in $WTFhaC_{new}$, directly interacts in $FhaC_{DIS}$ with the mutated residue Thr169 by formation of a hydrogen bond between the Leu38 backbone-N and the Thr169 side chain-OH (Fig. 5.6d). Apparently, this interaction triggers ordering also of the entire segment, where residues 39 to 42 are involved in further interactions with the same POTRA2 domain.

Biochemical data clearly indicate that the observed interactions around residues 33 and 38 (Fig. 5.6c,d) play a key role for the functional mechanism of FhaC. The double mutation (V169T,I176N), which was designed to interfere with β-augmentation substrate interactions of POTRA2, not only abolishes transport, but directly interferes with substrate interaction (Delattre *et al.* 2011); it thus affects a direct substrate binding site. We hypothesize that also in WTFhaC, the linker region 33–38 interacts at least transiently with the region around residues V169 and I176 on POTRA2. The H1 linker could thus be displaced by substrate binding, resulting in a destabilization of the contacts that lock the position of helix H1 to the barrel around residue Arg33. Indeed, EPR-based mobility assays on membrane-inserted FhaC have demonstrated a direct effect of substrate interaction on the mobility of residue 33 (Guérin *et al.* 2014): This residue is mostly immobile in the absence of a substrate and even remains partly immobile on deletion of the entire downstream H1 helix, demonstrating an inherent H1-independent component of tethering to POTRA1. In both cases, with and without H1, substrate addition drastically increases the mobility of residue 33. Altogether, this mechanism directly couples substrate binding to a preferential release of helix H1 into the periplasm (Fig. 5.7).

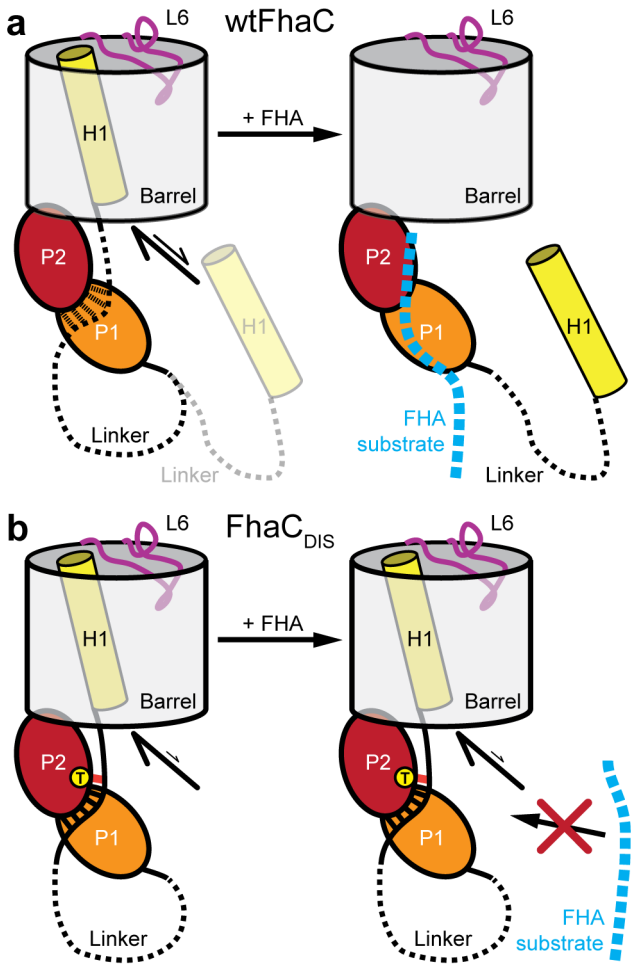

Figure 5.7 Plug helix H1 release mechanism of FhaC.
(**a**) In WTFhaC, the linker interacts weakly with POTRA domain 2, and the helix is preferentially inside the barrel. On substrate arrival, FHA competes with the linker for interaction with POTRA2, extruding the helix from the barrel and allowing the substrate to be transported. (**b**) In FhaC$_{DIS}$, the introduced hydrogen bond between Leu38 and Thr169 leads to stronger interactions between the linker and POTRA2, with which an arriving substrate cannot compete and thus will not be transported.

While recent structural and functional studies have provided important insights into Omp85 function, the underlying principles of the distinct translocase and insertase function remain unknown. The crystal structure of FhaC$_{DIS}$ now demonstrates a general structural conservation of the signature motifs in the lid-lock region in translocases and insertases of the Omp85 family. It also correlates variations in the signature sequences to the wider barrel shape of FhaC, which permits passage of the plug helix H1 all the way through the pore while the lid lock is formed.

Altogether with detailed previous studies on substrate interaction and FhaC mobility, the FhaC$_{DIS}$ structure reveals a competitive mechanism for coupling of substrate recognition and plug helix release. Most TpsB proteins are predicted to harbour a helical segment followed

by a disordered region at the N-terminus (Guérin *et al.* 2014). It is therefore probable that the mechanism revealed by this study will prove generally relevant to two-partner secretion. FhaC and related TPS systems play a prominent role in bacterial pathogenesis; identification of the competitive plugging mechanism may ultimately expose a novel target site for fighting bacterial infection.

5.4. Methods

5.4.1. Protein production and purification

The plasmid pFJD138–V169T–I176N, which encodes $FhaC_{DIS}$ with an N-terminal His6-tag (Delattre *et al.* 2011), was used to produce $FhaC_{DIS}$ for crystallization experiments. *E. coli* BL21(λ DE3)-omp5 transformed with pFJD138–V169T–I176N were grown at 37 °C in liquid LB broth to an OD_{600} of 1 and protein expression was induced overnight at 20 °C with 1 mM IPTG. Cells were collected, washed in 20 mM sodium phosphate (pH 7) and resuspended in the same buffer containing 0.01 mg mL^{-1} DNase and a mixture of protease inhibitors (Roche). Cells were broken by passages through a French pressure cell. After collecting the membrane fractions by ultracentrifugation (100,000*g* for 1 h), two steps of extraction were performed successively with 0.8 and 1.5% β-octyl glucoside. The second extract was subjected to chromatography onto a cation-exchange column Poros HS20 (Perkin-Elmer) equilibrated in 20 mM sodium phosphate (pH 7.0) with 1% β-octyl glucoside. FhaC was eluted with a linear 0–1 M gradient of NaCl. The FhaC-containing fractions were pooled and applied onto a 1 mL HiTrap chelating column (Amersham Biosciences) equilibrated in 20 mM sodium phosphate (pH 7.0), 1% β-octyl glucoside. FhaC was eluted by a pulse of 500 mM imidazole (pH 6.5) in the equilibration buffer. For crystallization, FhaC was concentrated to 26 mg mL^{-1} by using Vivaspin centrifugal devices with a 50 kDa cut-off (Vivascience).

5.4.2. Crystallization and data collection

Crystals were obtained at 20 °C using the hanging drop vapour diffusion method. The protein and precipitant solutions were mixed in a 1:1 ratio. Crystals were grown at a protein concentration of 26 mg mL^{-1} in 34% PEG1000, 1% β-octyl glucoside and 500 mM imidazole (pH 6.5). Diffraction data were collected at 100 K on beamline ID14-4 at the European Synchrotron Radiation Facility (Grenoble, France). All diffraction data were processed with XDS (Kabsch 2010). Data collection and refinement statistics are summarized in Table 5.1. Whereas the crystal packing remained isomorphous to the old crystal form, the diffraction limit increased to 2.5 Å. Model building was accomplished manually with Coot (Crystallographic Object Oriented Toolkit) (Emsley *et al.* 2010) from the CCP4 suite (Winn *et*

al. 2011). The refinement with Buster (Bricogne *et al.* 2011) led to an R_{work} of 21.7% and an R_{free} of 25.9% using data to 2.5 Å for $FhaC_{DIS}$ and R_{work}/R_{free} of 22.2% / 27.9% using data to 2.9 Å for the reprocessed WTFhaC data (Clantin *et al.* 2007). The final model for the $FhaC_{DIS}$ structure lacks the first two N-terminal residues, residues 296 and 297 of extracellular loop L3, 381 to 399 of L5, 478 to 481 of periplasmic turn T6, 499 to 503 of L7 and residues 537 and 538 of L8. Loop L6 and the linker between the helix and POTRA1 are well defined in the electron density. Furthermore, a total of three detergent molecules were well ordered and bound to FhaC. In addition, three PEG molecules were found inside the barrel and two PEG molecules are located close to the periplasmic pore in vicinity of the POTRA domain anchor. The updated $WTFhaC_{new}$ model lacks the first five N-terminal residues, residues 36–56 of the linker connecting the helix and POTRA1, residues 294–301 of L3, 342–350 of L4, 381–399 of L5, 475–481 of T6, 500–502 of L7 and 533–543 of L8. All structural differences between the $FhaC_{DIS}$ model and the superseded $WTFhaC_{old}$ model (PDB entry 2QDZ (Clantin *et al.* 2007)) are summarized in Supplementary Table 5.1. Composite omit maps after simulated annealing of the $FhaC_{DIS}$ structure and the superseded $WTFhaC_{old}$ structure against the $FhaC_{DIS}$ and the WTFhaC diffraction data (PDB entry 2QDZ (Clantin *et al.* 2007)) were generated using PHENIX (Adams *et al.* 2010).

5.4.3. Sequence alignments

Eleven TamA orthologs, ten BamA orthologs and ten TpsB proteins were selected from the NCBI database, showing pairwise sequence identities between 18 and 36% within each group (Gruss *et al.* 2013) (accession codes P0ADE4.1, WP_010374432.1, YP_006917734.1, YP_005378779.1, WP_006914415.1, WP_006956461.1, WP_007639592.1, YP_006416500.1, YP_007468392.1, WP_008316497.1, YP_006721763.1, YP_002998039.1, YP_001121414.1, WP_003783125.1, YP_001219350.1, WP_010501263.1, YP_865762.1, YP_007459313.1, YP_004865655.1, YP_002549812.1, WP_008996841.1, AAB30624.1, YP_335961.1, WP_005764711.1, YP_003741556.1, WP_002831157.1, YP_006646915.1, YP_004122309.1, WP_008291755.1, WP_005980414.1, YP_003307097.1). In addition, the *H. ducreyi* BamA sequence was added (NCBI accession code 4K3C_A) and a TpsB sequence (WP_004649222.1). Alignments, starting with the second last POTRA domains, were performed with Clustal Omega (Goujon *et al.* 2010, Sievers *et al.* 2011) and further edited taking into consideration available structural data (Supplementary Fig. 5.3).

5.5. Accession codes

Atomic coordinates and structure factors have been deposited in the Protein Data Bank with accession code 4QL0 for $FhaC_{DIS}$, and 4QKY for $WTFhaC_{new}$.

5.6. Author contributions

F.D. and B.C. purified and crystallized WTFhaC and $FhaC_{DIS}$. B.C. and V.V. collected diffraction data. All authors analysed data. T.M., B.C., F.G., F.J.-D., S.H. and V.V. wrote the paper

5.7. Acknowledgements

Crystallographic experiments were performed at the European Synchrotron Radiation Facility, Grenoble, France. We thank R. Ravelli for his support at beamline ID14. This work was supported by the French National Research Agency (Grant ANR-2010-BLANC 1306 DYN FHAC to F.J.-D), the Swiss National Science Foundation (Grant PP00P3_128419 to S.H.) and the European Research Council (FP7 contract MOMP 281764 to S.H.). F.G. acknowledges a fellowship by the Werner-Siemens Foundation.

5.8. Supplement

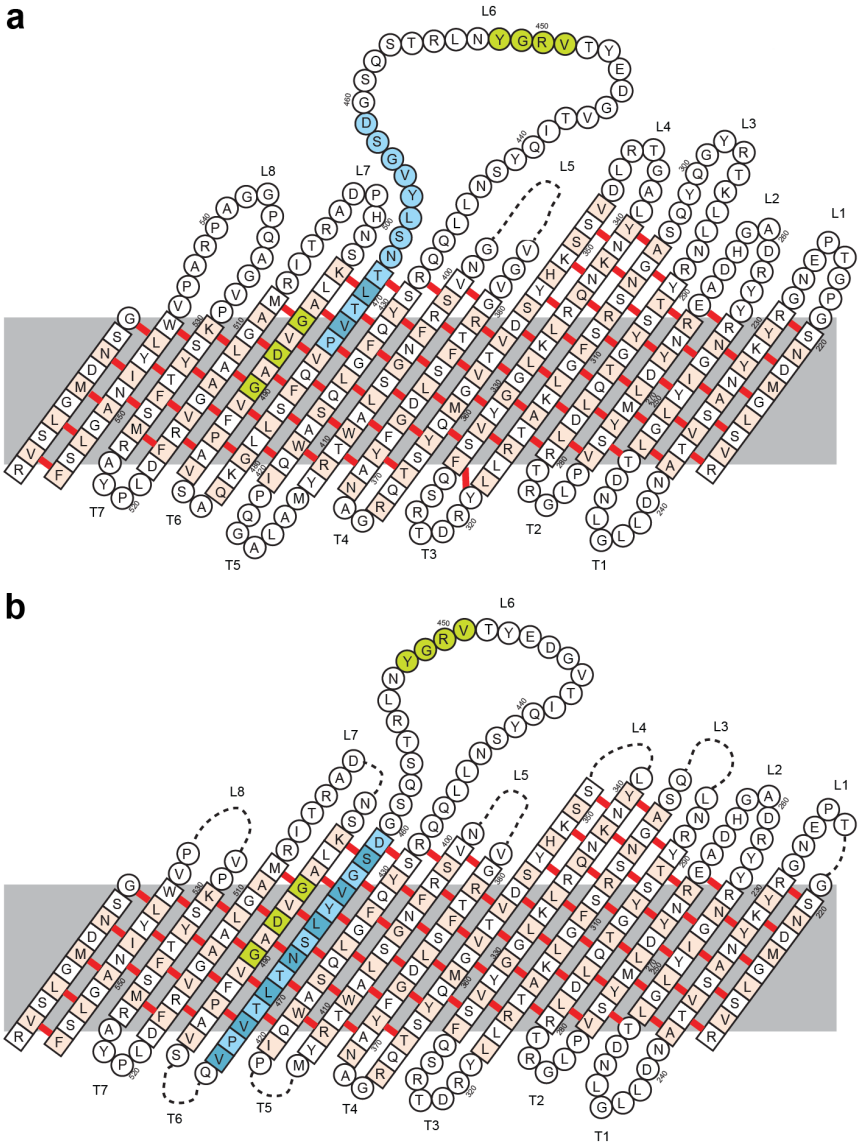

Supplementary Figure 5.1 Comparison of β-strand topologies in models of FhaC.

2D topology representations of (**a**) the superseded wtFhaC$_{old}$ structure (PDB entry 2QDZ (Clantin *et al.* 2007)) and (**b**) the structures of FhaC$_{DIS}$ (PDB entry 4QL0; this work) and wtFhaC$_{new}$ (PDB entry 4QKY; this work) as viewed from the barrel exterior. Residues forming β-strands are indicated by rectangles, residues of loops and turns by circles. The side chains of orange residues point towards the membrane. The extracellular loops are numbered L1 to L8 from N- to C-terminus, the periplasmic turns are numbered T1 to T7. Interstrand backbone hydrogen bond pairs are indicated by red lines between the corresponding residues. Strand 1 is repeated on the left hand side to show the hydrogen bonds that form to strand 16. The conserved motifs (I/V)RG(Y/F) (residues 449–452) and GxDxG (residues 490–494) are highlighted green. Residues of strand 12 are highlighted blue to show the register shift that appeared in the superseded wtFhaC$_{old}$ structure (Clantin *et al.* 2007) due to wrong tracing of the L6 loop.

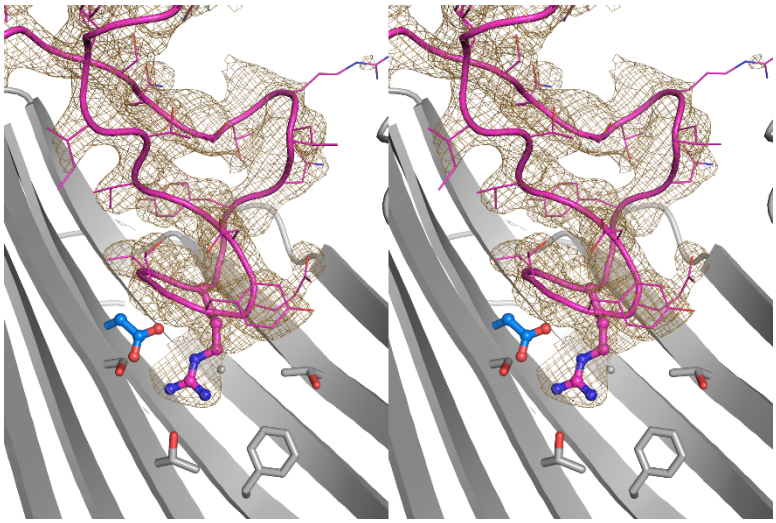

Supplementary Figure 5.2 Stereo view of electron density around the L6 loop of $FhaC_{DIS}$.
The $2F_oF_c$ map for $FhaC_{DIS}$ is shown in a radius of 2 Å around atoms belonging to the L6 loop (magenta) at 1σ contour level. Side chains of the L6 loop are shown as lines, selected side chains of the barrel (grey) are shown as sticks, and highly conserved residues as ball-and-stick.

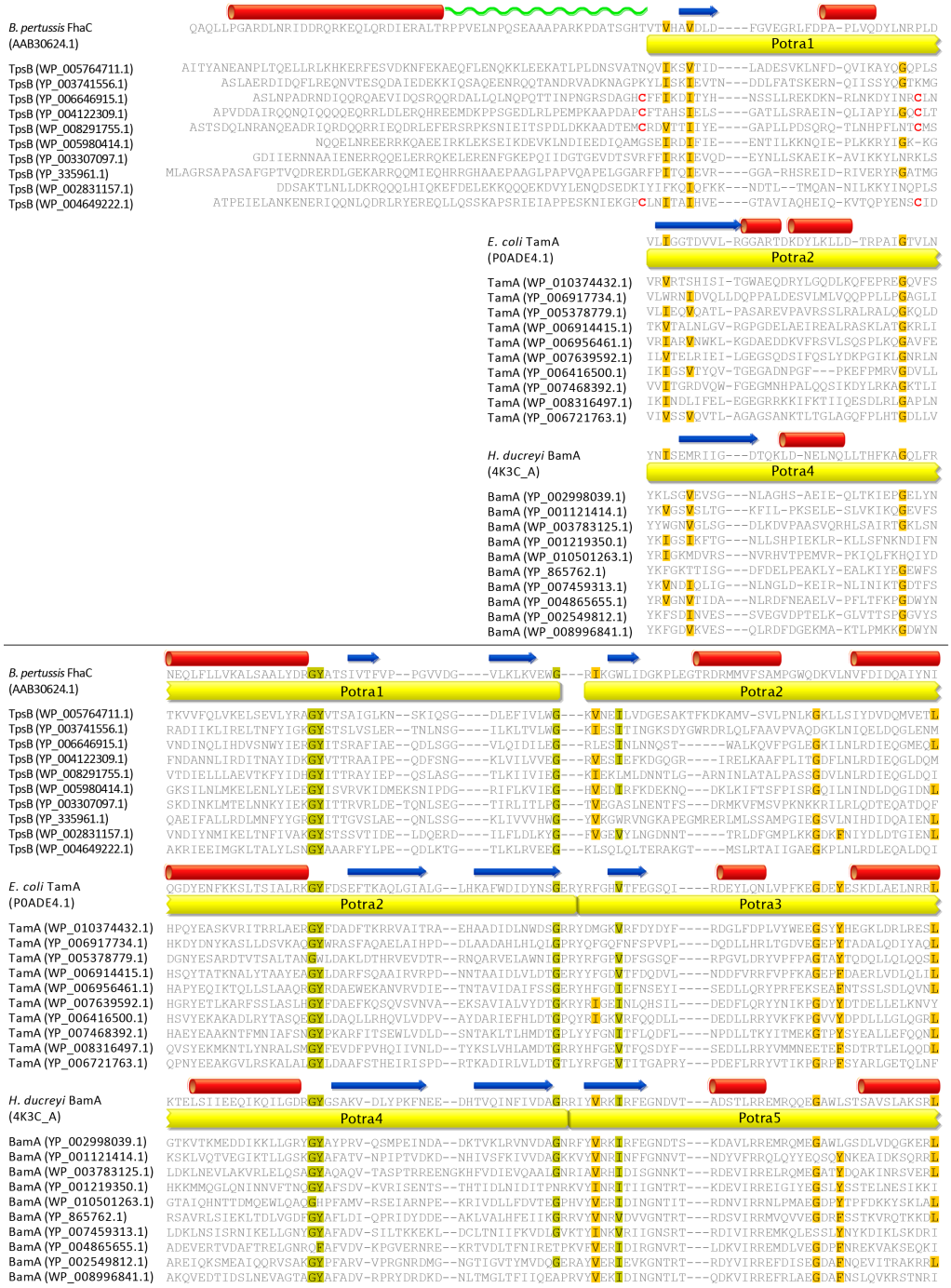
B. pertussis FhaC (AAB30624.1)
Potra1
TpsB (WP_005764711.1)
TpsB (YP_003741556.1)
TpsB (YP_006646915.1)
TpsB (YP_004122309.1)
TpsB (WP_008291755.1)
TpsB (WP_005980414.1)
TpsB (YP_003307097.1)
TpsB (YP_335961.1)
TpsB (WP_002831157.1)
TpsB (WP_004649222.1)
E. coli TamA (P0ADE4.1)
Potra2
TamA (WP_010374432.1)
TamA (YP_006917734.1)
TamA (YP_005378779.1)
TamA (WP_006914415.1)
TamA (WP_006956461.1)
TamA (WP_007639592.1)
TamA (YP_006416500.1)
TamA (YP_007468392.1)
TamA (WP_008316497.1)
TamA (YP_006721763.1)
H. ducreyi BamA (4K3C_A)
Potra4
BamA (YP_002998039.1)
BamA (YP_001121414.1)
BamA (WP_003783125.1)
BamA (YP_001219350.1)
BamA (WP_010501263.1)
BamA (YP_865762.1)
BamA (YP_007459313.1)
BamA (YP_004865655.1)
BamA (YP_002549812.1)
BamA (WP_008996841.1)
Potra3
Potra5

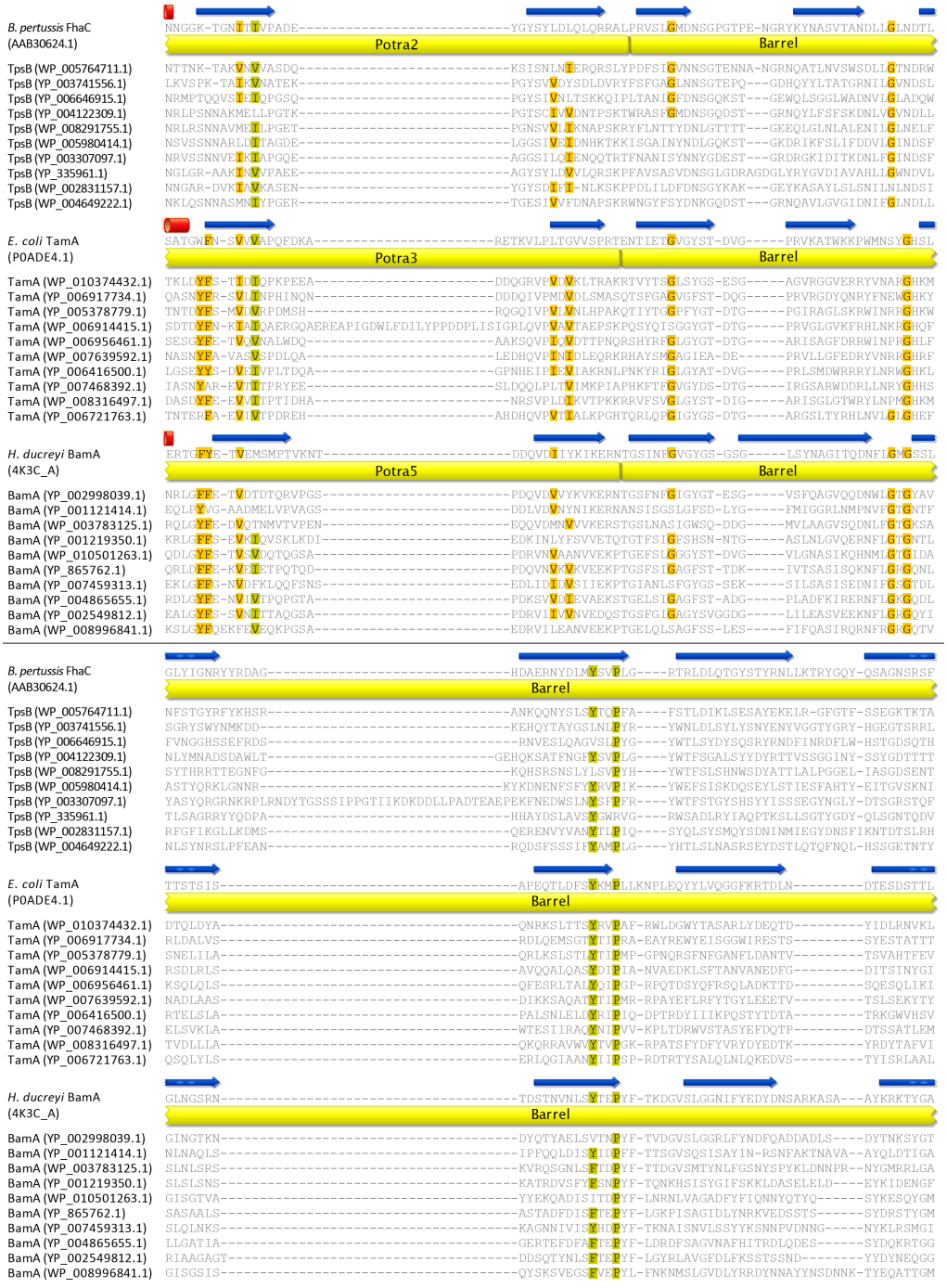
B. pertussis FhaC (AAB30624.1)
Potra2
Barrel
E. coli TamA (P0ADE4.1)
Potra3
Barrel
H. ducreyi BamA (4K3C_A)
Potra5
Barrel
E. coli TamA (P0ADE4.1)
Barrel
H. ducreyi BamA (4K3C_A)
Barrel

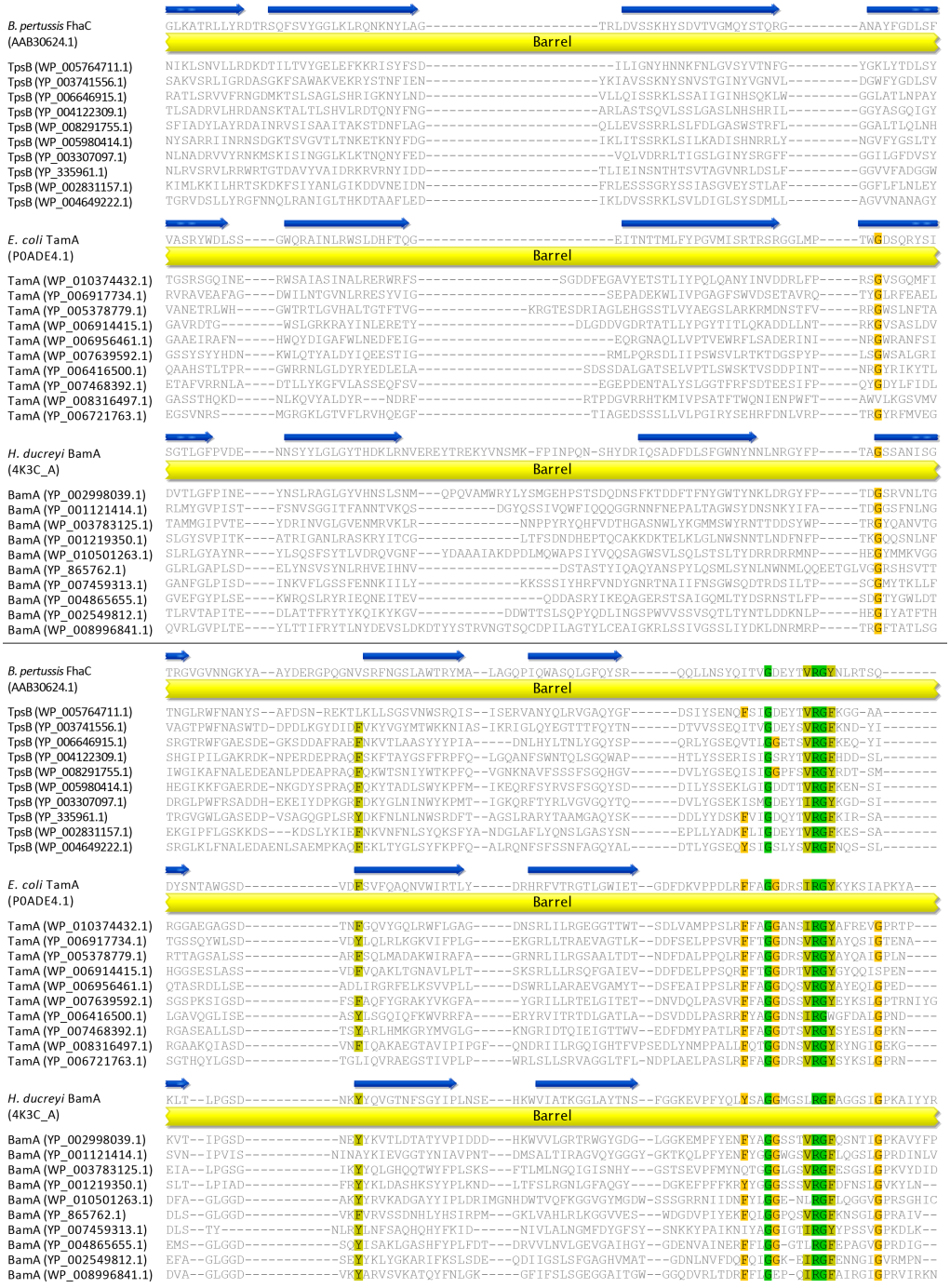
B. pertussis FhaC
(AAB30624.1)
Barrel
TpsB (WP_005764711.1)
TpsB (YP_003741556.1)
TpsB (YP_006646915.1)
TpsB (YP_004122309.1)
TpsB (WP_008291755.1)
TpsB (WP_005980414.1)
TpsB (YP_003307097.1)
TpsB (YP_335961.1)
TpsB (WP_002831157.1)
TpsB (WP_004649222.1)
E. coli TamA
(P0ADE4.1)
Barrel
TamA (WP_010374432.1)
TamA (YP_006917734.1)
TamA (YP_005378779.1)
TamA (WP_006914415.1)
TamA (WP_006956461.1)
TamA (WP_007639592.1)
TamA (YP_006416500.1)
TamA (YP_007468392.1)
TamA (WP_008316497.1)
TamA (YP_006721763.1)
H. ducreyi BamA
(4K3C_A)
Barrel
BamA (YP_002998039.1)
BamA (YP_001121414.1)
BamA (WP_003783125.1)
BamA (YP_001219350.1)
BamA (WP_010501263.1)
BamA (YP_865762.1)
BamA (YP_007459313.1)
BamA (WP_004865655.1)
BamA (WP_002549812.1)
BamA (WP_008996841.1)
B. pertussis FhaC
(AAB30624.1)
Barrel
TpsB (WP_005764711.1)
TpsB (YP_003741556.1)
TpsB (YP_006646915.1)
TpsB (YP_004122309.1)
TpsB (WP_008291755.1)
TpsB (WP_005980414.1)
TpsB (YP_003307097.1)
TpsB (YP_335961.1)
TpsB (WP_002831157.1)
TpsB (WP_004649222.1)
E. coli TamA
(P0ADE4.1)
Barrel
TamA (WP_010374432.1)
TamA (YP_006917734.1)
TamA (YP_005378779.1)
TamA (WP_006914415.1)
TamA (WP_006956461.1)
TamA (WP_007639592.1)
TamA (YP_006416500.1)
TamA (YP_007468392.1)
TamA (WP_008316497.1)
TamA (YP_006721763.1)
H. ducreyi BamA
(4K3C_A)
Barrel
BamA (YP_002998039.1)
BamA (YP_001121414.1)
BamA (WP_003783125.1)
BamA (YP_001219350.1)
BamA (WP_010501263.1)
BamA (YP_865762.1)
BamA (YP_007459313.1)
BamA (WP_004865655.1)
BamA (WP_002549812.1)
BamA (WP_008996841.1)

Supplementary Figure 5.3 Alignment of Omp85 sequences.

11 TpsB, 11 TamA and 11 BamA sequences beginning with the second last POTRA domains. For the known structures of *B. pertussis* FhaC (PDB entry 4QKY; this work), *E. coli* TamA (PDB entry 4C00 (Gruss *et al.* 2013)) and *H. ducreyi* BamA (PDB entry 4K3C (Noinaj *et al.* 2013)), α-helices and β-strands are indicated by red tubes and blue arrows, respectively, on top of the sequences. The sequences for the N-terminal helices and linkers of TpsB proteins are shown unaligned. Cysteines in the linker region and POTRA1 domain of TpsB proteins, plausibly forming disulfide bonds (see text), are highlighted in red.

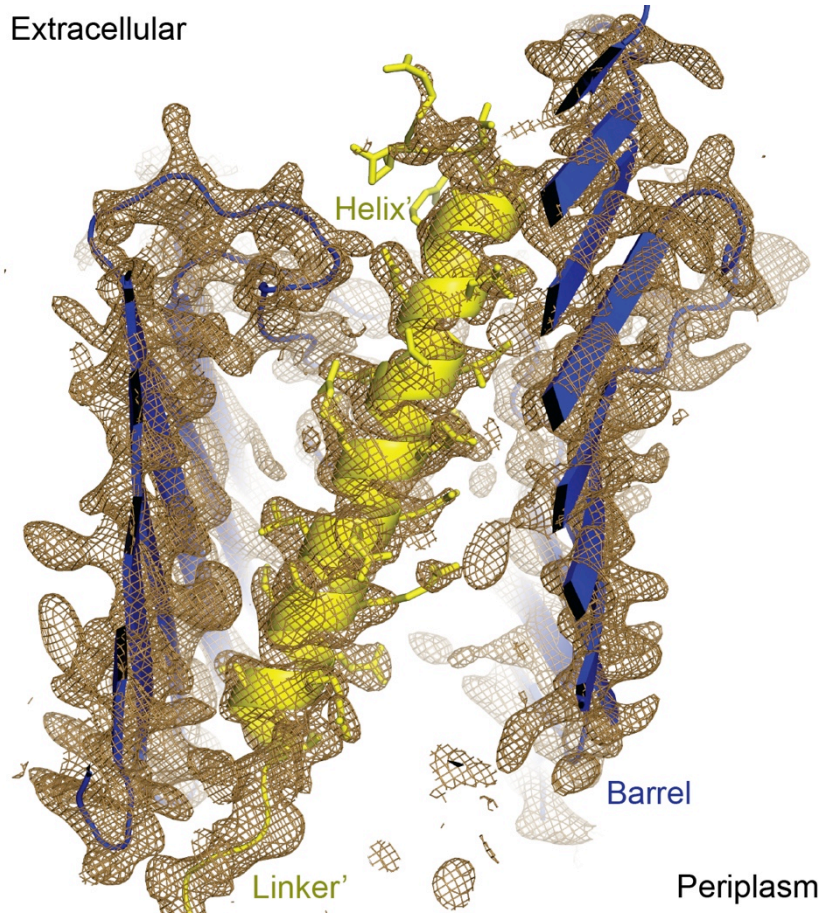

Supplementary Figure 5.4 Electron density around helix and barrel of $FhaC_{DIS}$.

The $2F_oF_c$ map for $FhaC_{DIS}$ is shown in a radius of 2.5 Å around atoms belonging to helix and linker (yellow) and the barrel (blue) at 1σ contour level.

Supplementary Table 5.1 Differences between FhaC structural models.

Region	**$FhaC_{DIS}$, residues**	**$wtFhaC_{old}$, corresponding residues**	**Variation**
N-terminal helix	Gln3-Asp10	Gln3-Gly7	Residues from symmetry-related molecules in different conformations
N-terminal helix	Leu11-Arg33	Ala8-Ala30	Residues from symmetry-related molecules aligned with offset 3
Linker	Pro34-His57	Leu31-Asp52	Not built in superseded $wtFhaC_{old}$ model, well resolved in $FhaC_{DIS}$ structure
POTRA1	Thr58-Thr60	Ala53-Ser55	Aligned with offset 5
POTRA1	Val61	Gly56-Val61	Extra loop in $wtFhaC_{old}$ model
POTRA1	Val70-Glu71	Val70-Gly72	Different conformations
POTRA1	Gly72-Pro77	Arg73-Ala78	Aligned with offset -1
POTRA1	Ala78-Asp83	Pro79-Asp83	Different conformations
Barrel L1	Pro222-G228	Pro222-G228	Different conformations
Barrel L3	Leu294-Lys295	Leu294-Lys295	Different conformations
Barrel L3	Thr296-Arg297	The296-Arg297	Not built in $FhaC_{DIS}$ model
Barrel L4	Gly343-Leu346	Gly343-Leu346	Different conformations
Barrel L5	Val381-Val383	Val381-Val383	Not built in $FhaC_{DIS}$ model
Barrel L5	Gly398-Asn399	Gly398-Asn399	Not built in $FhaC_{DIS}$ model
Barrel L6	Arg432		Position skipped in $wtFhaC_{old}$ model
Barrel L6	Gln433-Asn437	Arg432-Leu436	Aligned with offset 1
Barrel L6	Ser438		Position skipped in $wtFhaC_{old}$ model
Barrel L6	Tyr439-Glu446	Asn437-Gly444	Aligned with offset 2
Barrel L6	Tyr447	Asp445-Thr456	Extra loop in $wtFhaC_{old}$ model
Barrel L6	Thr448-Gly451	Ser457-Gly460	Aligned with offset -9
Barrel L6	Tyr452-Thr456	Asp461-Val464	Different conformations
Barrel L6, S12	Ser457-Gln475	Tyr465-Ala483	Aligned with offset -8
Barrel T6	Phe476-Ser477		Positions skipped in $wtFhaC_{old}$ model
Barrel T6	Leu478-Lys481		Not built in $FhaC_{DIS}$ model, positions skipped in $wtFhaC_{old}$ model
Barrel T6	Gln482-Ala483		Positions skipped in $wtFhaC_{old}$ model
Barrel L7	Asn499-Ala503	Asn499-Ala503	Not built in $FhaC_{DIS}$ model
Barrel T7	Leu519-Pro520	Leu519-Pro520	Different conformations
Barrel L8	Gly533-Pro536	Gly533-Pro536	Different conformations
Barrel L8	Gly537-Gly538	Gly537-Gly538	Not built in $FhaC_{DIS}$ model
Barrel L8	Ala539-Ala542	Ala539-Ala542	Different conformations

Comparison of differences between the superseded $wtFhaC_{old}$ structure (PDB entry 2QDZ (Clantin *et al.* 2007)) and $FhaC_{DIS}$ (PDB entry 4QL0; this work). Strands are indicated by "S", extracellular loops by "L" , periplasmic turns by "T".

CHAPTER 6:

Tom40 Sample Preparation for NMR Spectroscopy

6.1. Abstract

Tom40 is the central protein translocation pore of the TOM complex in the outer membrane of mitochondria. Whereas Tom40 has been investigated with various biophysical methods, also on the single molecule level, it has so far resisted structural research by NMR spectroscopy or X-ray crystallography. Here, a protocol for the preparation of Tom40 samples suitable for NMR experiments is described. Tom40 is recombinantly expressed in inclusion bodies in *E. coli* and refolded *in vitro*. The obtained NMR spectra prove the presence of β-strand secondary structure, but feature low experimental sensitivity due to micro-aggregation of refolded Tom40.

6.2. Introduction

The TOM complex in the outer membrane of mitochondria (OMM) mediates the import of nuclear encoded and cytosolic translated proteins across this membrane into mitochondria (Neupert and Herrmann 2007). Mitochondria-destined proteins either contain an N-terminal sorting signal, called presequence, with a length of 15 to 50 residues, which is positively charged and forms an amphipathic α-helix, or intrinsic targeting signals (Höhr *et al.* 2015, Neupert and Herrmann 2007, Schmidt *et al.* 2010). As about 99% of all mitochondrial proteins are encoded in the nucleus and mitochondria fulfill essential functions, including ATP synthesis, signaling and apoptosis, a functional TOM complex is crucial to eukaryotic cells (Chacinska *et al.* 2009).

Tom40 forms a β-barrel structure with presumably 19 strands, as suggested by close homology to the protein VDAC (Hiller *et al.* 2008) and biochemical experiments (Gessmann *et al.* 2011, Lackey *et al.* 2014). It constitutes the central translocation pore of the TOM complex (Chacinska *et al.* 2009, Hill *et al.* 1998, Suzuki *et al.* 2004, Vestweber *et al.* 1989). In addition, Tom5, Tom6 and Tom7 are part of the core complex and Tom20, Tom22 and Tom70 are associated receptors for substrates to be translocated (Ahting *et al.* 1999, Kato and Mihara 2008, Künkele *et al.* 1998, Model *et al.* 2002, Schmitt *et al.* 2005). These proteins span the OMM with a single α-helix and have cytosolic domains. Tom22 and Tom7 in addition possess small intermembrane space (IMS) domains. The TOM import mechanism is not understood in detail, but usually proteins are translocated in N- to C-terminal direction and it is thought that affinities for the substrates increase from the cytosolic parts of the receptors across the Tom40 pore to the IMS exposed domains, which thus directs the translocation path (Neupert and Herrmann 2007).

The TOM complex and Tom40 have resisted to structural characterization on an atomic level by NMR spectroscopy or X-ray crystallography due to unfavorable biochemical

properties of the protein (Yao *et al.* 2014). Electron micrographs of single particles show that the TOM complex contains two or three channels (Ahting *et al.* 1999, Becker *et al.* 2005, Künkele *et al.* 1998). Electrophysiology measurements of Tom40 or full TOM complex reconstituted in lipid bilayers, as well as liposome import assays evidence the channel properties of Tom40 and the ability to bind and transport presequences (Ahting *et al.* 1999, Becker *et al.* 2005, Hill *et al.* 1998, Künkele *et al.* 1998, Kuszak *et al.* 2015, Mahendran *et al.* 2012, Suzuki *et al.* 2004). Nevertheless, for understanding the molecular mechanisms of transport, structural information on the atomic level remains a key goal.

6.3. Results

6.3.1. hTom40 NMR spectroscopy

For NMR spectroscopy experiments, deuterated and ^{15}N-labeled hTom40 was expressed in inclusion bodies, purified via Ni-beads, refolded with detergent and then further purified via ion exchange chromatography. Purified protein was concentrated and the detergent concentration was adjusted for optimal properties in NMR measurements. To have a comparison for NMR spectral quality, the homologous hVDAC was prepared similarly following well-established protocols (Hiller *et al.* 2008). ^{15}N-filtered 1D-TROSY spectra of hTom40 show signal between 8.5 ppm and 9.5 ppm (Fig. 6.1a), indicating β-sheet content. Comparison with a high quality spectrum of hVDAC (Fig. 6.1b) however demonstrates that hTom40 reaches a relative sensitivity of only 3.5% of hVDAC (see Methods).

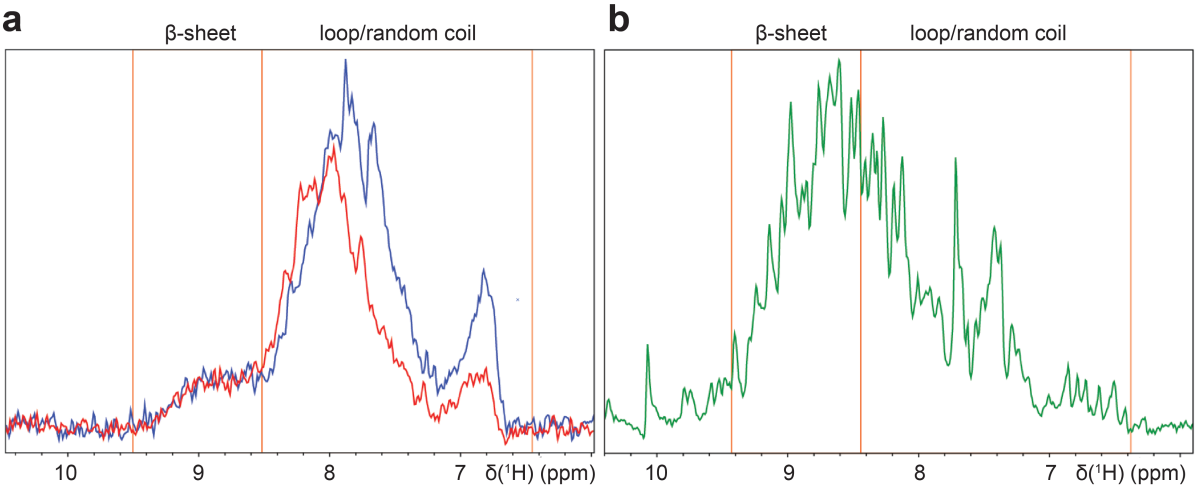

Figure 6.1 ^{15}N-filtered 1D-TROSY of hTom40 and hVDAC.
The NMR signal between 6 ppm and 10.4 ppm is shown for (**a**) hTom40 in LDAO micelles of two independent protein preparations (red and blue curve) and (**b**) hVDAC in LDAO micelles (green curve). The spectral regions showing β-sheet and random coil signal are indicated.

6.3.2. Analytical size exclusion chromatography

To analyze the reasons for the difference in spectral quality between the structurally similar hTom40 and hVDAC, refolded hTom40 was subjected to size exclusion chromatography (SEC). The chromatogram of the run demonstrates that the majority of the protein elutes in the void volume of the Superose 12 10/300 GL column (GE Healthcare) (Fig. 6.2a). Therefore, hTom40 forms soluble micro-aggregates, which is the reason for weak NMR signal due to slow tumbling rates. SDS-PAGE analysis shows that Tom40 even forms SDS-resistant dimers (Fig. 6.2b).

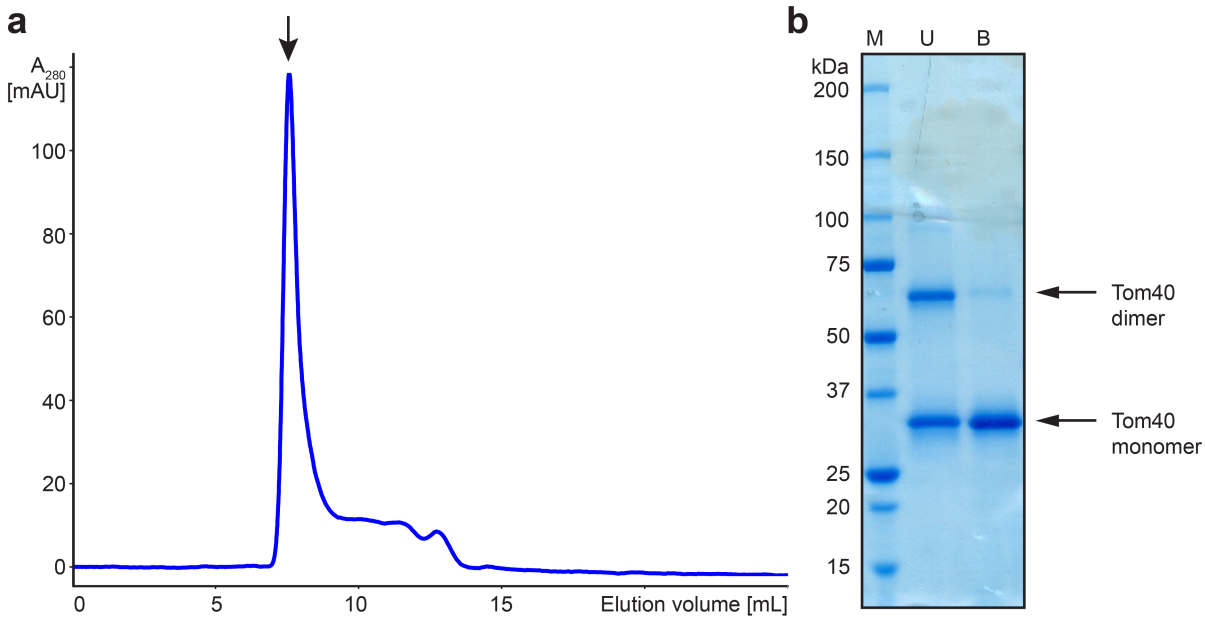

Figure 6.2 hTom40 SEC and SDS-PAGE analysis.
(**a**) A_{280} profile of a Superose 12 10/300 GL run of hTom40. The position of the void volume peak is indicated by an arrow. (**b**) SDS-PAGE analysis of unboiled hTom40 (“U”) and hTom40 boiled for approx. 10 min at 95 °C (“B”) in comparison with a molecular weight marker (“M”).

6.4. Discussion

6.4.1. hTom40 sample quality evaluation

The observation of β-sheet signal in the NMR spectrum of hTom40 (Fig 6.1a) suggests the presence of folded protein in our sample. However, the overall signal intensity is too weak for structure determination by NMR spectroscopy with the current preparations. A comparison with hVDAC indicates a relative signal intensity of only 3.5%. Since nearly 100% of hVDAC molecules in the sample are folded and monomeric, the current sample quality corresponds to 3.5% of all hTom40 molecules being folded and monomeric and thus contributing to β-sheet signal in the NMR spectra while the remaining majority of the protein

forms higher oligomers. Presumably, several different oligomeric hTom40 species exist in the sample, contributing in different extent to the overall signal. This latter view is additionally plausible regarding the elution profile of the analytical SEC (Fig. 6.2a).

6.4.2. hTom40 sample quality improvement

To come within reach of structure determination by NMR spectroscopy, the signal intensity needs to be significantly improved. A simple increase in protein concentration is not applicable and thus improvement can only be achieved by decreasing the micro-aggregation of the sample. This may be done by prevention of micro-aggregation during refolding, which would imply that once properly folded, hTom40 stays low-oligomeric. In a scenario where hTom40 would also continue forming micro-aggregates after refolding, a simple modification of the refolding protocol is not sufficient. The latter scenario is likely the case as *in vivo* Tom40 forms a complex with other proteins that surround it with single-span α-helices in the membrane and thus might contribute to stability. Therefore, the strong differences in behavior between the structurally similar proteins hTom40 and hVDAC may be partly based on the fact that the former is part of a protein complex, whereas the latter exists in monomeric form. Thus, one future way to go might be to purify the full TOM complex from isolated mitochondria instead of refolding Tom40, but this complex is likely not susceptible to NMR spectroscopy because of its large size of approx. 500 kDa (Ahting *et al.* 1999, Künkele *et al.* 1998). Alternatively, the regions of Tom40 that promote aggregation may be identified and mutated, or Tom40 may be stabilized in a different way by small molecules or peptides.

For larger complexes, X-ray crystallography is the method of choice for obtaining atomic structures. Since crystallization usually demands monodisperse samples, the same principal issues as for NMR spectroscopy need to be overcome in order to obtain material suitable for crystallization.

6.5. Methods

6.5.1. Plasmid construction

The DNA for human Tom40 was ordered from GenScript (Piscataway, NJ, USA) with optimized codons for expression in *E. coli*. Tom40Δ76 was amplified from this plasmid by PCR and then inserted into pET21d vector (Novagen) using restriction sites NcoI and XhoI to yield the hTom40Δ76 expression vector. It encodes hTom40Δ76 with an additional N-terminal Met-Ala and an additional C-terminal Leu-Glu followed by a His6-tag.

hVDAC was expressed from the plasmid described in Hiller *et al.* 2008, which encodes full-length human VDAC isoform 1 with an additional C-terminal Leu-Glu followed by a His6-tag in a pET21a vector (Novagen).

6.5.2. Expression, purification and refolding

Chemically competent *E. coli* BL21(λ DE3) or Lemo21(λ DE3) cells were transformed with the hTOM40 or hVDAC expression plasmid. After growth of cells in M9 medium containing D_2O and $^{15}NH_4Cl$ at 37 °C to an OD_{600} of 0.7–0.8, expression of the protein was induced by addition of 1 mM IPTG. Expression continued for 4–5 hours before cells were harvested.

Cells that expressed hTom40 were resuspended in PBS, supplemented with lysozyme, and lysed. Lysed cells containing expressed protein in inclusion body were pelleted for 30 min at 20,000*g*. The pellet was washed twice with 50 mM Tris, pH 8, and 100 mM NaCl and then resuspended in 20 mM Tris, pH 8, 150 mM NaCl, 6 M Guanidine hydrochloride (Gu-HCl), 5 mM imidazole and 5 mM β-mercaptoethanol (β-ME). The suspension was centrifuged and the supernatant added to 5 mL Ni-beads (GenScript). After incubation at room temperature the Ni-beads were first washed with the same buffer, before the protein was eluted with 500 mM imidazole in the same buffer. The eluted protein was dialyzed against 4 L of 20 mM Tris, pH 8, 150 mM NaCl and 5 mM β-ME and the precipitated protein then solubilized in 20 mM Tris, pH 8, 150 mM NaCl, 6 M Gu-HCl and 5 mM β-ME. Finally the protein solution was centrifuged to obtain a particle-free solution of Gu-HCl-denatured hTom40.

For hVDAC purification, well-established protocols were applied (Hiller *et al.* 2008) In brief, cells that expressed hVDAC were resuspended in TE-buffer, supplemented with lysozyme, and lysed. Lysed cells containing expressed protein in inclusion body were pelleted for 30 min at 20,000*g*. The pellet was first washed in TE buffer containing 2% Triton X-100 and then in detergent-free TE-buffer. Then, it was resuspended in 50 mM Tris, pH 7.5, 100 mM NaCl, 8 M Urea and 20 mM imidazole. The suspension was centrifuged and the supernatant added to 5 mL Ni-beads (GenScript). After incubation at room temperature the Ni-beads were first washed with the same buffer, before the protein was eluted with 250 mM imidazole in the same buffer. The eluted protein was dialyzed against 4 L of 50 mM Tris, pH 7.5, 50 mM NaCl, 1 mM EDTA and 5 mM DTT and the precipitated protein then solubilized in 50 mM NaPi, pH 7, 100 mM NaCl, 6 M Gu-HCl, 1 mM EDTA and 5 mM DTT. Finally the protein solution was centrifuged to obtain a particle-free solution of Gu-HCl-denatured hVDAC.

For protein refolding, denatured hVDAC or hTom40 was added dropwise into refolding buffers with tenfold volume, stirred rapidly with magnetic stirring bar. For hVDAC refolding,

well-established protocols were applied (Hiller *et al.* 2008). The refolding conditions for hVDAC were: 25 mM NaPi, pH 7, 100 mM NaCl, 1% LDAO, 5 mM DTT, 1 mM EDTA. The hVDAC refold was dialysed o/n against 25 mM NaPi, pH 6.5, 1 mM EDTA and 5 mM DTT and then centrifuged. The supernatant was loaded on a HiTrap SP HP cation exchange column (GE Healthcare). After the column was washed with 25 mM NaPi, pH 6.5, 0.1% LDAO and 5 mM DTT, the protein was eluted with a gradient to 1 M NaCl in the same buffer. The buffer of the eluted protein was exchanged by three rounds of concentrating in a 10 kDa c/o centrifugal unit and subsequent dilution with 25 mM MOPS-BisTris, pH 6.5, 0.05% LDAO and 5 mM DTT. Final protein concentration in the VDAC sample was 12.4 mg mL^{-1} (390 µM), the LDAO concentration was adjusted to 4.6% (200 mM).

The refolding conditions for hTom40 were: 20 mM Tris, pH 8, 150 mM NaCl, 1% LDAO and 5 mM β-ME. The hTom40 refold was dialysed o/n against 20 mM Tris, pH 9, 10 mM NaCl and 5 mM β-ME and then centrifuged. An equal volume of 20 mM Tris, pH 8.5, 15 mM NaCl, 0.1% LDAO and 5 mM β-ME was added to the supernatant, which was then loaded on a HiTrap Q FF anion exchange column (GE Healthcare). After the column was washed with 20 mM Tris, pH 8.5, 15 mM NaCl, 0.1% LDAO and 5 mM β-ME, the protein was eluted with a gradient to 1 M NaCl in the same buffer. The buffer of the eluted protein was exchanged by two rounds of concentrating in a 10 kDa c/o centrifugal unit and subsequent dilution with 20 mM Tris, pH 9, 50 mM NaCl, 0.05% LDAO and 5 mM β-ME. Final protein concentration in the hTom40 sample was 4.2 mg mL^{-1} (130 µM), the LDAO concentration was adjusted to 3.5% (150 mM).

6.5.3. NMR spectroscopy

NMR spectra were recorded at 35 °C on Bruker Avance-800 spectrometer triple-resonance probes. The total experiment time for the 2D [^{15}N,^{1}H]-TROSY HSQC was 6 h for hVDAC and 75 min for hTom40. The ^{1}H carrier was centered on the water resonance, the ^{15}N carrier at 117 ppm (hVDAC) / 115 ppm (hTom40). The interscan delay was set to 1 s. In the direct dimension, 1024 complex points were recorded in an acquisition time of 40 ms (hVDAC) / 32 ms (hTom40), multiplied with a 75°-shifted qsine bell (hVDAC) / sine bell (hTom40), zero-filled to 2048 points and Fourier transformed. NMR data were processed and analyzed using Topspin 2.1.

In order to compare the quality of hTom40 NMR spectra with hVDAC spectra, ^{15}N-filtered 1D-TROSY spectra of VDAC and hTom40 were overlaid. The hTom40 spectrum was scaled to superimpose with the VDAC spectrum in the β-sheet region between 8.5 and 9.5 ppm. To obtain a concentration- and acquisition-parameter-independent comparison of the sample qualities, the following formula was applied:

$$\frac{f_{hTom40}}{f_{hVDAC}} = \frac{N_{hVDAC} \times RG_{hVDAC} \times c_{hVDAC} \times \tau 90_{hTom40}}{N_{hTom40} \times RG_{hTom40} \times c_{hTom40} \times \tau 90_{hVDAC} \times SF_{hTom40}}$$

where f is a quality comparison factor, N the number of scans of the NMR measurements, c the protein concentration, RG the receiver gain during the NMR measurement; τ90 the length of the 90° ^{1}H-pulse and SF_{hTom40} is a scaling factor to overlay the recorded hTom40 spectrum with the hVDAC spectrum in the β-sheet signal region. For the actual acquisition parameters, sample concentrations and obtained NMR spectra in 6.3.1, the result of the formula with the variables replaced is:

$$\frac{f_{hTom40}}{f_{hVDAC}} = \frac{64 \times 203 \times 350\ \mu M \times 10.8\ \mu s}{4096 \times 203 \times 130\ \mu M \times 8.65\ \mu s \times 1.5} = 0.035 = 3.5\%$$

CHAPTER 7:

Conclusions and Outlook

7.1. Summary

This thesis revealed mechanistic insights into insertion and translocation processes mediated by Omp85 proteins. For the insertase TamA, which assembles autotransporter OMPs, a *bona fide* insertion mechanism based on coupled hybrid barrel formation with passenger domain secretion and subsequent lateral barrel release was inferred from the determined crystal structure. During TamA crystallization, a crystal seeding protocol for optimization of membrane protein crystals grown from bicelle solution was established. Interactions of TamA and its huge complex partner TamB could be demonstrated experimentally, and through computational co-evolution analysis the interaction sites in both proteins could be mapped.

For the translocase FhaC, a mechanism for substrate selection could be deduced from the crystal structure of a double mutant defective in substrate recognition, which at the same time allowed the correction of a formerly mistraced region in the wild-type FhaC crystal structure (Clantin *et al.* 2007). This region contains two highly conserved signature motifs in Omp85 proteins, located in barrel strand 13 and the extracellular L6 lid loop, which were now shown to form the same general structures and interactions both in Omp85 insertases and translocases. This structural motif, the “lid lock”, was therefore demonstrated to be a conserved structural feature both in Omp85 insertases and translocases. As both FhaC and TamA contribute to virulence in various organisms, these surface-accessible outer membrane proteins are relevant antibiotic targets, for which atomic structures and purification protocols are of great relevance.

For the VDAC-homologous translocase Tom40, which forms the central pore of the TOM complex in the outer mirochondrial membrane, an expression, refolding and purification protocol as a first basis towards *in vitro* experiments for functional and structural studies was established.

7.2. Omp85 insertion and translocation mechanisms

Autotransporter biogenesis has become a topic of controversial discussion (Bernstein 2007), since the initial hypothesis of its apparent simplicity was challenged by the observations that (i) barrel assembly and passenger domain translocation are coupled processes (Pavlova *et al.* 2013) and (ii) folded secondary structure elements too big for the narrow 12-stranded β-barrel can be secreted (Jong *et al.* 2007, Skillman *et al.* 2005). The suggested hybrid-barrel mechanism with passenger domain secretion and subsequent lateral release (Fig. 2.3) would elegantly resolve these issues and, in a slightly simplified form, can hold true for general OMP assembly. Interestingly, this mechanism resembles conceptionally

the dual role of the α-helical SecYEG for translocation and membrane insertion at the IM for a completely different class of proteins.

Even though the hybrid barrel mechanism has not yet been unambiguously proven experimentally, the computational co-evolution analysis between TamA and TamB in this work further supports the existence of hybrid barrels, in this case however with an interaction partner rather than a substrate. Furthermore, crosslinking studies demonstrated the necessity of opening between the first and the last BamA barrel strand (Noinaj *et al.* 2014) and a recent publication demonstrates that a BamA orthologue exhibits increased channel conductance, which correlates with barrel size, in presence of the last two strands of a substrate OMP, but not with the first two strands (Estrada Mallarino *et al.* 2015).

Besides hybrid barrel formation (Estrada Mallarino *et al.* 2015, Gruss *et al.* 2013, Kim *et al.* 2012, Noinaj *et al.* 2014, Noinaj *et al.* 2015, van den Berg 2013) (Fig. 7.1a), other currently discussed OMP assembly mechanisms include: Local distortion of the lipid bilayer to passively facilitate β-barrel assembly (Fig. 7.1b) (Gessmann *et al.* 2014, Noinaj *et al.* 2013, Noinaj *et al.* 2015, Selkrig *et al.* 2014, Sinnige *et al.* 2014), formation of an OMP barrel within the barrel lumen of BamA and subsequent lateral release into the membrane (Fig. 7.1c) (Bernstein 2007, van den Berg 2013), and preformation of an OMP barrel in the periplasm, stabilized by chaperones, before membrane insertion next to the Omp85 protein (Fig. 7.1d) (Bernstein 2015). The models of periplasmic preformation or formation inside BamA can be ruled out, as the former contradicts the observed fluid globule state of OMPs inside the chaperone Skp (Burmann *et al.* 2013, Callon *et al.* 2014) and the latter could only hold true for extremely small OMPs and misses any experimental evidence.

Local distortion via a thinning of the membrane next to BamA at the side of the interface between barrel strand 1 and 16 was shown by molecular dynamics simulation (Noinaj *et al.* 2013). In addition, the structures of BamA (Albrecht *et al.* 2014, Ni *et al.* 2014, Noinaj *et al.* 2013) and TamA (Gruss *et al.* 2013) show a narrowing between the aromatic girdles at the barrel exterior on this side, which in OMPs usually correlate with membrane boundaries. Experimentally, it was demonstrated that OMP folding *in vitro* is lipid headgroup-dependent and facilitated for thin membranes (Burgess *et al.* 2008, Gessmann *et al.* 2014, Patel *et al.* 2009, Patel and Kleinschmidt 2013, Pocanschi *et al.* 2006). This is well in line with the fact that *in vivo* spontaneous insertion of OMPs into the IM needs to be prevented to preserve the proton motive force and other concentration gradients across the IM and thus a local thinning of the OM could lead to spatially directed OMP assembly. Local membrane distortion next to TamA/BamA and hybrid barrel formation are mechanistically not mutually exclusive and a combination of both is in theory possible.

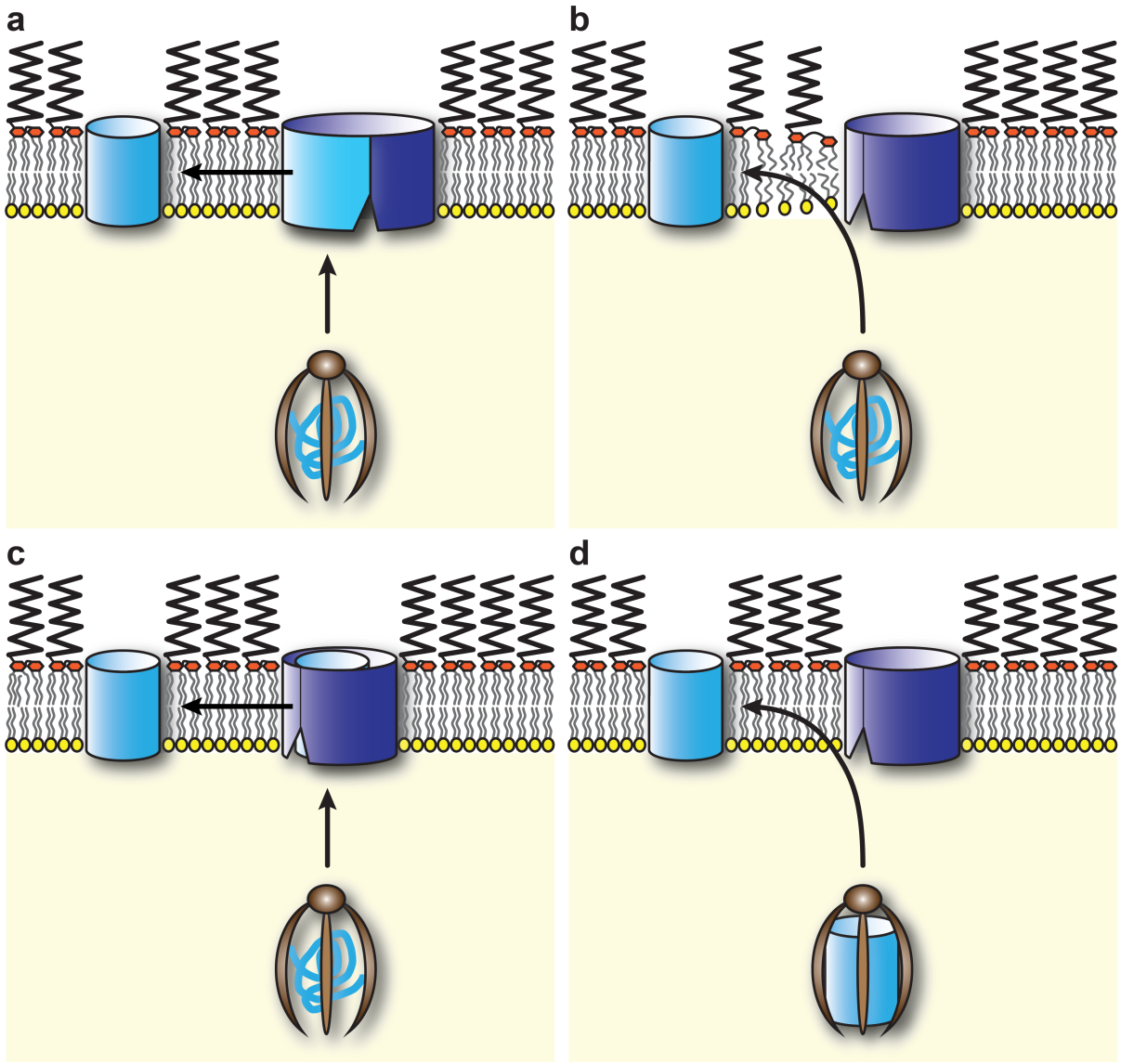

Figure 7.1 Current models for OMP assembly.
(**a**) Hybrid barrel mechanism: An unfolded OMP substrate (cyan, bottom) is stabilized by chaperones (brown) and brought to the Omp85 insertase, where it starts integrating its own barrel between Omp85 barrel strands 1 and 16 to form a hybrid barrel (cyan – blue, top right), which eventually disintegrates to release the mature membrane-inserted OMP (cyan, top left). (**b**) Distorted membrane mechanism: An unfolded OMP substrate (cyan, bottom) is stabilized by chaperones (brown) and brought to the Omp85 insertase (blue), where it inserts into the weakened lipid bilayer created by the Omp85 insertase to form the mature OMP (cyan, top left). (**c**) Omp85 lumen folding mechanism: An unfolded OMP substrate (cyan, bottom) is stabilized by chaperones (brown) and brought to the Omp85 insertase (blue), where it assembles in the lumen of the Omp85 barrel (blue) to form the mature OMP (cyan, top right) before lateral release into the membrane (cyan, top left). (**d**) Periplasmic preformation mechanism: A prefolded OMP substrate (cyan, bottom) is stabilized by chaperones (brown) and brought to the Omp85 insertase (blue), where it inserts into membrane (cyan, top left) next to the Omp85 protein (blue).

For the assumption of a passive insertion mechanism based on local membrane weakening, the directionality of OMP insertion, which *in vivo* is not random, needs to be considered. Moreover, the hydrophilic extracellular loops are generally longer than the periplasmic turns between the β-strands of an OMP (Mirus *et al.* 2010) and thus, at least for OMPs that do not contain additional periplasmic domains, it would seem energetically more favorable if such an OMP inserted upside down into the membrane in order to prevent the energetic barrier of membrane traversal of the long hydrophilic loops. Hence, at least a priming event in addition to facilitated insertion needs to take place to set the right orientation of the OMP. Furthermore, it makes sense for this priming event to occur in immediate membrane proximity in order to prevent reorientation before membrane insertion. The conserved β-signal in the most C-terminal strand of OMPs, which was shown to be necessary for OMP assembly (Struyvé *et al.* 1991), and to interact with several BAM subunits including BamA itself (Albrecht and Zeth 2011, Knowles *et al.* 2008, Robert *et al.* 2006), is the most likely motif to mediate this priming. Because of the reduced interactions between strands 1 and 16 of TamA and BamA (Gruss *et al.* 2013, Noinaj *et al.* 2013), the proof of necessity for them to open (Noinaj *et al.* 2014), and the predicted binding site at TamA barrel strand 1 for the β-signal-like C-terminus of TamB, found in this work, incorporation of the β-signal between strands 1 and 16 is from the current knowledge the most likely priming mechanism. In order to maintain the usually antiparallel strand pairing in an OMP barrel, the incorporation of a full hairpin, composed of the two last β-strands of the OMP seems favorable, which is equivalent to the first step in the proposed hybrid barrel formation mechanism.

Energetically, a hairpin insertion is reasonable: The hydrophilic loop between the two strands may use the aqueous TamA/BamA barrel interior for membrane traversal and after insertion, the hydrophobic and hydrophilic sidechains of the hairpin would be in a native-like membrane and aqueous environment, respectively. Broken hydrogen bonds between TamA/BamA strand 1 and 16, which are only few in comparison to other barrel strand pairs, would be replaced by even more hydrogen bonds: The hairpin replaces the lost hydrogen bonds on one side of the insertion site and forms additional ones on the other side. Moreover, the hairpin itself forms hydrogen bonds between its two strands.

Now, as the hairpin has set the right direction of the OMP in the membrane, complete OMP assembly into the distorted bilayer next to TamA/BamA may take place. For this to happen, the hydrogen bonds between the inserted OMP hairpin and the neighboring TamA/BamA strands need to be broken to release the hairpin from TamA/BamA in order that the rest of the barrel can assemble. As broken hydrogen bonds will be replaced again by new ones, this should not be energetically unfavorable and, furthermore, the interactions between any OMP and TamA/BamA would always be similarly independent of the number of

strands of an OMP barrel. However, this mechanism cannot suffice to explain the special case of autotransporter assembly, in which passenger domain secretion to the extracellular space is coupled to β-barrel assembly (Pavlova *et al.* 2013), and does not occur through the assembled autotransporter barrel (Bernstein 2007, Jong *et al.* 2007, Skillman *et al.* 2005).

A complete hybrid barrel formation resolves this mechanistic and topological riddle: After the first hairpin insertion, the next OMP strand pair would inserts next to the first strand pair and again more new hydrogen bonds are built than broken. This continues until the last strand pair has inserted and now the following N-terminal passenger domain can use the expanded hybrid barrel for membrane traversal. When its translocation has finished, the hybrid barrel disintegrates and the linker between the now extracellular passenger domain and barrel strand 1 at the periplasmic site ends up in the fully assembled autotransporter barrel.

Despite elegantly resolving the autotransporter assembly mechanism, this model does have a few weak points: For BamA, the number of strands of the OMP substrates can vary significantly between 8 (Pautsch and Schulz 1998) and 26 (Qiao *et al.* 2014) and therefore the hybrid barrel disintegration event needs to be timed correctly for each OMP in order to have all strands inserted. A solution to this problem may be that the disintegration due to rising instability, also for large hybrid barrels, is always kinetically slower than the hybrid barrel formation and thus, this mechanism works irrespective of the number of strands of an OMP. The second weak point is that the tilt angles of OMPs vary between approx. 35° and 45° (Pali and Marsh 2001) (Fig. 1.2b) and in a hybrid barrel both the tilt angles of TamA/BamA and the substrate need to be satisfied. However, the difference in tilt angles is not large and some flexibility in a hybrid barrel could suffice to satisfy the tilt angles both in the TamA/BamA region and the substrate OMP region.

Like for the OMP insertion mechanism, a detailed description of the TpsA translocation mechanism through the TpsB pore is still missing. Since Omp85 proteins share the same overall fold, the question remains whether insertion and translocation processes share a common mechanistic basis or are independent processes. A hybrid barrel mechanism could constitute a common mechanism, even though it is conceptionally not necessary for translocation. However, TpsA proteins share an N-terminal, approx. 250 residues long TPS domain, which is necessary and sufficient for translocation (Grass and St Geme 2000, Jacob-Dubuisson *et al.* 1997, Renauld-Mongenie *et al.* 1996, Schönherr *et al.* 1993). Since this domain contains amphipathic stretches of residues, which in the secreted soluble TpsA protein adopt β-helical structure (Fig. 1.7b), the formation of a hybrid barrel between a TpsB translocase and its TpsA substrate may exist as part of a recognition mode and translocation intermediate. A disintegration of the hybrid barrel would however not lead to a new OMP in

the membrane but instead would exclude the TPS sequence from the membrane environment and release it to the extracellular space.

7.3. L6 loop and lid lock function

All Omp85 structures determined to date represent resting states of these proteins. The cell exterior side of the barrel is closed in all structures but the closure differs between the insertases TamA (Gruss *et al.* 2013) and BamA (Albrecht *et al.* 2014, Ni *et al.* 2014, Noinaj *et al.* 2013), and the translocase FhaC (Clantin *et al.* 2007, Maier *et al.* 2015): Whereas in TamA and BamA the long extracellular loop L6 is mainly involved in barrel closure, supported by the inwards facing loops L3 and L4 (Fig. 5.5), loop L6 also contributes to barrel closure in FhaC, but the outwards facing loops L3 and L4 create a large gap, which is plugged by helix H1 (Fig. 5.5). Loop L6 adopts a very similar overall conformation in all proteins, except for a variable insertion site, which harbors additional residues in TamA and BamA as compared to FhaC (Fig. 5.4a, Supplementary Fig. 5.3). These additional residues form a loop heading towards the extracellular space and therefore the barrel would still be closed without them. An outwards closed barrel thus seems to be a conserved principle in the resting state of both insertases and translocases. It possibly contributes to barrel stability by compensating the reduced interactions between the first and last barrel strand, and prevents additional leakiness of the OM. The length of the flexible variable insertion site in L6 (Maier *et al.* 2015, Morgado *et al.* 2015) correlates with the number of barrel strands of the substrates of an Omp85 protein. BamA, which has substrates with up to 26 strands, contains 18.5 ± 8.6 additional residues (Supplementary Fig. 5.3), TamA, which has autotransporter substrates with 12 strands, contains 11.7 ± 4.2 additional residues, and for TpsB proteins, which have soluble secreted substrates, this variable insertion site is not filled at all (0 ± 0 residues). It is therefore tempting to speculate that in a hybrid barrel mechanism for OMP biogenesis these additional residues may structurally rearrange to stabilize the expanded hybrid barrel, possibly by interactions with other extracellular loops of TamA/BamA and/or the substrate OMP. This assumption would however speak against hybrid barrel formation as a common mechanistic principle for both insertion and translocation.

Loop L6 harbors one of the two highly conserved sequence motifs in Omp85 proteins, VRG(Y/F) (Delattre *et al.* 2010), which in all solved and corrected structures forms very similar interactions, including a salt bridge, with the other conserved motif (F/G)xDxG (Jacob-Dubuisson *et al.* 2013) at the barrel interior on strand 13. This conserved lid lock motif could therefore be essential to maintain the overall loop L6 structure and to contribute to stability during insertion or translocation. A more active role during insertion seems unlikely since crosslinking between the two motifs does not inhibit BamA function *in vivo* (Noinaj *et al.*

2014) and therefore unlocking of the two motifs is not required. However for FhaC, recent experimental data suggest that the salt bridge is broken during translocation of FHA, which would favor a more active role of the lid lock in translocation (Guérin *et al.* 2015).

The observed effect on barrel shapes of the GxDxG vs. FxDxG motifs in FhaC-like TpsB proteins and bacterial insertases, respectively (Fig. 5.4b, 5.5a), further implies a difference between insertion and translocation mechanisms. However it should be mentioned that in the not discussed HMW1B-like subfamily of TpsB proteins the motif is the same as in the insertase family (Jacob-Dubuisson *et al.* 2013). In this respect, it would also be of great relevance to study the lid lock structures in mitochondrial and chloroplast Omp85 proteins: Toc75 and OEP80 proteins in chloroplasts, involved in translocation and presumably also insertion, have an Fx(D/E)xGxDxG motif (Jacob-Dubuisson *et al.* 2013), which is like a fusion of an insertase with a translocase motif. The question to be answered here is which of the two negatively charged side chains is actually involved in lid lock formation and whether this double motif may hint at a dual role for these proteins, since little is known about OMP insertion into the chloroplast OEM and the actual insertase has not been identified yet. In contrast, in the mitochondrial insertase Sam50 the motif has changed to FxNxG (Jacob-Dubuisson *et al.* 2013), which abolishes the formation of a salt bridge with the still conserved Arg in the VRG(Y/F) motif. The question to be answered for Sam50 is whether still a lid lock-like structure forms, and whether a spatially close Asp or Glu residue in a different strand replaces the missing residue in this motif.

Overall, the Omp85 protein superfamily remains an exciting area of structural and functional studies.

Appendix

References

Adams PD, Afonine PV, Bunkoczi G, Chen VB, Davis IW, Echols N, . . . Zwart PH. PHENIX: a comprehensive Python-based system for macromolecular structure solution. *Acta Crystallogr D Biol Crystallogr* **66**, 213-221 (2010).

Adams PD, Grosse-Kunstleve RW, Hung LW, Ioerger TR, McCoy AJ, Moriarty NW, . . . Terwilliger TC. PHENIX: building new software for automated crystallographic structure determination. *Acta Crystallogr D Biol Crystallogr* **58**, 1948-1954 (2002).

Ahting U, Thun C, Hegerl R, Typke D, Nargang FE, Neupert W, Nussberger S. The TOM core complex: the general protein import pore of the outer membrane of mitochondria. *J Cell Biol* **147**, 959-968 (1999).

Akopian D, Shen K, Zhang X, Shan SO. Signal recognition particle: an essential protein-targeting machine. *Annu Rev Biochem* **82**, 693-721 (2013).

Alberts B, Johnson A, Lewis J, Raff M, Roberts K, Walter P. Molecular Biology of the Cell, 5th edition. *Garland Science: New York*, (2008).

Albrecht R, Schutz M, Oberhettinger P, Faulstich M, Bermejo I, Rudel T, . . . Zeth K. Structure of BamA, an essential factor in outer membrane protein biogenesis. *Acta Crystallogr D Biol Crystallogr* **70**, 1779-1789 (2014).

Albrecht R, Zeth K. Structural basis of outer membrane protein biogenesis in bacteria. *J Biol Chem* **286**, 27792-27803 (2011).

Anwari K, Webb CT, Poggio S, Perry AJ, Belousoff M, Celik N, . . . Lithgow T. The evolution of new lipoprotein subunits of the bacterial outer membrane BAM complex. *Mol Microbiol* **84**, 832-844 (2012).

Aoki SK, Pamma R, Hernday AD, Bickham JE, Braaten BA, Low DA. Contact-dependent inhibition of growth in Escherichia coli. *Science* **309**, 1245-1248 (2005).

Aramini JM, Huang YJ, Swapna GV, Cort JR, Rajan PK, Xiao R, . . . Montelione GT. Solution NMR structure of Escherichia coli ytfP expands the structural coverage of the UPF0131 protein domain family. *Proteins* **68**, 789-795 (2007).

Aramini JM, Swapna GV, Huang YJ, Rajan PK, Xiao R, Shastry R, . . . Montelione GT. 1H, 13C, and 15N resonance assignments for Escherichia coli ytfP, a member of the broadly conserved UPF0131 protein domain family. *J Biomol NMR* **33**, 197 (2005).

Barenkamp SJ, St Geme JW, 3rd. Genes encoding high-molecular-weight adhesion proteins of nontypeable Haemophilus influenzae are part of gene clusters. *Infect Immun* **62**, 3320-3328 (1994).

Baud C, Guerin J, Petit E, Lesne E, Dupre E, Locht C, Jacob-Dubuisson F. Translocation path of a substrate protein through its Omp85 transporter. *Nat Commun* **5**, 5271 (2014).

Baud C, Hodak H, Willery E, Drobecq H, Locht C, Jamin M, Jacob-Dubuisson F. Role of DegP for two-partner secretion in Bordetella. *Mol Microbiol* **74**, 315-329 (2009).

Bechtluft P, Nouwen N, Tans SJ, Driessen AJ. SecB--a chaperone dedicated to protein translocation. *Mol Biosyst* **6**, 620-627 (2010).

Becker L, Bannwarth M, Meisinger C, Hill K, Model K, Krimmer T, . . . Wagner R. Preprotein translocase of the outer mitochondrial membrane: reconstituted Tom40 forms a characteristic TOM pore. *J Mol Biol* **353**, 1011-1020 (2005).

Bennion D, Charlson ES, Coon E, Misra R. Dissection of β-barrel outer membrane protein assembly pathways through characterizing BamA POTRA 1 mutants of Escherichia coli. *Mol Microbiol* **77**, 1153-1171 (2010).

Bernstein HD. Are bacterial 'autotransporters' really transporters? *Trends Microbiol* **15**, 441-447 (2007).

Bernstein HD. Looks can be deceiving: recent insights into the mechanism of protein secretion by the autotransporter pathway. *Mol Microbiol* **97**, 205-215 (2015).

Betancor L, Fernandez MJ, Weissman KJ, Leadlay PF. Improved catalytic activity of a purified multienzyme from a modular polyketide synthase after coexpression with Streptomyces chaperonins in Escherichia coli. *Chembiochem* **9**, 2962-2966 (2008).

Bos MP, Robert V, Tommassen J. Functioning of outer membrane protein assembly factor Omp85 requires a single POTRA domain. *EMBO Rep* **8**, 1149-1154 (2007).

Braun M, Silhavy TJ. Imp/OstA is required for cell envelope biogenesis in Escherichia coli. *Mol Microbiol* **45**, 1289-1302 (2002).

Braun V. Covalent lipoprotein from the outer membrane of Escherichia coli. *Biochim Biophys Acta* **415**, 335-377 (1975).

Bricogne G, Blanc E, Brandl M, Flensburg C, Keller P, Paciorek W, . . . Womack TO. BUSTER. *Cambridge, United Kingdom: Global Phasing Ltd*, (2011).
Brix J, Dietmeier K, Pfanner N. Differential recognition of preproteins by the purified cytosolic domains of the mitochondrial import receptors Tom20, Tom22, and Tom70. *J Biol Chem* **272**, 20730-20735 (1997).
Burgess NK, Dao TP, Stanley AM, Fleming KG. β-Barrel proteins that reside in the Escherichia coli outer membrane in vivo demonstrate varied folding behavior in vitro. *J Biol Chem* **283**, 26748-26758 (2008).
Burmann BM, Wang C, Hiller S. Conformation and dynamics of the periplasmic membrane-protein-chaperone complexes OmpX-Skp and tOmpA-Skp. *Nat Struct Mol Biol* **20**, 1265-1272 (2013).
Buscher AZ, Grass S, Heuser J, Roth R, St Geme JW, 3rd. Surface anchoring of a bacterial adhesin secreted by the two-partner secretion pathway. *Mol Microbiol* **61**, 470-483 (2006).
Callon M, Burmann BM, Hiller S. Structural mapping of a chaperone-substrate interaction surface. *Angew Chem Int Ed Engl* **53**, 5069-5072 (2014).
Cannon KS, Or E, Clemons WM, Jr., Shibata Y, Rapoport TA. Disulfide bridge formation between SecY and a translocating polypeptide localizes the translocation pore to the center of SecY. *J Cell Biol* **169**, 219-225 (2005).
Chacinska A, Koehler CM, Milenkovic D, Lithgow T, Pfanner N. Importing mitochondrial proteins: machineries and mechanisms. *Cell* **138**, 628-644 (2009).
Chan NC, Lithgow T. The peripheral membrane subunits of the SAM complex function codependently in mitochondrial outer membrane biogenesis. *Mol Biol Cell* **19**, 126-136 (2008).
Chatterjee SN, Chaudhuri K. "Gram-Negative Bacteria: The cell Membranes" in Outer Membrane Vesicles of Bacteria. *SpringerBriefs in Microbiology, Springer, Berlin, Heidelberg*, 15-34 (2012).
Chen J. Molecular mechanism of the Escherichia coli maltose transporter. *Curr Opin Struct Biol* **23**, 492-498 (2013).
Clantin B, Delattre AS, Rucktooa P, Saint N, Meli AC, Locht C, . . . Villeret V. Structure of the membrane protein FhaC: a member of the Omp85-TpsB transporter superfamily. *Science* **317**, 957-961 (2007).
Clantin B, Hodak H, Willery E, Locht C, Jacob-Dubuisson F, Villeret V. The crystal structure of filamentous hemagglutinin secretion domain and its implications for the two-partner secretion pathway. *Proc Natl Acad Sci U S A* **101**, 6194-6199 (2004).
Costa TR, Felisberto-Rodrigues C, Meir A, Prevost MS, Redzej A, Trokter M, Waksman G. Secretion systems in Gram-negative bacteria: structural and mechanistic insights. *Nat Rev Microbiol* **13**, 343-359 (2015).
Cowan SW, Schirmer T, Rummel G, Steiert M, Ghosh R, Pauptit RA, . . . Rosenbusch JP. Crystal structures explain functional properties of two E. coli porins. *Nature* **358**, 727-733 (1992).
Cronan JE. Bacterial membrane lipids: where do we stand? *Annu Rev Microbiol* **57**, 203-224 (2003).
Dalbey RE, Kuhn A, Zhu L, Kiefer D. The membrane insertase YidC. *Biochim Biophys Acta* **1843**, 1489-1496 (2014).
Dautin N, Bernstein HD. Protein secretion in gram-negative bacteria via the autotransporter pathway. *Annu Rev Microbiol* **61**, 89-112 (2007).
Delattre AS, Clantin B, Saint N, Locht C, Villeret V, Jacob-Dubuisson F. Functional importance of a conserved sequence motif in FhaC, a prototypic member of the TpsB/Omp85 superfamily. *FEBS J* **277**, 4755-4765 (2010).
Delattre AS, Saint N, Clantin B, Willery E, Lippens G, Locht C, . . . Jacob-Dubuisson F. Substrate recognition by the POTRA domains of TpsB transporter FhaC. *Mol Microbiol* **81**, 99-112 (2011).
Deng M, Misra R. Examination of AsmA and its effect on the assembly of Escherichia coli outer membrane proteins. *Mol Microbiol* **21**, 605-612 (1996).
Doerrler WT, Raetz CR. Loss of outer membrane proteins without inhibition of lipid export in an Escherichia coli YaeT mutant. *J Biol Chem* **280**, 27679-27687 (2005).
Dong C, Hou HF, Yang X, Shen YQ, Dong YH. Structure of Escherichia coli BamD and its functional implications in outer membrane protein assembly. *Acta Crystallogr D Biol Crystallogr* **68**, 95-101 (2012a).
Dong C, Yang X, Hou HF, Shen YQ, Dong YH. Structure of Escherichia coli BamB and its interaction with POTRA domains of BamA. *Acta Crystallogr D Biol Crystallogr* **68**, 1134-1139 (2012b).
Du D, Wang Z, James NR, Voss JE, Klimont E, Ohene-Agyei T, . . . Luisi BF. Structure of the AcrAB-TolC multidrug efflux pump. *Nature* **509**, 512-515 (2014).
Eckart K, Eichacker L, Sohrt K, Schleiff E, Heins L, Soll J. A Toc75-like protein import channel is abundant in chloroplasts. *EMBO Rep* **3**, 557-562 (2002).

Egea PF, Stroud RM. Lateral opening of a translocon upon entry of protein suggests the mechanism of insertion into membranes. *Proc Natl Acad Sci U S A* **107**, 17182-17187 (2010).
Emsley P, Cowtan K. Coot: model-building tools for molecular graphics. *Acta Crystallogr D Biol Crystallogr* **60**, 2126-2132 (2004).
Emsley P, Lohkamp B, Scott WG, Cowtan K. Features and development of Coot. *Acta Crystallogr D Biol Crystallogr* **66**, 486-501 (2010).
Estrada Mallarino L, Fan E, Odermatt M, Muller M, Lin M, Liang J, . . . Welte W. TtOmp85, a β-barrel assembly protein, functions by barrel augmentation. *Biochemistry* **54**, 844-852 (2015).
Facey SJ, Kuhn A. Biogenesis of bacterial inner-membrane proteins. *Cell Mol Life Sci* **67**, 2343-2362 (2010).
Fan E, Fiedler S, Jacob-Dubuisson F, Muller M. Two-partner secretion of gram-negative bacteria: a single β-barrel protein enables transport across the outer membrane. *J Biol Chem* **287**, 2591-2599 (2012).
Flack FS, Loosmore S, Chong P, Thomas WR. The sequencing of the 80-kDa D15 protective surface antigen of Haemophilus influenzae. *Gene* **156**, 97-99 (1995).
Gabel F, Lensink MF, Clantin B, Jacob-Dubuisson F, Villeret V, Ebel C. Probing the conformation of FhaC with small-angle neutron scattering and molecular modeling. *Biophys J* **107**, 185-196 (2014).
Galdiero S, Falanga A, Cantisani M, Tarallo R, Della Pepa ME, D'Oriano V, Galdiero M. Microbe-host interactions: structure and role of Gram-negative bacterial porins. *Curr Protein Pept Sci* **13**, 843-854 (2012).
Gatzeva-Topalova PZ, Walton TA, Sousa MC. Crystal structure of YaeT: conformational flexibility and substrate recognition. *Structure* **16**, 1873-1881 (2008).
Gatzeva-Topalova PZ, Warner LR, Pardi A, Sousa MC. Structure and flexibility of the complete periplasmic domain of BamA: the protein insertion machine of the outer membrane. *Structure* **18**, 1492-1501 (2010).
Gentle I, Gabriel K, Beech P, Waller R, Lithgow T. The Omp85 family of proteins is essential for outer membrane biogenesis in mitochondria and bacteria. *J Cell Biol* **164**, 19-24 (2004).
Gentle IE, Burri L, Lithgow T. Molecular architecture and function of the Omp85 family of proteins. *Mol Microbiol* **58**, 1216-1225 (2005).
Gessmann D, Chung YH, Danoff EJ, Plummer AM, Sandlin CW, Zaccai NR, Fleming KG. Outer membrane β-barrel protein folding is physically controlled by periplasmic lipid head groups and BamA. *Proc Natl Acad Sci U S A* **111**, 5878-5883 (2014).
Gessmann D, Flinner N, Pfannstiel J, Schlosinger A, Schleiff E, Nussberger S, Mirus O. Structural elements of the mitochondrial preprotein-conducting channel Tom40 dissolved by bioinformatics and mass spectrometry. *Biochim Biophys Acta* **1807**, 1647-1657 (2011).
Glauert AM, Thornley MJ. The topography of the bacterial cell wall. *Annu Rev Microbiol* **23**, 159-198 (1969).
Gogala M, Becker T, Beatrix B, Armache JP, Barrio-Garcia C, Berninghausen O, Beckmann R. Structures of the Sec61 complex engaged in nascent peptide translocation or membrane insertion. *Nature* **506**, 107-110 (2014).
Goujon M, McWilliam H, Li W, Valentin F, Squizzato S, Paern J, Lopez R. A new bioinformatics analysis tools framework at EMBL-EBI. *Nucleic Acids Res* **38**, W695-699 (2010).
Gram C. Über die isolierte Färbung der Schizomyceten in Schnitt- und Trockenpräparaten. *Fortschritte der Medicin* **2**, 185-189 (1884).
Grass S, St Geme JW, 3rd. Maturation and secretion of the non-typable Haemophilus influenzae HMW1 adhesin: roles of the N-terminal and C-terminal domains. *Mol Microbiol* **36**, 55-67 (2000).
Gruss F, Zahringer F, Jakob RP, Burmann BM, Hiller S, Maier T. The structural basis of autotransporter translocation by TamA. *Nat Struct Mol Biol* **20**, 1318-1320 (2013).
Guedin S, Willery E, Tommassen J, Fort E, Drobecq H, Locht C, Jacob-Dubuisson F. Novel topological features of FhaC, the outer membrane transporter involved in the secretion of the Bordetella pertussis filamentous hemagglutinin. *J Biol Chem* **275**, 30202-30210 (2000).
Guérin J, Baud C, Touati N, Saint N, Willery E, Locht C, . . . Jacob-Dubuisson F. Conformational dynamics of protein transporter FhaC: large-scale motions of plug helix. *Mol Microbiol* **92**, 1164-1176 (2014).
Guérin J, Saint N, Baud C, Meli AC, Etienne E, Locht C, . . . Jacob-Dubuisson F. Dynamic interplay of membrane-proximal POTRA domain and conserved loop L6 in Omp85 transporter FhaC. *Mol Microbiol*, (2015).
Hagan CL, Kahne D. The reconstituted Escherichia coli Bam complex catalyzes multiple rounds of β-barrel assembly. *Biochemistry* **50**, 7444-7446 (2011).

Hagan CL, Kim S, Kahne D. Reconstitution of outer membrane protein assembly from purified components. *Science* **328**, 890-892 (2010).
Hagan CL, Silhavy TJ, Kahne D. β-Barrel membrane protein assembly by the Bam complex. *Annu Rev Biochem* **80**, 189-210 (2011).
Harrison SC. Peptide-surface association: the case of PDZ and PTB domains. *Cell* **86**, 341-343 (1996).
Heinz E, Lithgow T. A comprehensive analysis of the Omp85/TpsB protein superfamily structural diversity, taxonomic occurrence, and evolution. *Front Microbiol* **5**, 370 (2014).
Heinz E, Selkrig J, Belousoff MJ, Lithgow T. Evolution of the Translocation and Assembly Module (TAM). *Genome Biol Evol* **7**, 1628-1643 (2015).
Henderson IR, Cappello R, Nataro JP. Autotransporter proteins, evolution and redefining protein secretion. *Trends Microbiol* **8**, 529-532 (2000).
Henderson IR, Navarro-Garcia F, Nataro JP. The great escape: structure and function of the autotransporter proteins. *Trends Microbiol* **6**, 370-378 (1998).
Hennon SW, Soman R, Zhu L, Dalbey RE. YidC/Alb3/Oxa1 Family of Insertases. *J Biol Chem* **290**, 14866-14874 (2015).
Heuck A, Schleiffer A, Clausen T. Augmenting β-augmentation: structural basis of how BamB binds BamA and may support folding of outer membrane proteins. *J Mol Biol* **406**, 659-666 (2011).
Hill K, Model K, Ryan MT, Dietmeier K, Martin F, Wagner R, Pfanner N. Tom40 forms the hydrophilic channel of the mitochondrial import pore for preproteins. *Nature* **395**, 516-521 (1998).
Hiller S, Garces RG, Malia TJ, Orekhov VY, Colombini M, Wagner G. Solution structure of the integral human membrane protein VDAC-1 in detergent micelles. *Science* **321**, 1206-1210 (2008).
Hodak H, Clantin B, Willery E, Villeret V, Locht C, Jacob-Dubuisson F. Secretion signal of the filamentous haemagglutinin, a model two-partner secretion substrate. *Mol Microbiol* **61**, 368-382 (2006).
Hoffmann A, Bukau B, Kramer G. Structure and function of the molecular chaperone Trigger Factor. *Biochim Biophys Acta* **1803**, 650-661 (2010).
Höhr AI, Straub SP, Warscheid B, Becker T, Wiedemann N. Assembly of β-barrel proteins in the mitochondrial outer membrane. *Biochim Biophys Acta* **1853**, 74-88 (2015).
Hsu SC, Patel R, Bedard J, Jarvis P, Inoue K. Two distinct Omp85 paralogs in the chloroplast outer envelope membrane are essential for embryogenesis in Arabidopsis thaliana. *Plant Signal Behav* **3**, 1134-1135 (2008).
Hsueh YC, Flinner N, Gross LE, Haarmann R, Mirus O, Sommer MS, Schleiff E. The chloroplast outer envelope protein P39 in Arabidopsis thaliana belongs to the Omp85 protein family. *Proteins*, (2014).
Hutchings MI, Palmer T, Harrington DJ, Sutcliffe IC. Lipoprotein biogenesis in Gram-positive bacteria: knowing when to hold 'em, knowing when to fold 'em. *Trends Microbiol* **17**, 13-21 (2009).
Huysmans GH, Baldwin SA, Brockwell DJ, Radford SE. The transition state for folding of an outer membrane protein. *Proc Natl Acad Sci U S A* **107**, 4099-4104 (2010).
Ieva R, Bernstein HD. Interaction of an autotransporter passenger domain with BamA during its translocation across the bacterial outer membrane. *Proc Natl Acad Sci U S A* **106**, 19120-19125 (2009).
Ieva R, Tian P, Peterson JH, Bernstein HD. Sequential and spatially restricted interactions of assembly factors with an autotransporter β domain. *Proc Natl Acad Sci U S A* **108**, E383-391 (2011).
Jacob-Dubuisson F, Antoine R, Locht C. Autotransporter proteins, evolution and redefining protein secretion: response. *Trends Microbiol* **8**, 533-534 (2000).
Jacob-Dubuisson F, Buisine C, Willery E, Renauld-Mongenie G, Locht C. Lack of functional complementation between Bordetella pertussis filamentous hemagglutinin and Proteus mirabilis HpmA hemolysin secretion machineries. *J Bacteriol* **179**, 775-783 (1997).
Jacob-Dubuisson F, Guerin J, Baelen S, Clantin B. Two-partner secretion: as simple as it sounds? *Res Microbiol* **164**, 583-595 (2013).
Jacob-Dubuisson F, Locht C, Antoine R. Two-partner secretion in Gram-negative bacteria: a thrifty, specific pathway for large virulence proteins. *Mol Microbiol* **40**, 306-313 (2001).
Jaehme M, Slotboom DJ. Diversity of membrane transport proteins for vitamins in bacteria and archaea. *Biochim Biophys Acta* **1850**, 565-576 (2015).
Jansen KB, Baker SL, Sousa MC. Crystal structure of BamB from Pseudomonas aeruginosa and functional evaluation of its conserved structural features. *PLoS One* **7**, e49749 (2012).

Jansen KB, Baker SL, Sousa MC. Crystal structure of BamB bound to a periplasmic domain fragment of BamA, the central component of the β-barrel assembly machine. *J Biol Chem* **290**, 2126-2136 (2015).
Jong WS, ten Hagen-Jongman CM, den Blaauwen T, Slotboom DJ, Tame JR, Wickstrom D, . . . Luirink J. Limited tolerance towards folded elements during secretion of the autotransporter Hbp. *Mol Microbiol* **63**, 1524-1536 (2007).
Julio SM, Cotter PA. Characterization of the filamentous hemagglutinin-like protein FhaS in Bordetella bronchiseptica. *Infect Immun* **73**, 4960-4971 (2005).
Kabsch W. Xds. *Acta Crystallogr D Biol Crystallogr* **66**, 125-132 (2010).
Kajava AV, Steven AC. The turn of the screw: variations of the abundant β-solenoid motif in passenger domains of Type V secretory proteins. *J Struct Biol* **155**, 306-315 (2006).
Kapust RB, Tozser J, Fox JD, Anderson DE, Cherry S, Copeland TD, Waugh DS. Tobacco etch virus protease: mechanism of autolysis and rational design of stable mutants with wild-type catalytic proficiency. *Protein Eng* **14**, 993-1000 (2001).
Kato H, Mihara K. Identification of Tom5 and Tom6 in the preprotein translocase complex of human mitochondrial outer membrane. *Biochem Biophys Res Commun* **369**, 958-963 (2008).
Keeling PJ. The endosymbiotic origin, diversification and fate of plastids. *Philos Trans R Soc Lond B Biol Sci* **365**, 729-748 (2010).
Kim KH, Aulakh S, Paetzel M. Crystal structure of β-barrel assembly machinery BamCD protein complex. *J Biol Chem* **286**, 39116-39121 (2011a).
Kim KH, Aulakh S, Paetzel M. The bacterial outer membrane β-barrel assembly machinery. *Protein Sci* **21**, 751-768 (2012).
Kim KH, Aulakh S, Tan W, Paetzel M. Crystallographic analysis of the C-terminal domain of the Escherichia coli lipoprotein BamC. *Acta Crystallogr Sect F Struct Biol Cryst Commun* **67**, 1350-1358 (2011b).
Kim KH, Kang HS, Okon M, Escobar-Cabrera E, McIntosh LP, Paetzel M. Structural characterization of Escherichia coli BamE, a lipoprotein component of the β-barrel assembly machinery complex. *Biochemistry* **50**, 1081-1090 (2011c).
Kim KH, Paetzel M. Crystal structure of Escherichia coli BamB, a lipoprotein component of the β-barrel assembly machinery complex. *J Mol Biol* **406**, 667-678 (2011).
Kim S, Malinverni JC, Sliz P, Silhavy TJ, Harrison SC, Kahne D. Structure and function of an essential component of the outer membrane protein assembly machine. *Science* **317**, 961-964 (2007).
Knowles TJ, Browning DF, Jeeves M, Maderbocus R, Rajesh S, Sridhar P, . . . Overduin M. Structure and function of BamE within the outer membrane and the β-barrel assembly machine. *EMBO Rep* **12**, 123-128 (2011).
Knowles TJ, Jeeves M, Bobat S, Dancea F, McClelland D, Palmer T, . . . Henderson IR. Fold and function of polypeptide transport-associated domains responsible for delivering unfolded proteins to membranes. *Mol Microbiol* **68**, 1216-1227 (2008).
Koebnik R, Locher KP, Van Gelder P. Structure and function of bacterial outer membrane proteins: barrels in a nutshell. *Mol Microbiol* **37**, 239-253 (2000).
Koenig P, Mirus O, Haarmann R, Sommer MS, Sinning I, Schleiff E, Tews I. Conserved properties of polypeptide transport-associated (POTRA) domains derived from cyanobacterial Omp85. *J Biol Chem* **285**, 18016-18024 (2010).
Koronakis V, Sharff A, Koronakis E, Luisi B, Hughes C. Crystal structure of the bacterial membrane protein TolC central to multidrug efflux and protein export. *Nature* **405**, 914-919 (2000).
Krause RM, McCarty M. Studies on the chemical structure of the streptococcal cell wall. I. The identification of a mucopeptide in the cell walls of groups A and A-variant streptococci. *J Exp Med* **114**, 127-140 (1961).
Kudva R, Denks K, Kuhn P, Vogt A, Muller M, Koch HG. Protein translocation across the inner membrane of Gram-negative bacteria: the Sec and Tat dependent protein transport pathways. *Res Microbiol* **164**, 505-534 (2013).
Kumazaki K, Kishimoto T, Furukawa A, Mori H, Tanaka Y, Dohmae N, . . . Nureki O. Crystal structure of Escherichia coli YidC, a membrane protein chaperone and insertase. *Sci Rep* **4**, 7299 (2014).
Künkele KP, Heins S, Dembowski M, Nargang FE, Benz R, Thieffry M, . . . Neupert W. The preprotein translocation channel of the outer membrane of mitochondria. *Cell* **93**, 1009-1019 (1998).
Kuszak AJ, Jacobs D, Gurnev PA, Shiota T, Louis J, Lithgow T, . . . Buchanan SK. Evidence of distinct channel conformations and substrate binding affinities for the mitochondrial outer membrane protein translocase pore Tom40. *J Biol Chem*, (2015).
Kutik S, Stojanovski D, Becker L, Becker T, Meinecke M, Kruger V, . . . Wiedemann N. Dissecting membrane insertion of mitochondrial β-barrel proteins. *Cell* **132**, 1011-1024 (2008).

Kutschera U, Niklas KJ. Endosymbiosis, cell evolution, and speciation. *Theory Biosci* **124**, 1-24 (2005).
Labischinski H, Goodell EW, Goodell A, Hochberg ML. Direct proof of a "more-than-single-layered" peptidoglycan architecture of Escherichia coli W7: a neutron small-angle scattering study. *J Bacteriol* **173**, 751-756 (1991).
Lackey SW, Taylor RD, Go NE, Wong A, Sherman EL, Nargang FE. Evidence supporting the 19 β-strand model for Tom40 from cysteine scanning and protease site accessibility studies. *J Biol Chem* **289**, 21640-21650 (2014).
Langer G, Cohen SX, Lamzin VS, Perrakis A. Automated macromolecular model building for X-ray crystallography using ARP/wARP version 7. *Nat Protoc* **3**, 1171-1179 (2008).
Leo JC, Grin I, Linke D. Type V secretion: mechanism(s) of autotransport through the bacterial outer membrane. *Philos Trans R Soc Lond B Biol Sci* **367**, 1088-1101 (2012).
Mahendran KR, Romero-Ruiz M, Schlosinger A, Winterhalter M, Nussberger S. Protein translocation through Tom40: kinetics of peptide release. *Biophys J* **102**, 39-47 (2012).
Maier T, Clantin B, Gruss F, Dewitte F, Delattre AS, Jacob-Dubuisson F, . . . Villeret V. Conserved Omp85 lid-lock structure and substrate recognition in FhaC. *Nat Commun* **6**, 7452 (2015).
Maier T, Ferbitz L, Deuerling E, Ban N. A cradle for new proteins: trigger factor at the ribosome. *Curr Opin Struct Biol* **15**, 204-212 (2005).
Malinverni JC, Werner J, Kim S, Sklar JG, Kahne D, Misra R, Silhavy TJ. YfiO stabilizes the YaeT complex and is essential for outer membrane protein assembly in Escherichia coli. *Mol Microbiol* **61**, 151-164 (2006).
Manning DS, Reschke DK, Judd RC. Omp85 proteins of Neisseria gonorrhoeae and Neisseria meningitidis are similar to Haemophilus influenzae D-15-Ag and Pasteurella multocida Oma87. *Microb Pathog* **25**, 11-21 (1998).
Mayer A, Nargang FE, Neupert W, Lill R. MOM22 is a receptor for mitochondrial targeting sequences and cooperates with MOM19. *EMBO J* **14**, 4204-4211 (1995).
McCoy AJ, Grosse-Kunstleve RW, Adams PD, Winn MD, Storoni LC, Read RJ. Phaser crystallographic software. *J Appl Crystallogr* **40**, 658-674 (2007).
Milenkovic D, Kozjak V, Wiedemann N, Lohaus C, Meyer HE, Guiard B, . . . Meisinger C. Sam35 of the mitochondrial protein sorting and assembly machinery is a peripheral outer membrane protein essential for cell viability. *J Biol Chem* **279**, 22781-22785 (2004).
Mirus O, Hahn A, Schleiff E. "Outer Membrane Proteins" in Prokaryotic Cell Wall Compounds. Structure and Biochemistry (eds. König H, Claus H, Varma A). *Springer, Berlin, Heidelberg*, 175-230 (2010).
Model K, Prinz T, Ruiz T, Radermacher M, Krimmer T, Kuhlbrandt W, . . . Meisinger C. Protein translocase of the outer mitochondrial membrane: role of import receptors in the structural organization of the TOM complex. *J Mol Biol* **316**, 657-666 (2002).
Morgado L, Zeth K, Burmann BM, Maier T, Hiller S. Characterization of the insertase BamA in three different membrane mimetics by solution NMR spectroscopy. *J Biomol NMR* **61**, 333-345 (2015).
Neupert W, Herrmann JM. Translocation of proteins into mitochondria. *Annu Rev Biochem* **76**, 723-749 (2007).
Ni D, Wang Y, Yang X, Zhou H, Hou X, Cao B, . . . Huang Y. Structural and functional analysis of the β-barrel domain of BamA from Escherichia coli. *FASEB J* **28**, 2677-2685 (2014).
Nicolaisen K, Missbach S, Hsueh YC, Ertel F, Fulgosi H, Sommer MS, Schleiff E. The Omp85-type outer membrane protein p36 of Arabidopsis thaliana evolved by recent gene duplication. *J Plant Res* **128**, 317-325 (2015).
Nikaido H. Molecular Basis of Bacterial Outer Membrane Permeability Revisited. *Microbiology and Molecular Biology Reviews* **67**, 593-656 (2003).
Noel CR, Mazar J, Melvin JA, Sexton JA, Cotter PA. The prodomain of the Bordetella two-partner secretion pathway protein FhaB remains intracellular yet affects the conformation of the mature C-terminal domain. *Mol Microbiol* **86**, 988-1006 (2012).
Noinaj N, Buchanan SK. Structural insights into the transport of small molecules across membranes. *Curr Opin Struct Biol* **27**, 8-15 (2014).
Noinaj N, Fairman JW, Buchanan SK. The crystal structure of BamB suggests interactions with BamA and its role within the BAM complex. *J Mol Biol* **407**, 248-260 (2011).
Noinaj N, Guillier M, Barnard TJ, Buchanan SK. TonB-dependent transporters: regulation, structure, and function. *Annu Rev Microbiol* **64**, 43-60 (2010).
Noinaj N, Kuszak AJ, Balusek C, Gumbart JC, Buchanan SK. Lateral opening and exit pore formation are required for BamA function. *Structure* **22**, 1055-1062 (2014).

Noinaj N, Kuszak AJ, Gumbart JC, Lukacik P, Chang H, Easley NC, . . . Buchanan SK. Structural insight into the biogenesis of β-barrel membrane proteins. *Nature* **501**, 385-390 (2013).
Noinaj N, Rollauer SE, Buchanan SK. The β-barrel membrane protein insertase machinery from Gram-negative bacteria. *Curr Opin Struct Biol* **31**, 35-42 (2015).
Norell D, Heuck A, Tran-Thi TA, Gotzke H, Jacob-Dubuisson F, Clausen T, . . . Fan E. Versatile in vitro system to study translocation and functional integration of bacterial outer membrane proteins. *Nat Commun* **5**, 5396 (2014).
Oberhettinger P, Leo JC, Linke D, Autenrieth IB, Schutz MS. The inverse autotransporter intimin exports its passenger domain via a hairpin intermediate. *J Biol Chem* **290**, 1837-1849 (2015).
Oldham ML, Khare D, Quiocho FA, Davidson AL, Chen J. Crystal structure of a catalytic intermediate of the maltose transporter. *Nature* **450**, 515-521 (2007).
Oomen CJ, van Ulsen P, van Gelder P, Feijen M, Tommassen J, Gros P. Structure of the translocator domain of a bacterial autotransporter. *EMBO J* **23**, 1257-1266 (2004).
Ovchinnikov S, Kamisetty H, Baker D. Robust and accurate prediction of residue-residue interactions across protein interfaces using evolutionary information. *Elife* **3**, e02030 (2014).
Page MG. The role of the outer membrane of Gram-negative bacteria in antibiotic resistance: Ajax' shield or Achilles' heel? *Handb Exp Pharmacol*, 67-86 (2012).
Paila YD, Richardson LG, Schnell DJ. New insights into the mechanism of chloroplast protein import and its integration with protein quality control, organelle biogenesis and development. *J Mol Biol* **427**, 1038-1060 (2015).
Pali T, Marsh D. Tilt, twist, and coiling in β-barrel membrane proteins: relation to infrared dichroism. *Biophys J* **80**, 2789-2797 (2001).
Palmer T, Berks BC. The twin-arginine translocation (Tat) protein export pathway. *Nat Rev Microbiol* **10**, 483-496 (2012).
Palomino C, Marin E, Fernandez LA. The fimbrial usher FimD follows the SurA-BamB pathway for its assembly in the outer membrane of Escherichia coli. *J Bacteriol* **193**, 5222-5230 (2011).
Papanikou E, Karamanou S, Economou A. Bacterial protein secretion through the translocase nanomachine. *Nat Rev Microbiol* **5**, 839-851 (2007).
Park E, Menetret JF, Gumbart JC, Ludtke SJ, Li W, Whynot A, . . . Akey CW. Structure of the SecY channel during initiation of protein translocation. *Nature* **506**, 102-106 (2014).
Park E, Rapoport TA. Mechanisms of Sec61/SecY-mediated protein translocation across membranes. *Annu Rev Biophys* **41**, 21-40 (2012).
Paschen SA, Waizenegger T, Stan T, Preuss M, Cyrklaff M, Hell K, . . . Neupert W. Evolutionary conservation of biogenesis of β-barrel membrane proteins. *Nature* **426**, 862-866 (2003).
Patel GJ, Behrens-Kneip S, Holst O, Kleinschmidt JH. The periplasmic chaperone Skp facilitates targeting, insertion, and folding of OmpA into lipid membranes with a negative membrane surface potential. *Biochemistry* **48**, 10235-10245 (2009).
Patel GJ, Kleinschmidt JH. The lipid bilayer-inserted membrane protein BamA of Escherichia coli facilitates insertion and folding of outer membrane protein A from its complex with Skp. *Biochemistry* **52**, 3974-3986 (2013).
Patel R, Smith SM, Robinson C. Protein transport by the bacterial Tat pathway. *Biochim Biophys Acta* **1843**, 1620-1628 (2014).
Pautsch A, Schulz GE. Structure of the outer membrane protein A transmembrane domain. *Nat Struct Biol* **5**, 1013-1017 (1998).
Pavlova O, Peterson JH, Ieva R, Bernstein HD. Mechanistic link between β barrel assembly and the initiation of autotransporter secretion. *Proc Natl Acad Sci U S A* **110**, E938-947 (2013).
Pei J, Grishin NV. AL2CO: calculation of positional conservation in a protein sequence alignment. *Bioinformatics* **17**, 700-712 (2001).
Pfanner N, Wiedemann N, Meisinger C, Lithgow T. Assembling the mitochondrial outer membrane. *Nat Struct Mol Biol* **11**, 1044-1048 (2004).
Phan G, Remaut H, Wang T, Allen WJ, Pirker KF, Lebedev A, . . . Waksman G. Crystal structure of the FimD usher bound to its cognate FimC-FimH substrate. *Nature* **474**, 49-53 (2011).
Plamondon P, Luke NR, Campagnari AA. Identification of a novel two-partner secretion locus in Moraxella catarrhalis. *Infect Immun* **75**, 2929-2936 (2007).
Pocanschi CL, Apell HJ, Puntervoll P, Hogh B, Jensen HB, Welte W, Kleinschmidt JH. The major outer membrane protein of Fusobacterium nucleatum (FomA) folds and inserts into lipid bilayers via parallel folding pathways. *J Mol Biol* **355**, 548-561 (2006).
Pohlner J, Halter R, Beyreuther K, Meyer TF. Gene structure and extracellular secretion of Neisseria gonorrhoeae IgA protease. *Nature* **325**, 458-462 (1987).

Poole K, Schiebel E, Braun V. Molecular characterization of the hemolysin determinant of Serratia marcescens. *J Bacteriol* **170**, 3177-3188 (1988).
Prieto AI, Hernandez SB, Cota I, Pucciarelli MG, Orlov Y, Ramos-Morales F, . . . Casadesus J. Roles of the outer membrane protein AsmA of Salmonella enterica in the control of marRAB expression and invasion of epithelial cells. *J Bacteriol* **191**, 3615-3622 (2009).
Prilipov A, Phale PS, Van Gelder P, Rosenbusch JP, Koebnik R. Coupling site-directed mutagenesis with high-level expression: large scale production of mutant porins from E. coli. *FEMS Microbiol Lett* **163**, 65-72 (1998).
Pusnik M, Schmidt O, Perry AJ, Oeljeklaus S, Niemann M, Warscheid B, . . . Schneider A. Mitochondrial preprotein translocase of trypanosomatids has a bacterial origin. *Curr Biol* **21**, 1738-1743 (2011).
Qiao S, Luo Q, Zhao Y, Zhang XC, Huang Y. Structural basis for lipopolysaccharide insertion in the bacterial outer membrane. *Nature* **511**, 108-111 (2014).
Qu J, Mayer C, Behrens S, Holst O, Kleinschmidt JH. The trimeric periplasmic chaperone Skp of Escherichia coli forms 1:1 complexes with outer membrane proteins via hydrophobic and electrostatic interactions. *J Mol Biol* **374**, 91-105 (2007).
Renauld-Mongenie G, Cornette J, Mielcarek N, Menozzi FD, Locht C. Distinct roles of the N-terminal and C-terminal precursor domains in the biogenesis of the Bordetella pertussis filamentous hemagglutinin. *J Bacteriol* **178**, 1053-1060 (1996).
Ricci DP, Hagan CL, Kahne D, Silhavy TJ. Activation of the Escherichia coli β-barrel assembly machine (Bam) is required for essential components to interact properly with substrate. *Proc Natl Acad Sci U S A* **109**, 3487-3491 (2012).
Rigel NW, Schwalm J, Ricci DP, Silhavy TJ. BamE modulates the Escherichia coli β-barrel assembly machine component BamA. *J Bacteriol* **194**, 1002-1008 (2012).
Robert V, Volokhina EB, Senf F, Bos MP, Van Gelder P, Tommassen J. Assembly factor Omp85 recognizes its outer membrane protein substrates by a species-specific C-terminal motif. *PLoS Biol* **4**, e377 (2006).
Robertson JW, Kasianowicz JJ, Banerjee S. Analytical approaches for studying transporters, channels and porins. *Chem Rev* **112**, 6227-6249 (2012).
Rossiter AE, Leyton DL, Tveen-Jensen K, Browning DF, Sevastsyanovich Y, Knowles TJ, . . . Henderson IR. The essential β-barrel assembly machinery complex components BamD and BamA are required for autotransporter biogenesis. *J Bacteriol* **193**, 4250-4253 (2011).
Rottem S. Interaction of mycoplasmas with host cells. *Physiol Rev* **83**, 417-432 (2003).
Ruffolo CG, Adler B. Cloning, sequencing, expression, and protective capacity of the oma87 gene encoding the Pasteurella multocida 87-kilodalton outer membrane antigen. *Infect Immun* **64**, 3161-3167 (1996).
Sanchez-Pulido L, Devos D, Genevrois S, Vicente M, Valencia A. POTRA: a conserved domain in the FtsQ family and a class of β-barrel outer membrane proteins. *Trends Biochem Sci* **28**, 523-526 (2003).
Sandoval CM, Baker SL, Jansen K, Metzner SI, Sousa MC. Crystal structure of BamD: an essential component of the β-Barrel assembly machinery of gram-negative bacteria. *J Mol Biol* **409**, 348-357 (2011).
Sauri A, Soprova Z, Wickstrom D, de Gier JW, Van der Schors RC, Smit AB, . . . Luirink J. The Bam (Omp85) complex is involved in secretion of the autotransporter haemoglobin protease. *Microbiology* **155**, 3982-3991 (2009).
Sauri A, Ten Hagen-Jongman CM, van Ulsen P, Luirink J. Estimating the size of the active translocation pore of an autotransporter. *J Mol Biol* **416**, 335-345 (2012).
Scheurwater EM, Burrows LL. Maintaining network security: how macromolecular structures cross the peptidoglycan layer. *FEMS Microbiol Lett* **318**, 1-9 (2011).
Schiebel E, Schwarz H, Braun V. Subcellular location and unique secretion of the hemolysin of Serratia marcescens. *J Biol Chem* **264**, 16311-16320 (1989).
Schirmer T, Keller TA, Wang YF, Rosenbusch JP. Structural basis for sugar translocation through maltoporin channels at 3.1 A resolution. *Science* **267**, 512-514 (1995).
Schmidt O, Pfanner N, Meisinger C. Mitochondrial protein import: from proteomics to functional mechanisms. *Nat Rev Mol Cell Biol* **11**, 655-667 (2010).
Schmitt S, Ahting U, Eichacker L, Granvogl B, Go NE, Nargang FE, . . . Nussberger S. Role of Tom5 in maintaining the structural stability of the TOM complex of mitochondria. *J Biol Chem* **280**, 14499-14506 (2005).
Schnell DJ, Kessler F, Blobel G. Isolation of components of the chloroplast protein import machinery. *Science* **266**, 1007-1012 (1994).

Schönherr R, Tsolis R, Focareta T, Braun V. Amino acid replacements in the Serratia marcescens haemolysin ShlA define sites involved in activation and secretion. *Molecular Microbiology* **9**, 1229-1237 (1993).
Selkrig J, Belousoff MJ, Headey SJ, Heinz E, Shiota T, Shen HH, . . . Lithgow T. Conserved features in TamA enable interaction with TamB to drive the activity of the translocation and assembly module. *Sci Rep* **5**, 12905 (2015).
Selkrig J, Leyton DL, Webb CT, Lithgow T. Assembly of β-barrel proteins into bacterial outer membranes. *Biochim Biophys Acta* **1843**, 1542-1550 (2014).
Selkrig J, Mosbahi K, Webb CT, Belousoff MJ, Perry AJ, Wells TJ, . . . Lithgow T. Discovery of an archetypal protein transport system in bacterial outer membranes. *Nat Struct Mol Biol* **19**, 506-510, S501 (2012).
Serra DO, Conover MS, Arnal L, Sloan GP, Rodriguez ME, Yantorno OM, Deora R. FHA-mediated cell-substrate and cell-cell adhesions are critical for Bordetella pertussis biofilm formation on abiotic surfaces and in the mouse nose and the trachea. *PLoS One* **6**, e28811 (2011).
Shahid SA, Bardiaux B, Franks WT, Krabben L, Habeck M, van Rossum BJ, Linke D. Membrane-protein structure determination by solid-state NMR spectroscopy of microcrystals. *Nat Methods* **9**, 1212-1217 (2012).
Sheldrick GM. Experimental phasing with SHELXC/D/E: combining chain tracing with density modification. *Acta Crystallogr D Biol Crystallogr* **66**, 479-485 (2010).
Shen HH, Leyton DL, Shiota T, Belousoff MJ, Noinaj N, Lu J, . . . Lithgow T. Reconstitution of a nanomachine driving the assembly of proteins into bacterial outer membranes. *Nat Commun* **5**, 5078 (2014).
Shi LX, Theg SM. The chloroplast protein import system: from algae to trees. *Biochim Biophys Acta* **1833**, 314-331 (2013).
Shi Y. Common folds and transport mechanisms of secondary active transporters. *Annu Rev Biophys* **42**, 51-72 (2013).
Sievers F, Wilm A, Dineen D, Gibson TJ, Karplus K, Li W, . . . Higgins DG. Fast, scalable generation of high-quality protein multiple sequence alignments using Clustal Omega. *Mol Syst Biol* **7**, 539 (2011).
Silhavy TJ, Kahne D, Walker S. The bacterial cell envelope. *Cold Spring Harb Perspect Biol* **2**, a000414 (2010).
Sinnige T, Weingarth M, Renault M, Baker L, Tommassen J, Baldus M. Solid-state NMR studies of full-length BamA in lipid bilayers suggest limited overall POTRA mobility. *J Mol Biol* **426**, 2009-2021 (2014).
Skillman KM, Barnard TJ, Peterson JH, Ghirlando R, Bernstein HD. Efficient secretion of a folded protein domain by a monomeric bacterial autotransporter. *Mol Microbiol* **58**, 945-958 (2005).
Sklar JG, Wu T, Gronenberg LS, Malinverni JC, Kahne D, Silhavy TJ. Lipoprotein SmpA is a component of the YaeT complex that assembles outer membrane proteins in Escherichia coli. *Proc Natl Acad Sci U S A* **104**, 6400-6405 (2007a).
Sklar JG, Wu T, Kahne D, Silhavy TJ. Defining the roles of the periplasmic chaperones SurA, Skp, and DegP in Escherichia coli. *Genes Dev* **21**, 2473-2484 (2007b).
Smith KP, Voogt RD, Ruiz T, Mintz KP. The conserved carboxyl domain of MorC, an inner membrane protein of Aggregatibacter actinomycetemcomitans, is essential for membrane function. *Mol Oral Microbiol*, (2015).
Sommer MS, Daum B, Gross LE, Weis BL, Mirus O, Abram L, . . . Schleiff E. Chloroplast Omp85 proteins change orientation during evolution. *Proc Natl Acad Sci U S A* **108**, 13841-13846 (2011).
Spiess M. Protein translocation: the Sec61/SecYEG translocon caught in the act. *Curr Biol* **24**, R317-319 (2014).
St Geme JW, 3rd, Falkow S, Barenkamp SJ. High-molecular-weight proteins of nontypable Haemophilus influenzae mediate attachment to human epithelial cells. *Proc Natl Acad Sci U S A* **90**, 2875-2879 (1993).
St Geme JW, 3rd, Grass S. Secretion of the Haemophilus influenzae HMW1 and HMW2 adhesins involves a periplasmic intermediate and requires the HMWB and HMWC proteins. *Mol Microbiol* **27**, 617-630 (1998).
Stegmeier JF, Andersen C. Characterization of pores formed by YaeT (Omp85) from Escherichia coli. *J Biochem* **140**, 275-283 (2006).
Stegmeier JF, Gluck A, Sukumaran S, Mantele W, Andersen C. Characterisation of YtfM, a second member of the Omp85 family in Escherichia coli. *Biol Chem* **388**, 37-46 (2007).
Strange RE, Dark FA. An Unidentified Amino-sugar present in Cell Walls and Spores of Various Bacteria. *Nature* **177**, 186-188 (1956).

Struyvé M, Moons M, Tommassen J. Carboxy-terminal phenylalanine is essential for the correct assembly of a bacterial outer membrane protein. *J Mol Biol* **218**, 141-148 (1991).
Surana NK, Grass S, Hardy GG, Li H, Thanassi DG, Geme JW, 3rd. Evidence for conservation of architecture and physical properties of Omp85-like proteins throughout evolution. *Proc Natl Acad Sci U S A* **101**, 14497-14502 (2004).
Surrey T, Jahnig F. Refolding and oriented insertion of a membrane protein into a lipid bilayer. *Proc Natl Acad Sci U S A* **89**, 7457-7461 (1992).
Surrey T, Schmid A, Jahnig F. Folding and membrane insertion of the trimeric β-barrel protein OmpF. *Biochemistry* **35**, 2283-2288 (1996).
Suzuki H, Kadowaki T, Maeda M, Sasaki H, Nabekura J, Sakaguchi M, Mihara K. Membrane-embedded C-terminal segment of rat mitochondrial TOM40 constitutes protein-conducting pore with enriched β-structure. *J Biol Chem* **279**, 50619-50629 (2004).
Sveshnikova N, Grimm R, Soll J, Schleiff E. Topology studies of the chloroplast protein import channel Toc75. *Biol Chem* **381**, 687-693 (2000).
Tamm LK, Hong H, Liang B. Folding and assembly of β-barrel membrane proteins. *Biochim Biophys Acta* **1666**, 250-263 (2004).
Thomas WR, Callow MG, Dilworth RJ, Audesho AA. Expression in Escherichia coli of a high-molecular-weight protective surface antigen found in nontypeable and type b Haemophilus influenzae. *Infect Immun* **58**, 1909-1913 (1990).
Timmis JN, Ayliffe MA, Huang CY, Martin W. Endosymbiotic gene transfer: organelle genomes forge eukaryotic chromosomes. *Nat Rev Genet* **5**, 123-135 (2004).
Tokuda H. Biogenesis of outer membranes in Gram-negative bacteria. *Biosci Biotechnol Biochem* **73**, 465-473 (2009).
Tommassen J. Assembly of outer-membrane proteins in bacteria and mitochondria. *Microbiology* **156**, 2587-2596 (2010).
Tranel PJ, Froehlich J, Goyal A, Keegstra K. A component of the chloroplastic protein import apparatus is targeted to the outer envelope membrane via a novel pathway. *EMBO J* **14**, 2436-2446 (1995).
Tranel PJ, Keegstra K. A novel, bipartite transit peptide targets OEP75 to the outer membrane of the chloroplastic envelope. *Plant Cell* **8**, 2093-2104 (1996).
Turnbull WB, Daranas AH. On the value of c: can low affinity systems be studied by isothermal titration calorimetry? *J Am Chem Soc* **125**, 14859-14866 (2003).
Typas A, Banzhaf M, Gross CA, Vollmer W. From the regulation of peptidoglycan synthesis to bacterial growth and morphology. *Nat Rev Microbiol* **10**, 123-136 (2012).
Ujwal R, Bowie JU. Crystallizing membrane proteins using lipidic bicelles. *Methods* **55**, 337-341 (2011).
Ulrich T, Rapaport D. Biogenesis of β-barrel proteins in evolutionary context. *Int J Med Microbiol* **305**, 259-264 (2015).
Valent QA, Scotti PA, High S, de Gier JW, von Heijne G, Lentzen G, . . . Luirink J. The Escherichia coli SRP and SecB targeting pathways converge at the translocon. *EMBO J* **17**, 2504-2512 (1998).
van den Berg B. Crystal structure of a full-length autotransporter. *J Mol Biol* **396**, 627-633 (2010).
van den Berg B. Lateral gates: β-barrels get in on the act. *Nat Struct Mol Biol* **20**, 1237-1239 (2013).
Van den Berg B, Clemons WM, Jr., Collinson I, Modis Y, Hartmann E, Harrison SC, Rapoport TA. X-ray structure of a protein-conducting channel. *Nature* **427**, 36-44 (2004).
van Ulsen P, Rahman S, Jong WS, Daleke-Schermerhorn MH, Luirink J. Type V secretion: from biogenesis to biotechnology. *Biochim Biophys Acta* **1843**, 1592-1611 (2014).
van Ulsen P, Rutten L, Feller M, Tommassen J, van der Ende A. Two-partner secretion systems of Neisseria meningitidis associated with invasive clonal complexes. *Infect Immun* **76**, 4649-4658 (2008).
Vestweber D, Brunner J, Baker A, Schatz G. A 42K outer-membrane protein is a component of the yeast mitochondrial protein import site. *Nature* **341**, 205-209 (1989).
Vinothkumar KR, Henderson R. Structures of membrane proteins. *Q Rev Biophys* **43**, 65-158 (2010).
Vollmer W, Bertsche U. Murein (peptidoglycan) structure, architecture and biosynthesis in Escherichia coli. *Biochim Biophys Acta* **1778**, 1714-1734 (2008).
Vollmer W, Blanot D, de Pedro MA. Peptidoglycan structure and architecture. *FEMS Microbiol Rev* **32**, 149-167 (2008a).
Vollmer W, Joris B, Charlier P, Foster S. Bacterial peptidoglycan (murein) hydrolases. *FEMS Microbiol Rev* **32**, 259-286 (2008b).
Volokhina EB, Beckers F, Tommassen J, Bos MP. The β-barrel outer membrane protein assembly complex of Neisseria meningitidis. *J Bacteriol* **191**, 7074-7085 (2009).

Volokhina EB, Grijpstra J, Stork M, Schilders I, Tommassen J, Bos MP. Role of the periplasmic chaperones Skp, SurA, and DegQ in outer membrane protein biogenesis in Neisseria meningitidis. *J Bacteriol* **193**, 1612-1621 (2011).
von Heijne G. Membrane-protein topology. *Nat Rev Mol Cell Biol* **7**, 909-918 (2006).
Voulhoux R, Bos MP, Geurtsen J, Mols M, Tommassen J. Role of a highly conserved bacterial protein in outer membrane protein assembly. *Science* **299**, 262-265 (2003).
Vuong P, Bennion D, Mantei J, Frost D, Misra R. Analysis of YfgL and YaeT interactions through bioinformatics, mutagenesis, and biochemistry. *J Bacteriol* **190**, 1507-1517 (2008).
Walther DM, Rapaport D, Tommassen J. Biogenesis of β-barrel membrane proteins in bacteria and eukaryotes: evolutionary conservation and divergence. *Cell Mol Life Sci* **66**, 2789-2804 (2009).
Weaver TM, Smith JA, Hocking JM, Bailey LJ, Wawrzyn GT, Howard DR, . . . Thompson JR. Structural and functional studies of truncated hemolysin A from Proteus mirabilis. *J Biol Chem* **284**, 22297-22309 (2009).
Werner J, Misra R. YaeT (Omp85) affects the assembly of lipid-dependent and lipid-independent outer membrane proteins of Escherichia coli. *Mol Microbiol* **57**, 1450-1459 (2005).
Whitfield C, Trent MS. Biosynthesis and export of bacterial lipopolysaccharides. *Annu Rev Biochem* **83**, 99-128 (2014).
Wiedemann N, Kozjak V, Chacinska A, Schonfisch B, Rospert S, Ryan MT, . . . Meisinger C. Machinery for protein sorting and assembly in the mitochondrial outer membrane. *Nature* **424**, 565-571 (2003).
Wilkens S. Structure and mechanism of ABC transporters. *F1000Prime Rep* **7**, 14 (2015).
Willems RJ, Geuijen C, van der Heide HG, Renauld G, Bertin P, van den Akker WM, . . . Mooi FR. Mutational analysis of the Bordetella pertussis fim/fha gene cluster: identification of a gene with sequence similarities to haemolysin accessory genes involved in export of FHA. *Mol Microbiol* **11**, 337-347 (1994).
Wimley WC. The versatile β-barrel membrane protein. *Current Opinion in Structural Biology* **13**, 404-411 (2003).
Winn MD, Ballard CC, Cowtan KD, Dodson EJ, Emsley P, Evans PR, . . . Wilson KS. Overview of the CCP4 suite and current developments. *Acta Crystallogr D Biol Crystallogr* **67**, 235-242 (2011).
Wirth C, Condemine G, Boiteux C, Berneche S, Schirmer T, Peneff CM. NanC crystal structure, a model for outer-membrane channels of the acidic sugar-specific KdgM porin family. *J Mol Biol* **394**, 718-731 (2009).
Wu T, Malinverni J, Ruiz N, Kim S, Silhavy TJ, Kahne D. Identification of a multicomponent complex required for outer membrane biogenesis in Escherichia coli. *Cell* **121**, 235-245 (2005).
Xie K, Dalbey RE. Inserting proteins into the bacterial cytoplasmic membrane using the Sec and YidC translocases. *Nat Rev Microbiol* **6**, 234-244 (2008).
Xu X, Wang S, Hu YX, McKay DB. The periplasmic bacterial molecular chaperone SurA adapts its structure to bind peptides in different conformations to assert a sequence preference for aromatic residues. *J Mol Biol* **373**, 367-381 (2007).
Yamamoto H, Itoh N, Kawano S, Yatsukawa Y, Momose T, Makio T, . . . Endo T. Dual role of the receptor Tom20 in specificity and efficiency of protein import into mitochondria. *Proc Natl Acad Sci U S A* **108**, 91-96 (2011).
Yao X, Durr UH, Gattin Z, Laukat Y, Narayanan RL, Bruckner AK, . . . Zweckstetter M. NMR-based detection of hydrogen/deuterium exchange in liposome-embedded membrane proteins. *PLoS One* **9**, e112374 (2014).
Yen MR, Peabody CR, Partovi SM, Zhai Y, Tseng YH, Saier MH. Protein-translocating outer membrane porins of Gram-negative bacteria. *Biochim Biophys Acta* **1562**, 6-31 (2002).
Yeo HJ, Yokoyama T, Walkiewicz K, Kim Y, Grass S, Geme JW, 3rd. The structure of the Haemophilus influenzae HMW1 pro-piece reveals a structural domain essential for bacterial two-partner secretion. *J Biol Chem* **282**, 31076-31084 (2007).
Zhang H, Gao ZQ, Hou HF, Xu JH, Li LF, Su XD, Dong YH. High-resolution structure of a new crystal form of BamA POTRA4-5 from Escherichia coli. *Acta Crystallogr Sect F Struct Biol Cryst Commun* **67**, 734-738 (2011).
Zhang YM, Rock CO. Membrane lipid homeostasis in bacteria. *Nat Rev Microbiol* **6**, 222-233 (2008).
Zimmer J, Nam Y, Rapoport TA. Structure of a complex of the ATPase SecA and the protein-translocation channel. *Nature* **455**, 936-943 (2008).
Zückert WR. Secretion of bacterial lipoproteins: through the cytoplasmic membrane, the periplasm and beyond. *Biochim Biophys Acta* **1843**, 1509-1516 (2014).

Acknowledgements

First of all, I would like to thank my supervisors Timm and Sebastian for providing me with a research topic for my Ph.D. work, for successfully guiding me through it, and for the knowledge and cutting-edge state-of-the-art equipment they offered. Furthermore, they kept being supportive and motivating throughout my Ph.D. and from time to time gave me that little push that is needed if it wouldn't come from within. Also, I would like to thank Martin Spiess for being part of my Ph.D. advisory committee.

Next, I would like to thank all former and current members of Timm's and Sebastian's groups for scientific and non-scientific discussions. I would like to thank Björn for introduction to the TOM project and NMR spectroscopy and Roman for his initiative in the TAM project. Especially, I would like to thank Moritz, Stefan, Dominik and Cedric for being good friends and for having the one or other beer together, accompanied by highly intellectual conversations.

Last, I would like to thank the Biozentrum as well as the Werner Siemens Foundation and the Fellowships for Excellence for hiring me and giving me this great scientific opportunity in this interdisciplinary scientific working environment.